

CRUSHING BEHAVIOR OF ALUMINUM FOAM-FILLED COMPOSITE TUBES

**A Thesis Submitted to
the Graduate School of Engineering and Sciences of
İzmir Institute of Technology
in Partial Fulfillment of the Requirements for the Degree of**

MASTER OF SCIENCE

in Mechanical Engineering

**by
Sinan YÜKSEL**

**July 2005
İZMİR**

We approve the thesis of **Sinan YÜKSEL**

Date of Signature

26 July 2005

Assoc. Prof. Dr. Mustafa GÜDEN
Supervisor
Department of Mechanical Engineering
İzmir Institute of Technology

26 July 2005

Assoc. Prof. Dr. Metin TANOĞLU
Co-Supervisor
Department of Mechanical Engineering
İzmir Institute of Technology

26 July 2005

Assoc. Prof. Dr. Bülent YARDIMOĞLU
Department of Mechanical Engineering
İzmir Institute of Technology

26 July 2005

Assoc. Prof. Dr. Engin AKTAŞ
Department of Civil Engineering
İzmir Institute of Technology

26 July 2005

Assoc. Prof. Dr. Barış ÖZERDEM
Department of Mechanical Engineering
İzmir Institute of Technology

Assoc. Prof. Dr. Semahat ÖZDEMİR
Head of the Graduate School

ACKNOWLEDGEMENTS

I would like to thank my advisors Assoc. Prof. Dr. Mustafa Gden and Assoc. Prof. Dr. Metin Tanođlu for their guidance and encouragement. They shared their all knowledge and expertise with me during this research. Besides, I am also very thankful to IZTECH CMR, IZTECH Atelier staff, my project friend Halit Kavi because of their helps during the experimental and production steps of the study. I am also grateful to the support provided by TBTAK (Project MSAG 227). Finally I would like to thank my family for their patience and support.

ABSTRACT

An experimental study has been conducted in order to determine the effect of Al-foam filling on the composite and hybrid (Al metal and composite) composite tubes. Tubes and fillers used in the experiments were prepared using the tube rolling and foaming from powder compacts methods, respectively. The composite was prepared using E-glass fiber fabric (2x2 twill fiber construction of 165 g/m^2 areal density) and polyester matrix with a 45/45 fiber angle to the tube axis. The quasi-static crush tests were conducted axially on the empty, hybrid and foam filled tubes at 25 mm/min crosshead speed. The deformation sequences of the tubes were further recorded during the tests in order to identify the crushing modes of the tubes. Two failure mechanisms literally known as progressive crushing and catastrophic failure (compression shear) were observed during the crushing of empty composite tubes. The progressive crushing mode led to higher crushing loads hence Specific Absorbed Energies (SAE). The predominant progressive crushing mode of empty tubes of thinner wall section was attributed to the surface end defects introduced during sectioning of the tubes. In hybrid tubes, the deformation mode of Al tube was found to be a more complex form of the diamond mode of deformation, leading to higher SAE values than the sum of the SAEs of empty composite and empty metal tube. The increased load and SAE values of hybrid tubes were attributed to the constraining effect of the composite to the metal tube folding. Results further showed that when the progressive crushing mode was taken into account hybrid tubes had lower SAE values than those of empty composite tubes. The foam filling of the composite tubes however showed two different results. It increased the foam filled tube crush loads over the sum of the crush loads of empty composite tube and foam. In the latter case it was not effective in increasing crush loads over the sum of the crush loads of empty composite tube and foam in the progressive crushing region. These two effects were discussed in terms of possible interactions between composite tube and foam.

ÖZET

Alüminyum (Al) köpük dolgunun, kompozit tüp ve Al-kompozit ikili tüplerin düşük deformasyon hızlarındaki ezilme davranışlarına ve soğurdukları enerji miktarlarına etkilerini belirlemek amaçlı deneysel bir çalışma yapılmıştır. Dolgu amaçlı kullanılan kapalı hücreli Al köpükler patentlenmiş bir proses kullanılarak üretilmiştir. Kompozit tüpler ise sonsuz fiberlerle filament sarma ve cam fiber kumaşlarla tüp sarma yöntemleriyle üretilmiştir. Düşük deformasyon hızlı (25mm/dak) deformasyon testleri değişik geometrik özelliklerde üretilmiş, boş ve Al köpük dolu tekli ve Al-kompozit ikili tüplere uygulanmıştır. Yapılan bu testlerin bazıları tüplerin deformasyon mekanizmalarının saptanabilmesi amacıyla test sürecinde kamerayla kaydedilmiştir. Benzeri malzemelerde başka çalışmalarda da karşılaşılmış olan ilerleyen ezilme ve tüp yapısında yırtılmalar şeklinde deformasyon mekanizmaları gözlemlenmiştir. İlerleyen ezilme şeklinde deforme olan tüplerde ezilme yük değerleri ve dolayısıyla da soğurulan enerji ve birim kütlenin soğurduğu enerji (SAE) değerleri daha yüksek olmuştur. İlerleyen ezilme modu tüp sarma sonrasında test numunesi buyutuna kesilirken tüp sonlarında oluşan hatalardan dolayı ince duvar kalınlığı olan tüplerde daha baskın oluşmuştur. İkili tüplerde, Al tüp daha karmaşık bir elmas modunda deforme olmuş ve bu değişiklik tek başına Al ve kompozit tüplerin ezilmesinin SAE değerleri toplamından daha büyük bir SAE değeri oluşmasına neden olmuştur. Bunun nedeni ezilme sırasında kompozit tüpün Al tüpün ezilme sırasındaki katlanmalarına etkisi olmasıdır. Bu karşılıklı etkileşim etkisi olarak adlandırılmaktadır. Kompozit tüplerde köpük dolgu kullanmanın ayrı ayrı ezilme yük değerleri toplamının üstünde değerlere ulaşması ve ezilmenin başlangıç aşamalarında kararlılık etkisi olmasına rağmen, aynı etki ilerleyen ezilme bölgesinde gözlemlenmemiştir. Bunun nedeni olabilecek olası etkileşimlerin üstünde durulmuştur. Köpük dolgulu ikili tüplerde de, dolgunun Al tüpün iç yöndeki katlanlarına gösterdiği dirençten dolayı oluşan kuvvetten aksenal yırtılmayla deforme olan kompozit tüpten dolayı, dolgunun ezilme yük ve SAE değerlerinde kararlılık sağlayıcı etkisi gözlemlenmemiştir.

TABLE OF CONTENTS

NOMENCLATURE	ix
LIST OF FIGURES	xi
LIST OF TABLES.....	xvii
CHAPTER 1. INTRODUCTION	1
CHAPTER 2. MANUFACTURING METHODS OF CLOSED CELL ALUMINUM FOAMS AND FIBER REINFORCED POLYESTER COMPOSITE TUBES.....	3
2.1. Manufacturing Methods of Closed Cell Aluminum Foams.....	3
2.1.1. Foaming of Melts by Gas Injection	3
2.1.2. Foaming of Melts with Blowing Agents.....	5
2.1.3. Foaming from Powder Compacts	6
2.1.4. Accumulative Roll-bonding Technique (ARB).....	9
2.1.5. Laser Assisted Aluminum Foaming	10
2.2. Manufacturing Methods of Fiber Reinforced Polyester Tubes	12
2.2.1. Filament Winding	12
2.2.2. Pultrusion	13
2.2.3. Resin Transfer Molding (RTM).....	15
2.2.4. Tube Rolling	15
2.2.5. Braiding	17
CHAPTER 3. CRUSHING BEHAVIOUR OF Al-FOAMS, EMPTY TUBES AND FOAM FILLED TUBES	18
3.1. Crushing Behavior of Al Foams	18
3.1.1. Linear Elasticity	19
3.1.2. Elastic and Plastic Collapse	21

3.1.3. Densification.....	22
3.1.4. Anisotropy	23
3.2. Terminologies Used In Crush Analysis	23
3.3. Crushing Behavior Of Composite Tubes.....	26
3.3.1. Fiber Micro Buckling.....	28
3.3.2. Euler Buckling	29
3.3.3. Tube Inversion	29
3.3.4. Progressive Crushing	29
3.3.5. Axisymmetric and Diamond Shaped Buckling	31
3.3.6. Crushing Behavior of Filament Wound Tubes.....	32
3.4. Crushing Behavior of Al Tubes	33
3.5. Crushing Behavior of Foam Filled Tubes.....	35
CHAPTER 4. MATERIALS AND PROCESSING	38
4.1. Al Closed Cell Foams	38
4.1.1. Closed Cell Al Foam Preparation	38
4.1.2. Aluminum Foam Filler Sample Preparation.....	44
4.1.3. Compression Mechanical Properties of Al Foams	46
4.2. Preparation of Glass Fiber Reinforced Composite Tubes	48
4.2.1. Filament Winding	48
4.2.2. Tube Rolling	50
CHAPTER 5. PREPARATION OF EMPTY, FOAM-FILLED, HYBRID AND FOAM FILLED HYBRID TUBES	51
5.1. Composite Tubes	51
5.1.1. Composite Tubes Prepared by Filament Winding.....	52
5.1.2. Composite Tubes Prepared by Tube Rolling Method Using Different Fabrics	53
5.1.3. Composite Tubes Prepared by Tube Rolling Method with Different Fiber Angles.....	54
5.1.4. Composite Tubes Prepared by Tube Rolling Method with Different Wall Thickness.....	54
5.1.5. Aluminum Foam-Filled Rolled Composite Tubes.....	55
5.2. Hybrid Tubes	56

5.2.1. Empty Hybrid Tubes.....	57
5.2.2. Al-Foam Filled Hybrid Tubes.....	58
5.3. Compression Tests and Calculations Methods	59
CHAPTER 6. RESULTS AND DISCUSSION.....	60
6.1. Compression Behavior of Empty Tubes.....	60
6.1.1. Single Composite Tubes	60
6.1.2. Empty Al and Composite Hybrid Tubes.....	72
6.2. Compression Behavior of Al-Foam Filled Tubes.....	80
6.2.1. Al-Foam Filled Composite Tubes.....	80
6.2.1. Al-Foam Filled Al-Composite Hybrid Tubes.....	86
CHAPTER 7. CONCLUSIONS.....	91
REFERENCES	93

NOMENCLATURE

A_E	Crush force efficiency
σ_p	Plateau stress of the foam
C	Strengthening coefficient of the foam filling
D	Mean diameter
D_C	Deformation capacity
E	Absorbed energy
E^*	Elastic modulus of the foam
E_s	Elastic modulus of the solid material
L	Total length of deformation element
σ_{ys}	Yield stress of the solid material
δ_{max}	Maximum total efficiency displacement
m_t	Total mass of deformation element
ν^*	Poisson ratio
ϕ	Fraction of solid
P_a	Average crush load of empty tubes
δ	Displacement
P_{at}	Atmospheric pressure
σ_U	The ultimate tensile stress of the tube material
σ_0	Mean plastic flow stress of the tube material
$\sigma_{0.2}$	Proof strength of the tube material
P_{max}	Maximum deformation load
P_0	Initial gas pressure of the foam cells
R	Anisotropy ratio
σ_{pl}^*	Plastic collapse stress of foam
SAE	Specific absorbed energy
S_E	Stroke efficiency
t	Thickness of tube
T_E	Total crush efficiency
ε_d	Densification strain of foam
ρ^*	Foam density

ρ_c	Tube material density
ρ_s	Solid material density
σ_c	Collapse stress of the foam
σ_{el}^*	Elastic collapse stress of foam
θ	Fiber angle

LIST OF FIGURES

<u>Figure</u>	<u>Page</u>
Figure 2.1. Foaming of melt by gas injection	4
Figure 2.2. Preferable particle (calcium) volume fraction and particle size range of stabilizing powders	4
Figure 2.3. Direct foaming of melts by adding gas-releasing agent	6
Figure 2.4. Effect of calcium (Ca) fraction and stirring time on the viscosity of Al melt	6
Figure 2.5. Foaming from powder compacts	7
Figure 2.6. (a) Complicated foam parts (b) sandwich foam panel	8
Figure 2.7. (a) schematic of the manufacturing process of a perform sheet through ARB process (b) prediction of gradual distribution of added blowing Agent articles	10
Figure 2.8. The block diagram of laser assisted AlSi7 foaming for three processing speeds, in decreasing order (1) > (2) > (3).....	11
Figure 2.9. Filament winding process set up	12
Figure 2.10. Pultrusion process set-up.....	14
Figure 2.11. Tube rolling process	15
Figure 2.12. Braiding set up for formation of fiberglass perform for composite coupling shaft	17
Figure 3.1. Cubic models of a) open-cell and b) closed-cell foams	18
Figure 3.2. Compression stress-strain curve of Al foam with 0.45 g/cm ³ density, showing distinct deformation regions	19
Figure 3.3. The mechanisms of foam deformation: a) open-cell foam, sequentially cell wall bending, cell wall axial deformation and fluid flow between cells and b) closed-cell foams, sequentially cell wall bending and contraction, membrane stretching and enclosed gas pressure	20
Figure 3.4. The deforming Al foam sample at various percent strains.....	21
Figure 3.5. Deformation mechanism of Al foam under compressive load.....	22
Figure 3.6. Terminologies used in the crush analysis of tubes.....	25
Figure 3.7. Various variables that influence the energy absorption characteristics of composite materials	26

Figure 3.8. Deformation types of tubular composite structures under compression. (a) Fiber micro buckling, (b) Euler buckling, (c) tube inversion, (d) progressive brittle crushing, (e) axisymmetric buckling and (f) diamond shape buckling	27
Figure 3.9. (a) Nominal stress-nominal strain behavior for braids of initial helix angle $\theta=23^\circ$ and 30° failing by micro buckling in compression. (b) The sawtooth fracture path of a compressive specimen which has failed by micro buckling	28
Figure 3.10. Progressively crushing of composite tubes by (a) fragmentation and (b) splaying modes.....	30
Figure 3.11. Load displacement curves of (a) static and (b) impact tests of composite tubes.....	30
Figure 3.12. (a) Sectioned crush tube sample showing frond formation and center wall crack, (b) Sectioned non-crimp fabric tube showing frond formation with high degree of post-crush integrity	31
Figure 3.13. Image of a $\theta =40^\circ$ braid tube failed by diamond shape buckling.....	32
Figure 3.14. Transition of collapse mode with respect to ply angle: (a) $\theta =75^\circ$, in traverse shearing, (b) $\theta = 45^\circ$ in local buckling, (c) $\theta =15^\circ$ in lamina bending.....	32
Figure 3.15. Alexander's concertina mode of deformation model.....	34
Figure 3.16. Concertina mode of circular tube deformation; inward and outward folding	35
Figure 3.17. Compression behavior of Al foam filled Al tube.....	36
Figure 3.18. Cross-sectioned braided tube with polyurethane core after uniaxial compression, $\theta=40^\circ$	37
Figure 3.19. Cut-away section of an epoxy foam-filled hybrid tube after the axial test.....	37
Figure 4.1. Schematic of foam preparation process.....	39
Figure 4.2. Foaming furnace, hot mould carrier and foaming mould.....	40
Figure 4.3. Cold compaction die.....	41

Figure 4.4. (a) Cold compacted precursor (92% dense) and (b) hot forged precursor (99% dense)	42
Figure 4.5. (a) Machining of the forged precursor material and (b) machined precursor	42
Figure 4.6. Foaming in the furnace with a steel mold closed at the top and bottom	43
Figure 4.7. Foamed precursor that completely filled foaming the mold	44
Figure 4.8. Pictures of Al foam and precursor material, showing 4 times expansion of initial thickness of the precursor	44
Figure 4.9. View of machining foam fillers using electrical discharge machine	45
Figure 4.10. An electrical discharge machined cylindrical Al foam sample	45
Figure 4.11. Compressive stress-strain curves of the prepared Al foams at various densities	46
Figure 4.12. Typical plateau stress vs. relative density curves of the Al foams	47
Figure 4.13. Glass fibers used to prepare tubes, (a) fiber fabric and (b) continuous fiber tow	48
Figure 4.14. Mandrel and the de-molding ring	49
Figure 4.15. Sectioned filament wound composite tube test specimens	49
Figure 4.16. Rolled and cut to length composite tube compression test specimens	50
Figure 5.1. Representation of geometrical parameters of fiber reinforced composite tubes	51
Figure 5.2. Filament wound tubes: (a) side and (b) cross-sectional view and (c) compression test specimens	52
Figure 5.3. Rolled tube showing homogeneous outer diameter and thickness: (a) side and (b) cross-sectional view	53
Figure 5.4. (a) E-glass woven fabric with (b) 2x2 twill fiber construction	54
Figure 5.5. Rolled tubes of different thickness coded as TE	55
Figure 5.6. (a) Machined filler Al-foam samples and (b) foam filled composite tube with thickness of 0.56 mm	56
Figure 5.7. Empty aluminum-composite hybrid tubes	57
Figure 5.8. Al foam-filled hybrid tube top views and layers	58
Figure 6.1. Load-displacement curves of filament wound composite tubes	60
Figure 6.2. Photographs of a filament wound composite tube failed by (a) buckling and (b) separation of tows	61

Figure 6.3. Load-displacement curves of composite tubes manufactured by tube rolling with two different fabric densities and varying thickness: a) 100 g/cm ² , t=0.86 mm and 200 g/cm ² , b) t=0.71 mm, (c) t=1.07 mm and d) t=1.53 mm	62
Figure 6.4. Crushing modes of the composite tubes of 0/90, a) progressive crushing and catastrophic failure (b) compression shear and (c) axial splitting and radial crack	62
Figure 6.5. Load-displacement curves of the composite tubes with 45/45 fiber angle prepared using E-glass fiber fabric of 2x2 twill fiber construction of 165 g/m ² areal density, average wall thickness: (a) t = 0.55 mm (b) t = 0.82 mm and (c) t=1.32 mm	64
Figure 6.6. (a) Load-displacement curve of a composite tube with 45/45 fiber angle prepared using E-glass fiber fabric of 2x2 twill fiber construction of 165 g/m ² areal density, wall thickness 0.41 mm and (b) corresponding view of the deformation at various displacements numbered in (a) showing progressive crushing mode	65
Figure 6.7. (a) Load-displacement curve of a composite tube with 45/45 fiber angle prepared using E-glass fiber fabric of 2x2 twill fiber construction of 165 g/m ² areal density, wall thickness 0.59 mm and (b) corresponding view of the deformation at various displacements numbered in (a) showing catastrophic failure crushing mode	67
Figure 6.8. Micrographs showing (a) a crack on the surface of a tube, formed as result of fiber and matrix fracture b) a broken fiber and c) fiber/matrix interface debonding in the crack region.....	68
Figure 6.9. Comparison of the (a) load and (b) SAE values of the empty composite tubes of different thickness and empty Al tube	70
Figure 6.10. (a) Effect of the tube mass on the maximum and mean loads and (b) SAE values of empty composite tubes with 45/45 fiber angle.....	71
Figure 6.11. Load, mean load and SAE basing on the mean load vs. displacement curves of empty Al tube of 27 mm in length and 0.29 mm in thickness.....	71
Figure 6.12. Load vs. displacement curves of hybrid tubes	73

Figure 6.13. Effect of the tube mass on the (a) maximum and mean loads and (b) SAE values of hybrid composite tubes with 45/45 fiber angle and (c) comparison of SAE values of hybrid tubes with empty composite and Al tubes	73
Figure 6.14. (a) Load-displacement curve of a hybrid tube with 45/45 fiber angle and (b) corresponding view of the deformation at various displacements numbered in (a) showing progressive crushing mode	75
Figure 6.15. (a) Load-displacement curve of a hybrid tube with 45/45 fiber angle and (b) corresponding view of the deformation at various displacements numbered in (a) showing compression shear mode crushing mode	76
Figure 6.16. Pictures of the progressive crushed hybrid tube after 20 mm deformation in (a) from back and (b) from front.....	77
Figure 6.17. Partially crushed empty Al tube: (a) back and (b) front views	78
Figure 6.18. Pictures of the hybrid tube after 20 mm deformation in Figure 6.14 taken from the backside of the crushing	78
Figure 6.19. Comparison of crushing loads of hybrid tubes with empty composite and composite tubes and their sum	79
Figure 6.20. Comparison of SAE values of the hybrid tubes with empty composite and Al tubes and their sum.....	80
Figure 6.21. Load-displacement curves of foam filled and empty composite tubes	81
Figure 6.22. (a) Load-displacement curve of a foam filled (0.33 g/cm ³) tube with 45/45 fiber angle and (b) corresponding views of the deformation at various displacements numbered in (a) showing progressive crushing mode.....	82
Figure 6.23. Maximum and mean crush loads vs. foam densities in filled and empty tubes	83
Figure 6.24. Comparison of foam filled tube crush loads with empty composite and Al foam and their sum (a) 0.25 g/cm ³ , (b) 0.33 g/cm ³ and (c) 0.44 and 0.27 g/cm ³	85
Figure 6.25. Comparison of SAE values of the foam filled tubes with empty composite and the sum of composite tube and the foam	86
Figure 6.26. Load-displacement curves of foam filled hybrid, empty hybrid and composite tubes.....	87

Figure 6.27. Comparisons of load-displacement curves hybrid tube with (a) the sum of crush loads of composite tube, Al tube and foam and (b) foam filled composite and Al tubes	88
Figure 6.28. (a) Image of the Al-foam filled hybrid tube after compression (b) deformation mechanism of the Al tube of the foam filled hybrid tube.....	89
Figure 6.29. Deformed views of (a) foam filled Al tube (Kavi et al., 2004) and (b) and (c) foam filled hybrid tube	89
Figure 6.30. SAE vs. Displacements of empty hybrid and composite tube and foam filled hybrid and composite tubes.....	90

LIST OF TABLES

<u>Table</u>	<u>Page</u>
Table 4.1. Specifications of powders used in foam manufacturing.....	40
Table 4.2. Specifications of the initially prepared cold compacted precursors	41
Table 4.3. Coefficients of Equation 4.1 for each foam density studied.....	48
Table 5.1. Wall thickness and fabric areal density of composites with 0/90 fiber lay-up	53
Table 5.2. Geometric parameters of composite tubes prepared for determining the thickness effect	55
Table 5.3. The properties of the foam filled composite tubes	56
Table 5.4. Mechanical properties of Al tube material	57
Table 5.5. Geometric parameters of tested empty Al tube	57
Table 5.6. Properties of empty hybrid tubes	58
Table 5.7. Properties of al foam filled hybrid tubes	58
Table 6.1. Compression test results of empty composite tubes with 45/45 fiber angle..	66
Table 6.2. Compression test results of Al-Composite hybrid tubes	72
Table 6.3. Compression test results of Al-foam filled composite tubes	81

CHAPTER 1

INTRODUCTION

Crashworthiness and impact resistance are directly related to structural integrity and passenger safety. The vital importance of the crashworthiness has motivated researchers to concentrate on the designing of passive novel structural components that are capable of absorbing the crash energy in a controlled manner. The protection of passengers in the event of an accident is an important issue mainly in the automotive, railway and aerospace industries. Any generic technology that can provide enhanced levels of protection in these industries is of considerable interest. Most interesting recent developments have however been witnessed in the automotive industry as increasingly stringent crashworthiness legislation coupled with rising consumer awareness of safety issues and cost pressures from insurance companies.

The crash protection system in automobiles is solely based on the axial folding of columnar metal structures, which has been known for several decades as an excellent energy-absorbing mechanism. Components based upon this principle are also utilized in high-volume industrial products such as trains and any other sector where energy, during a crash situation, needs to be absorbed in a controlled way. Energy absorbers in automobiles, referred as crash boxes, are generally inserted between the bumper cross members and the body. Its predefined shape helps to prevent the costly damages to the supporting parts. The screwed-on crash boxes can also be replaced easily with a relatively low expense.

The crushing behavior of columnar structures including rectangular and circular metal and composite tubes were studied extensively over the 30 years. In the last decade, the scientific interest shifted through filling the columnar structures with light-weight foams because foam-filling results in an increase in the specific energy absorption over the sum of the specific energy absorption of the foam alone and tube alone. This is known as interaction effect and can potentially be used in many diverse engineering applications including main frames of structural parts.

Studies of foam-filled tubes generally were on the foam-filled metal tubes and there have been only few studies on the crushing behavior of foam filled composite and foam filled composite/metal hybrid tubes. In filled metal tubes, the energy absorption

simply resulted from the tube folding, foam crushing and interaction between tube wall and filler. However, the effect of foam filling on the crushing behavior of composite tubes and hybrid tubes has not been known. Therefore these two tube systems, composite and composite/metal tube, were investigated in this thesis in terms of foam filling effects to their crushing behavior. Tubes were prepared using E-glass fibers and polyester matrix and the filler, Al closed cell foam, prepared by foaming from powder compact processes.

The content of the thesis is as follows: Chapter II summarizes Al foam and composite tube processing methods, Chapter III is a review of crushing behavior foams, metal and composite tubes and foam filled tubes. Chapter IV is on the characterization of used filler materials and Chapter V is on the preparation of the single and filled tubes. Results of the compression tests of the tubular energy absorbers manufactured and discussion are given in Chapter VI followed by the conclusions, Chapter VI.

CHAPTER 2

MANUFACTURING METHODS OF CLOSED CELL ALUMINUM FOAMS AND FIBER REINFORCED POLYESTER COMPOSITE TUBES

2.1. Manufacturing Methods of Closed Cell Aluminum Foams

Al closed cell foam can be manufactured by 1) foaming of melts by gas injection, 2) foaming of melts with blowing agents, 3) foaming from powder compacts, 4) accumulative roll-bonding technique and 5) laser assisted foaming. The first three methods are currently used to produce commercial Al foam while the others are still in the development stages.

2.1.1. Foaming of Melts by Gas Injection

Foaming of melts by gas injection is currently used by Alcan N. Hydro (Norway) and Cymat Aluminum Corporation (Canada) (Banhart and Baumeister 1998, Banhart 2000a). Ceramic particles like SiC, Al₂O₃, or magnesium oxide, are added in order to enhance the viscosity of the liquid metal to be foamed. In the second step, the melt is foamed by injecting gas (air or nitrogen) using rotating air injection shaft which generates fine gas bubbles and distributes them homogeneously in the melt (see Figure 2.1) (Gibson and Simone 1997). Since the bubbles are stabilized by ceramic particles, they can be pulled off melt surface using a conveyor belt. Finally, the foam is cooled down below the melting point of metal matrix. Typical volume fraction range of the ceramic particles used in the process is between 10 and 20% with a mean particle size between 5 μm and 20 μm as depicted in Figure 2.2 (Prakash et al. 1995). Typical density, average cell size and cell wall thickness are 0.069- 0.54g/cm³, 3-25 mm, and 50-85 μm, respectively (Gibson and Simone 1997). Average cell size, average cell wall thickness and density can be adjusted by varying processing parameters including gas injection rate and rotating shaft speed.

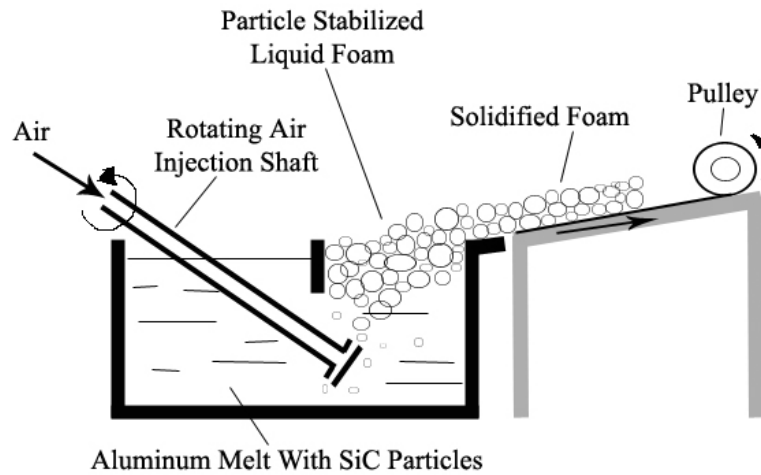


Figure 2.1. Foaming of melt by gas injection.

(Source : Gibson and Simone 1997)

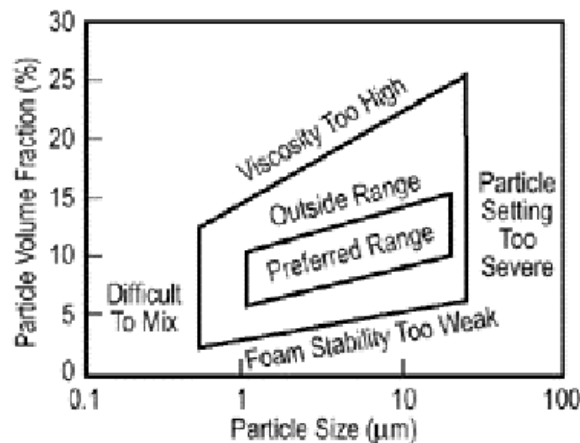


Figure 2.2. Preferable particle (calcium) volume fraction and particle size range of stabilizing powders.

(Source: Prakash et al. 1995)

Drainage is usually observed in the foamed slabs, which causes density and pore size gradients. The conveyor belt also induces shearing forces, leading to the formation of elongated cells. Solidified foams with dense outer surface layers can be directly used or machined into any desired shape. However, machining of these foams may be difficult due to the presence of hard ceramic particles in the metal matrix. The process has the capability for continuous production of large volumes of low-density metal matrix composite foams at a relatively lower cost. The main disadvantage of direct foaming is the necessity for the secondary processes such as cutting and machining.

2.1.2. Foaming of Melts with Blowing Agents

The second method of Al closed-cell foam production is to add a foaming or blowing agent (e.g. TiH₂) into liquid metal. As the foaming agent decomposes, the released gas drives the foaming process (Figure 2.3) (Miyoshi et al. 2000, Banhart 2000b). Before foaming, 1.5 wt.% calcium metal is added into the liquid Al at 680 °C and then the melt is stirred quickly (Figure 2.3). The viscosity of the melt increases with increasing stirring time because of the formation of oxide and/or metallic compounds (calcium oxide, calcium-aluminum oxide, or Al₄Ca intermetallic) which thickens the metallic melt (Banhart 1998). The effects of calcium volume fraction and stirring time on the viscosity of an Al melt are shown in Figure 2.4 (Banhart 2000b). In a later stage of the process, after adjusting the viscosity of the liquid metal, TiH₂ with an amount of 1.6 wt.% is added into the melt, which releases hydrogen gas in the hot viscous liquid according to the following reaction:



Above reaction results in the expansion of the liquid metal and fills the foaming vessel with liquid foam at a constant pressure. Finally, the liquid foam is cooled down below the melting point of the foamed alloy quickly and the solidified Al foam is further processed for specific applications.

Al foams produced by the process, *Alporas*TM, is the most homogeneous foams produced currently (Banhart 2000b). Typical densities of the cast foams are between 0.18 g/cm³ and 0.24 g/cm³ with an average pore size ranging from 2 mm to 10 mm (Miyoshi et al. 2000, Banhart 2000b). The viscosity of the molten Al can also be adjusted by injecting oxygen, air and other gas mixtures through the melt which causes the formation of Al₂O₃ particles and by adding viscosity enhancing additives directly such as Al₂O₃ and SiC particles. Complicated temperature cycles, difficulty in the adjustment of variables and the need for secondary processing (machining) are the disadvantages of the process.

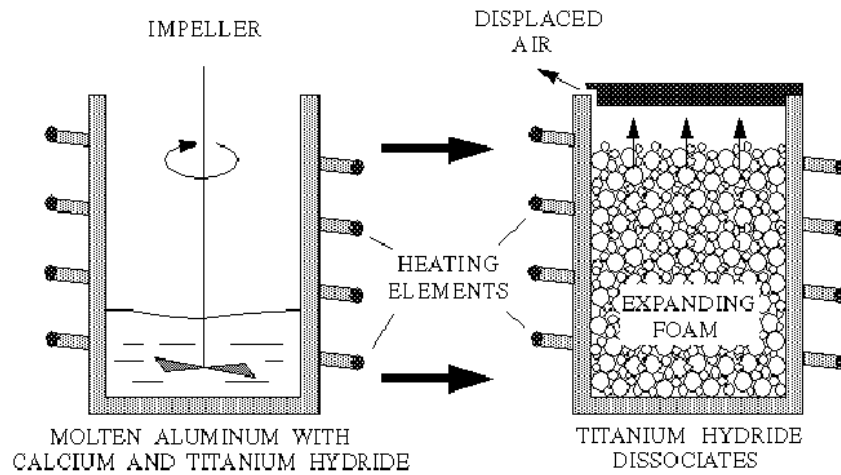


Figure 2.3. Direct foaming of melts by adding gas-releasing agent.

(Source: Banhart 2000b)

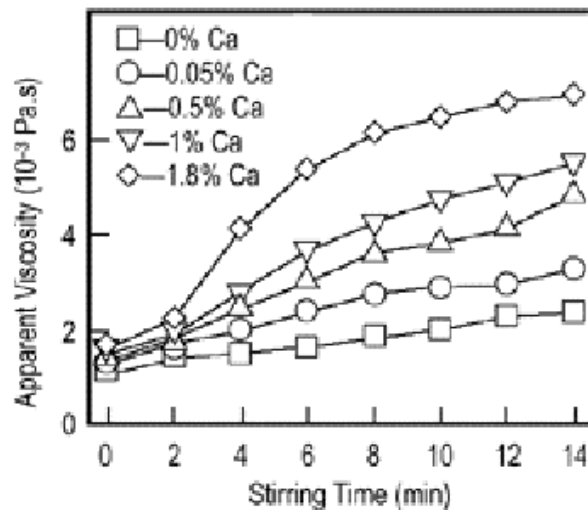


Figure 2.4 Effect of calcium (Ca) fraction and stirring time on the viscosity of Al melt.

(Source: Banhart 2000b)

2.1.3. Foaming from Powder Compacts

The process starts with mixing metal powders with a blowing agent which upon heating releases a foaming gas (Figure 2.5) (Baumgartner et al. 2000). Metal powder-blowing agent mixture is then compressed to a dense, semi-finished foamable product via metal forming processes such as hot compaction, extrusion and rolling (Figure 2.5). In a final step, the semi-finished product is heated to a temperature near to the melting point of the metal. During heating, the blowing agent decomposes and subsequently

releases gas, leading to the expansion of the molten or mushy metal and the formation of a highly porous structure.

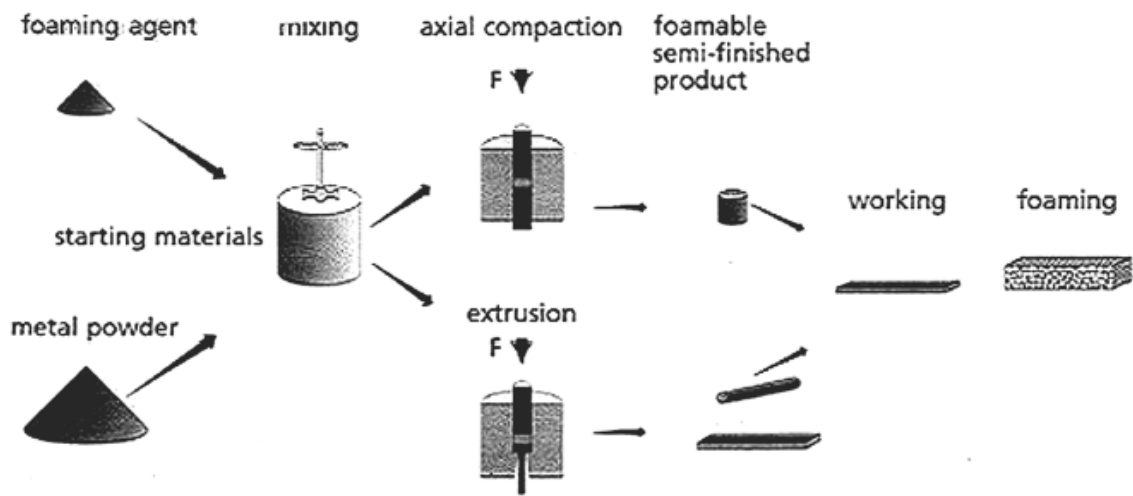


Figure 2.5. Foaming from powder compacts.

(Source: Baumgartner et al. 2000)

Besides metal hydrides (e.g., TiH_2), carbonates (e.g., calcium carbonate, potassium carbonate, sodium carbonate and sodium bicarbonate), hydrates (e.g., aluminum sulphate hydrate and aluminum hydroxide) or substances that evaporate quickly (e.g., mercury compounds or pulverized organic substances) can also be used as blowing agent.

For efficient foaming, it is very critical to form a gas-tight semi finished product in which the blowing agent is entrapped fully in the metallic matrix. Therefore the temperature and the pressure of hot compaction must be high enough to bond the individual metal powder particles and form a gas-tight seal around the blowing agent particles so that early decomposition of the blowing agent and the escape of H_2 gas before the melting of semi-finished product are avoided. In compaction by rolling, a temperature range between $350\text{ }^\circ\text{C}$ and $400\text{ }^\circ\text{C}$ is sufficient for the diffusion between the particles (Baumeister and Schrader 1992).

The amount of blowing agent for foaming of Al and its alloys has been found to be small. Calculations have shown that 0.6 wt. % TiH_2 in a foamable Al compact would give an expansion factor of 17, a value almost 4 times higher than the experimentally found expansion factor (4-5) (Baumgartner et al. 2000). This indicates that, only small portion of the released hydrogen (25%) is effective in forming pores and the rest is lost during foaming.

The time needed for full expansion of the semi-finished product depends on the temperature and size of the precursor and ranges from a few seconds to several minutes. The process is not only restricted to Al and its alloys, but also tin, zinc, brass, lead, gold, and some other metals and alloys can also be foamed using appropriate blowing agents and process parameters (Yu et al. 1998).

If a piece of foamable product is foamed in a furnace, the result will be a lump of metal foam with an undefined shape unless the expansion is limited. This is done by inserting the foamable semi-finished material into a mold and expanding it by heating. This process results in near-net shaped parts with a closed and dense outer skin and a highly porous cellular core. Complicated parts can be manufactured by pouring the expanding liquid foam into a mold (Figure 2.6 (a)). Sandwich panels consisting of a foamed metal core and two metal face sheets can be manufactured by bonding the face sheets to a piece of foam with adhesives. Another way is to roll clad Al or steel sheets into a sheet of foamable material and allow the foamable core to expand while the face sheets remain dense (Figure 2.6 (b)). By this method, Al foam structures can be combined with steel or titanium face sheets as well as with Al face sheets. In the latter case, Al sheets with melting points that are higher than the core material must be used to avoid melting of the face sheets during foaming.

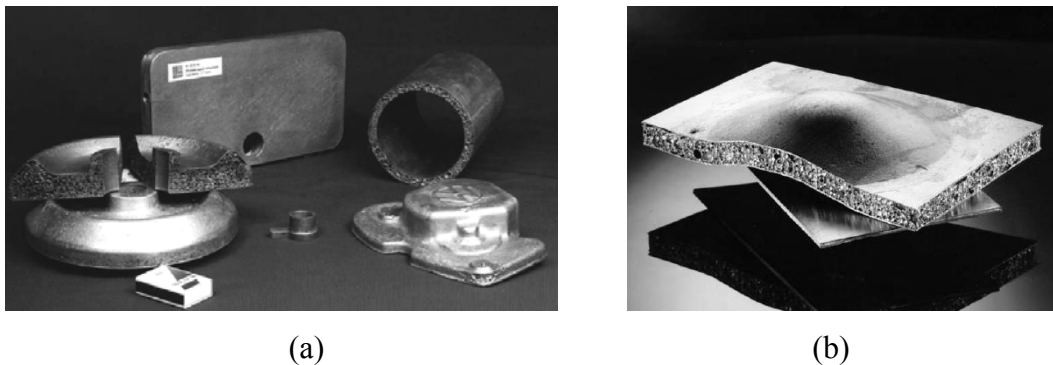


Figure 2.6 (a) complicated foam parts (b) sandwich foam panel.

(Source: Web_1 2005)

It is also possible, with this process by applying suitable heating, to produce bodies that have continuously or discontinuously changing densities over the cross section. If the foaming process is interrupted after a certain time at a constant temperature, a certain density will be obtained and if the foaming process is continued further, a higher density value will result. For example, structures having higher foam

densities on the locations exposed to higher external loads could be manufactured by this method. If the hot compaction process is performed inside a mold, the powder mixture will be surrounded completely or partially by a blowing agent free metal powder. Upon foaming, this forms a dense or less porous cover layer and a highly porous foam core. This offers advantages for the joining similar or different structures and for the production of foam core structures that require a dense cover such as car doors and frames.

Foaming from powder compacts process has been recently modified by incorporating TiH_2 particles directly into an Al melt instead of using powders to prepare a foamable precursor material. To avoid premature H_2 evolution, the melt should be quickly cooled down below its melting point after mixing or the blowing agent has to be passivated to prevent it from releasing gas before solidification. The former technique, called *Foamcast* is carried out in a die-casting machine and the TiH_2 is injected into the die simultaneously with the melt (Banhart 2000a). The resulting cast part is virtually dense and could be foamed by remelting in analogy to foaming from powder compacts; however, achieving a homogeneous distribution of TiH_2 powders in the die is difficult. The latter route requires that TiH_2 powders be subjected to a heat treatment cycle that forms an oxide layer on each particle, which delays the decomposition of TiH_2 . TiH_2 is then added to the melt and the melt can be cooled at comparatively slow rates after stirring. Melts containing SiC particles are used to obtain stable foams. The name *Formgrip* has been given to this process which is an acronym of foaming of reinforced metals by gas release in precursors (Gergely and Clyne 2000).

2.1.4. Accumulative Roll-Bonding Technique (ARB)

This process is recently proposed by Kitazono et al. (2004) and based on the dispersion of foaming agent into bulk metal sheets through sequential rolling. The stages of process are schematically illustrated in Figure 2.7 (a) (Kitazono et al. 2004). Two metal strips are stacked together with blowing agent powder (TiH_2) in between them. The stacked strips are then roll-bonded by the reduction of thickness. The bonded strips are then cut and after surface treatment, they are stacked again and roll-bonded. After several roll-bonding cycles, rolled foamable precursor composite in which the blowing agent particles dispersed in a metal matrix is obtained (Figure 2.7 (b))

(Kitazono et al. 2004). The composite is used as the starting material for the following high temperature foaming process.

The microstructure of the manufactured preform using ARB method is the same as the precursor produced by powder metallurgy process. Closed-cell aluminum foams with about 40% porosity were successfully produced through the ARB process. This process has the potential to produce a large scale sandwich structure comprising a foam core and skin plates using conventional cladding techniques

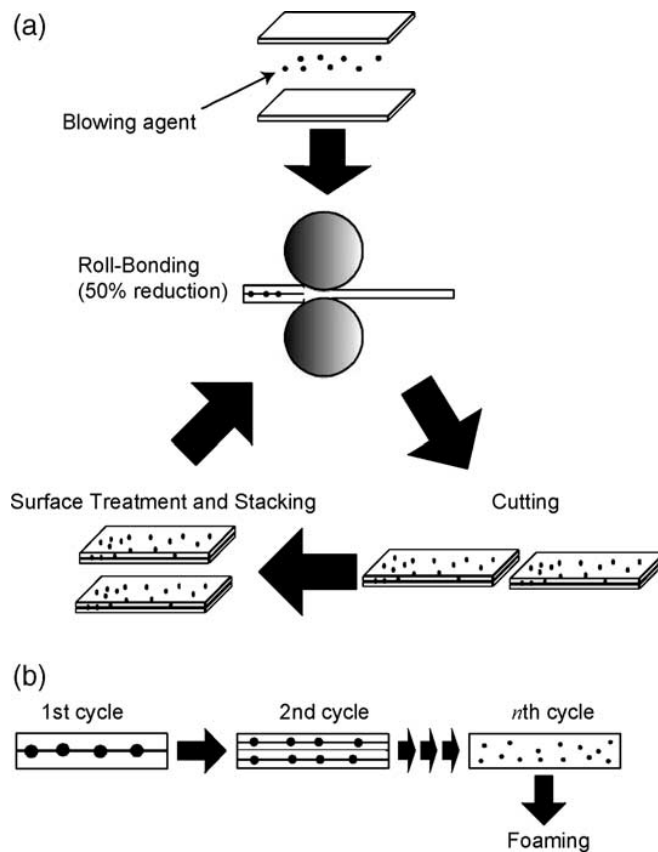


Figure 2.7. (a) schematic of the manufacturing process of a preform sheet through ARB process (b) prediction of gradual distribution of added blowing agent particles.

(Source: Kitazono et al. 2004)

2.1.5. Laser Assisted Aluminum Foaming

This process is recently proposed by Kathuria (2001). The basic principle of laser assisted foaming is shown schematically in Figure 2.8. The precursor material with

blowing agent, prepared by P/M process, is foamed by heating it up to its melting point by a high power laser beam irradiation. The uni-directional expansion of the foamable precursor material can be observed during the entire foaming process in the irradiation direction. The expansion in the other directions is relatively negligibly small.

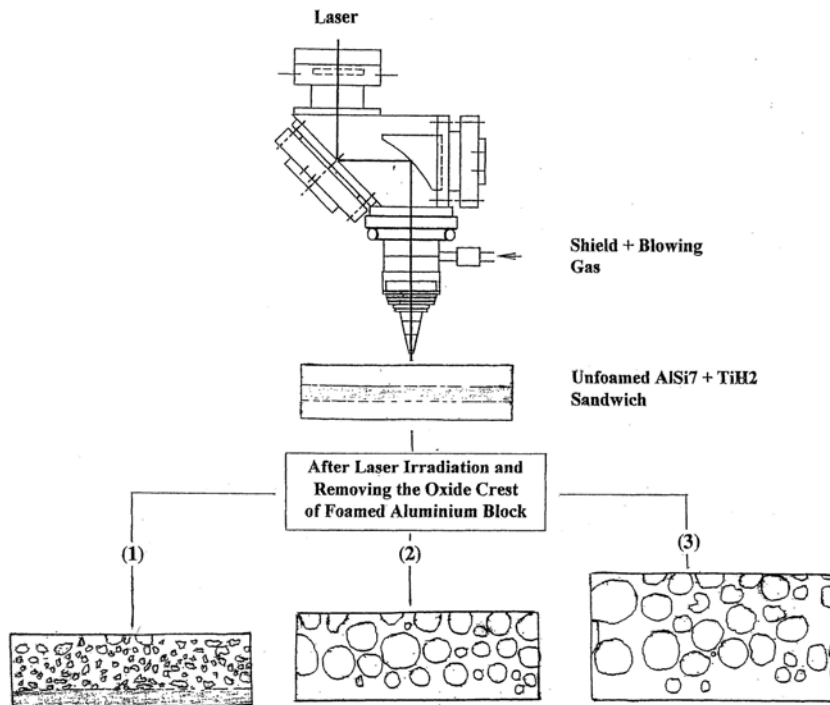


Figure 2.8. The block diagram of laser assisted AlSi7 foaming for three processing speeds, in decreasing order (1) > (2) > (3)

(Source: Kathuria 2001)

Besides H_2 evolution and foaming, the shield gas Ar is an additional help for the formation of the porosity and may also become trapped inside the solidified foam. In the conventional thermal melting process, the average temperature gradient of the interface varies as the bulk temperature is lower. This is accompanied by a slow cooling rate and hence a long time for the stabilization of the pores to occur. However, in the case of laser process the average temperature gradient of the interface is much higher; thus, a faster cooling rate results in the pore stabilization. Figure 2.8 also illustrates how the processing speed could affect the cell morphology and the expansion ratio of the buildup foam.

The foamable Al-alloy sandwich samples fabricated according to the P/M procedure are used in this technique. Porous structures with relative densities of 0.33-0.39 and porosity of (61-67%) can be fabricated by using this method.

2.2. Manufacturing Methods of Fiber Reinforced Polyester Tubes

Fiber reinforced composite tubes can be manufactured by 1) filament winding, 2) pultrusion, 3) RTM, 4) tube rolling and 5) braiding.

2.2.1. Filament Winding

The basis of this method is high-speed precise lay-down of continuous reinforcement in predescribed patterns. Fibres pass through a resin bath before being wound onto a male mandrel in a variety of orientations. The mandrel can be cylindrical, round, or any shape that does not have reentrant curvature. (Peters and Humphrey, 1998) Fiber orientation is controlled by the fibre feeding mechanism and rate of rotation of the mandrel. By winding continuous strands of carbon fiber, fiberglass or other material in very precise patterns, structures can be built with properties stronger than steel at much lighter weights. The schematic set up for this process is shown in Figure 2.9 (WEB_2 2004).

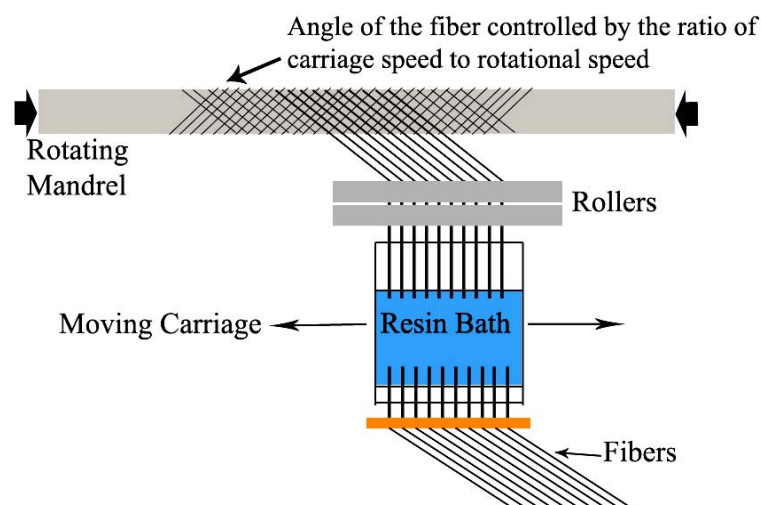


Figure 2.9. Filament winding process set up

(Source: WEB_2 2004)

Any resin can be used in this process like epoxy, polyester, vinylester and phenolic. Also any fibre can be used in the application of this process. The fibres are used straight from a creel and not woven or stitched into a fabric form.

The primary advantages of filament winding are:

- This can be a very fast and therefore economic method of laying material down.
- The capacity to use continuous fibers over whole component area (without joints) and to orient fibers easily in load direction.
- Resin content can be controlled by metering the resin onto each fibre tow through nips or dies.
- Fibre cost is minimized since there is no secondary process to convert fibre into fabric prior to use.

The primary disadvantages of filament winding are:

- The process is limited to convex shaped components.
- Fibre cannot easily be laid exactly along the length of a component.
- Mandrel costs for large components can be high.
- Inability to change fiber path easily (in one lamina)
- The external surface of the component is unmoulded, and therefore cosmetically unattractive.
- Low viscosity resins usually need to be used with their attendant lower mechanical and health and safety properties.

2.2.2. Pultrusion

Pultrusion is an automated process for manufacturing composite materials into continuous, constant cross-sectional profiles. Fibres are pulled from a creel through a resin bath and then on through a heated die. The matrix used is typically a thermosetting resin, which chemically reacts when heat is introduced to create an exothermic reaction. The die completes the impregnation of the fibre, controls the resin content and cures the material into its final shape as it passes through the die. The resulting profile is shaped

to the point at which it cannot be reshaped unlike thermoplastics. This cured profile is then automatically cut to length.

Fabrics may also be introduced into the die to provide fibre direction other than at 0° . Although pultrusion is a continuous process, producing a profile of constant cross-section, a variant known as 'pulforming' allows for some variation to be introduced into the cross-section (Martin and Sumerak 1998). The process pulls the materials through the die for impregnation, and then clamps them in a mould for curing. This makes the process non-continuous, but accommodating of small changes in cross-section. A typical set up of pultrusion process is shown in Figure 2.10 (WEB_2 2004).

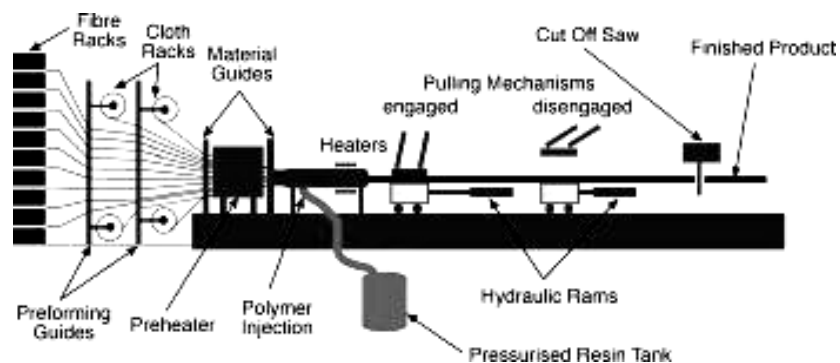


Figure 2.10 Pultrusion process set-up

Polymers for which the process is very common are epoxy, polyester, vinylester and phenolic. The main advantages and disadvantages of this technique of composite tube manufacturing are as follows:

Advantages:

- This can be a very fast, and therefore economic, way of impregnating and curing materials.
- Resin content can be accurately controlled.
- Fibre cost is minimized since the majority is taken from a creel.
- Structural properties of laminates can be very good since the profiles have very straight fibres and high fibre volume fractions can be obtained.
- Resin impregnation area can be enclosed thus limiting volatile emissions.

Disadvantages:

- Limited to constant or near constant cross-section components
- Heated die costs can be high.

2.2.3. Resin Transfer Molding (RTM)

Resin transfer molding (RTM) is one of the methods to process composite tubes. With this process, a dry fiber preform is placed within a tubular mold and resin is injected into the mold under pressure (Turner et al. 2005). The method of evacuating excess resin varies between techniques.

With traditional RTM, the mold consists of a minimum of two pieces and result in a seam along the length of the tube. However, expandable mandrel RTM has a one-piece mold that produces no seams which are both a cosmetic defect and can lead to premature structural failure in especially thin-walled structures. The substantial thermal expansion of Teflon allows the preform to fit within the outer mold. Excess resin is removed by heating the entire mold. As the mandrel expands against the tube, a consistent wall thickness is created along the entire length of the mold.

2.2.4. Tube Rolling

The common element in most tube rolling methods is that the material to be wrapped is laid out on a flat surface with no tension applied. Compaction and densification of the material during the wrapping process is accomplished by contact pressure between the mandrel and the material, as shown in Figure 2.11 (Roy 1998).

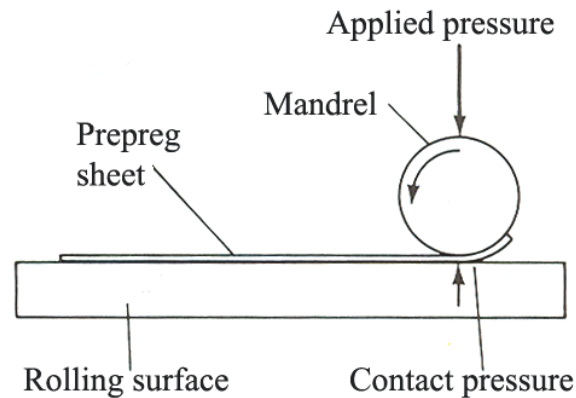


Figure 2.11 Tube rolling process

(Source: Roy 1998)

To facilitate a tight wrap, the material to be rolled should have sufficient tack to adhere to the mandrel and to itself. In some instances, it may be necessary to apply a tacking agent to the mandrel or to heat the mandrel.

Typically fabrics are used when $0^\circ/90^\circ$ fiber orientation is required. Tubes made with this fiber orientation have good longitudinal and circumferential properties, but poor torsional values. For the tubes that require a higher degree of refinement in structural properties, unidirectional tapes are used (Roy 1998). It is possible to achieve any combination of axial, hoop, and torsional mechanical properties with unidirectional tapes by using a predetermined combination of wraps.

Both forms of the material require cutting of patterns in preparation for rolling. Prepreg pattern design is determined by the product being fabricated, the material form employed, and the equipment being used for the fabrication. Generally, tubes made from prepreg fabrics are convolute wrapped, whereas tube based unidirectional prepreg tapes can be either convolute or spiral wrapped.

After cure, some amount of sanding or grinding usually required. Sanding produces a good quality surface for cosmetic purposes, whereas centerless grinding is used when precise diameter control is required. Centerless sanders are widely used for high production rate items such as golf shafts and fishing rods.

2.2.5 Braiding

Braiding is a textile process that is known for its simplicity and versatility. Braided structures are unique in their high level of conformability, torsional stability, and damage resistance (Ko 1998).

Braiding process, as shown in Figure 2.12, has many similarities to filament winding. Dry or prepreg yarns, tapes or tow can be braided over a rotating and removable form or mandrel in a controlled manner to assume various shapes, fiber orientations, and fiber volume fractions. Although braiding cannot achieve as high volume fraction as filament winding, braids can assume more complex shapes than filament wound preforms.

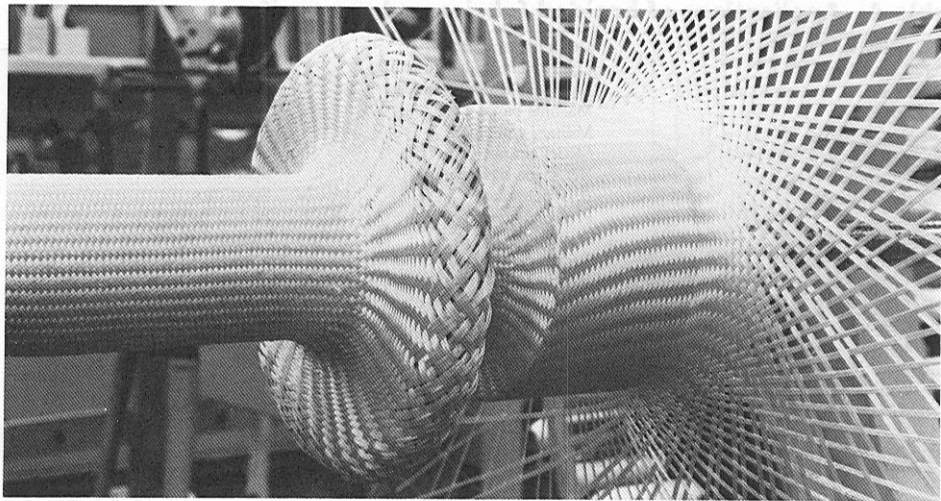


Figure 2.12. Braiding set up for formation of fiberglass preform for composite coupling shaft.

(Source: Ko 1998)

By using the three dimensional braiding process, not only can the intralaminar failure of filament wound or tape laid-up composites be prevented, but the low interlaminar properties of the laminated composites can also be prevented (Ko 1998).

CHAPTER 3

CRUSHING BEHAVIOUR OF Al-FOAMS, EMPTY TUBES AND FOAM FILLED TUBES

3.1. Crushing Behavior of Al Foams

Foams are the light-weight cellular structured materials. Synthetic foams are usually inspired from nature and they may be considered in two groups in terms of their cell structure; open and closed-cell foams. Simplest cubic models of open-cell and closed-cell foams are shown in Figures 3.1(a) and (b) (Gibson and Ashby 1997), respectively. Foams may also be classified into three groups in terms of their mechanical behavior: elastomeric, elastic-plastic and elastic-brittle.

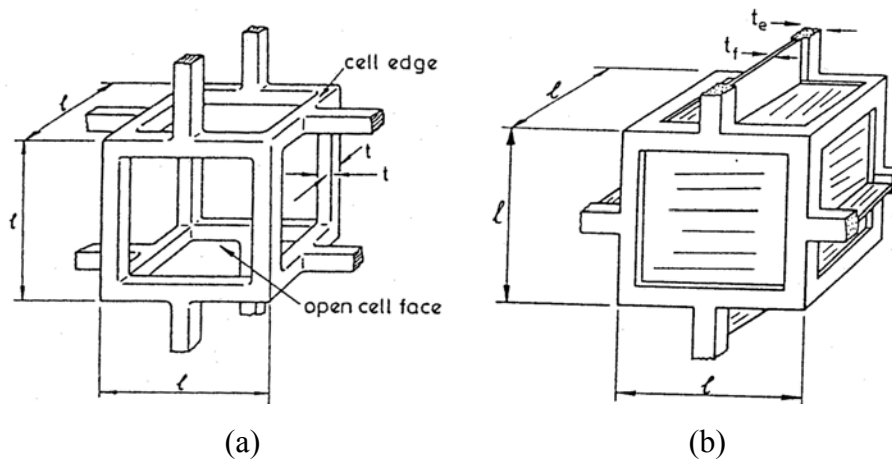


Figure 3.1. Cubic models of a) open-cell and b) closed-cell foams.

(Source: Gibson and Ashby 1997)

Under compressive loads, Al foams show characteristic stress-strain behavior. Compressive stress-strain curve consists of three consecutive regions: linear elastic region, collapse region and densification region in which the properties approach those of fully-dense alloy (Figure 3.2).

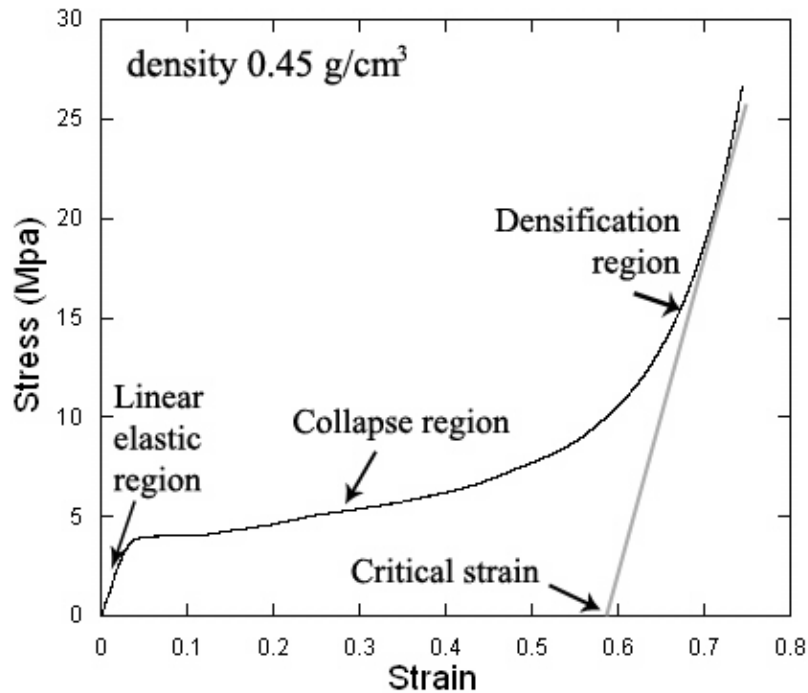


Figure 3.2. Compression stress-strain curve of Al foam with 0.45 g/cm³ density, showing distinct deformation regions.

3.1.1. Linear Elasticity

Open cell foam of low relative densities (the ratio between foam density and solid foam material density (ρ^*/ρ_s)), deforms primarily by cell wall bending (Maiti et al. 1984). With increasing relative density ($\rho^*/\rho_s > 0.1$), cell edge compression plays a significant role. Fluid flow through open-cell foam contributes to the elastic module if the fluid has a high viscosity or the strain rate is exceptionally high. Besides cell edge deformation, the thin membranes of the closed cell foams, which form the cell faces, stretch normal to the compression axis and therefore contribute to the modulus. If the membranes do not rupture, the compression of the cell fluid trapped within the cells also increases the modulus. Each of these mechanisms contributing to the linear-elastic response of the foams is shown schematically in Figures 3.3(a) and (b) for open and closed-cell foams, respectively (Gibson and Ashby 1997).

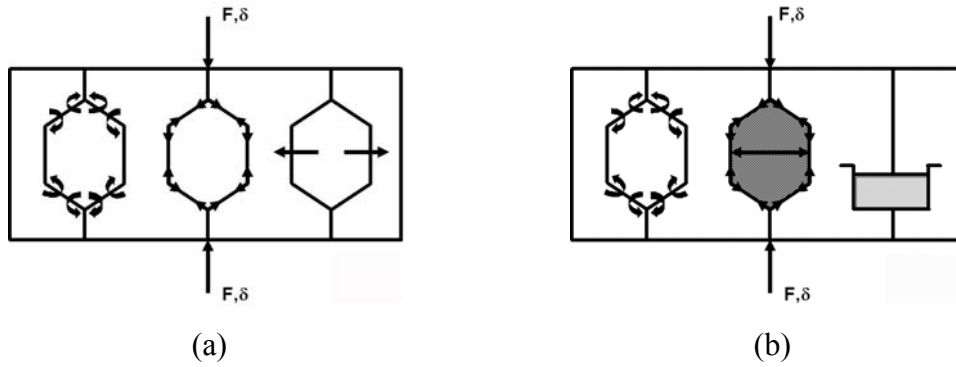


Figure 3.3. The mechanisms of foam deformation: a) open-cell foam, sequentially cell wall bending, cell wall axial deformation and fluid flow between cells and b) closed-cell foams, sequentially cell wall bending and contraction, membrane stretching and enclosed gas pressure.

(Source: Gibson and Ashby 1997)

The simplest model of foam structure is the cubic model, which encompasses cubic array of members of length l and square cross-section of side t (Figure 3.1). The structure and shape of the cells in the actual foam structure are more complex than those of the cubic model. The deformation and failure mechanisms of the cubic model are however quite similar to those of real foams and therefore it is very useful in predicting mechanical properties.

The elastic modulus of the open cell foams (E^*), which is calculated from the linear-elastic deflection of a beam of length l loaded at its mid point by a load F , is given as (Gibson and Ashby 1997);

$$\frac{E^*}{E_s} = C_1 \left(\frac{\rho^*}{\rho_s} \right) \quad (3.1)$$

where s refers to the solid material from which the foam is made and C_1 is a constant. The experimental elastic modulus of open-cell foams showed that C_1 is nearly equal to unity. The experimental results have further showed that the Poisson ratio (ν^*) was around 0.3 (Gibson and Ashby 1997).

In closed-cell foams, a fraction of the solid, represented by ϕ , is contained in the cell edges having a thickness of t_e and the remaining fraction, $(1-\phi)$, is in the cell faces

of a thickness of t_f . By including enclosed gas pressure, the Elastic modulus of closed-cell foams of the cubic model is expressed as (Gibson and Ashby 1997),

$$\frac{E^*}{E_s} = C_1 \phi^2 \left(\frac{\rho^*}{\rho_s} \right) + C_1' (1 - \phi) \frac{\rho^*}{\rho_s} + \frac{P_0 (1 - 2\nu^*)}{E_s \left(1 - \frac{\rho^*}{\rho_s} \right)} \quad (3.2)$$

where P_0 is the initial pressure of the cell fluid and C_1 and C_1' are the constants. The first, second and third terms of Equation 3.2 refer to cell wall bending, membrane stretching and enclosed gas pressure, respectively.

3.1.2. Elastic and Plastic Collapse

Linear elasticity is generally limited to 5% or less strain values. Foams made from material that have a yield point such as rigid polymers and ductile metals collapse plastically when loaded beyond the linear-elastic region. Plastic collapse gives a horizontal plateau in the stress-strain curve with unrecoverable strain. Both elastic buckling and plastic failure are localized; a deformation band is usually formed transverse to the loading axis and propagates through undeformed sections of the foam with increasing strain until all the foam section is filled with the band (Gibson and Ashby 1997). Following the elastic region the deformation was localized in the regions marked with black arrows shown in Figure 3.4 (Yuksel and Guden 2005).

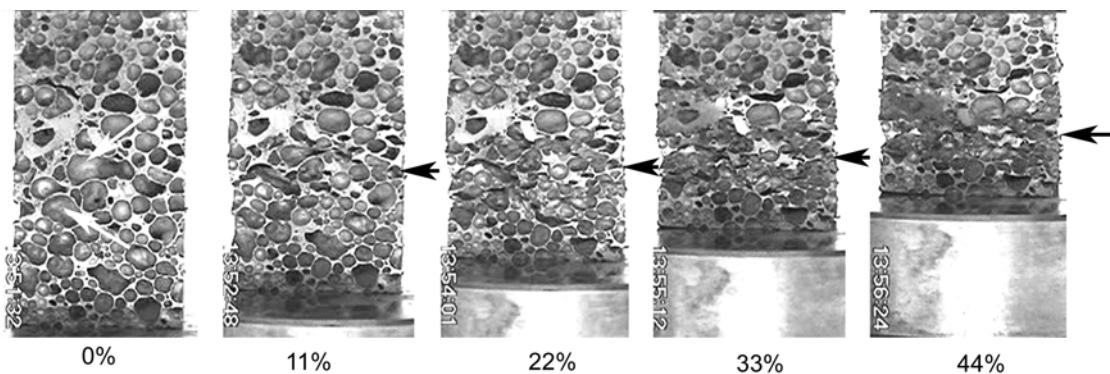


Figure 3.4. The deforming Al foam sample at various percent strains.

(Source: Yuksel and Guden 2005)

It is also seen that the deformation localization starts from the locations of the largest cell size or the lowest density (weakest link), marked with white arrows at 0% strain in Figure 3.4. Microscopic analyses of the localized regions have shown that the main deformation mechanism in Al foams was the cell wall bending, i.e. cell edges buckled over cell walls (Figure 3.5) (Yuksel and Guden 2005).

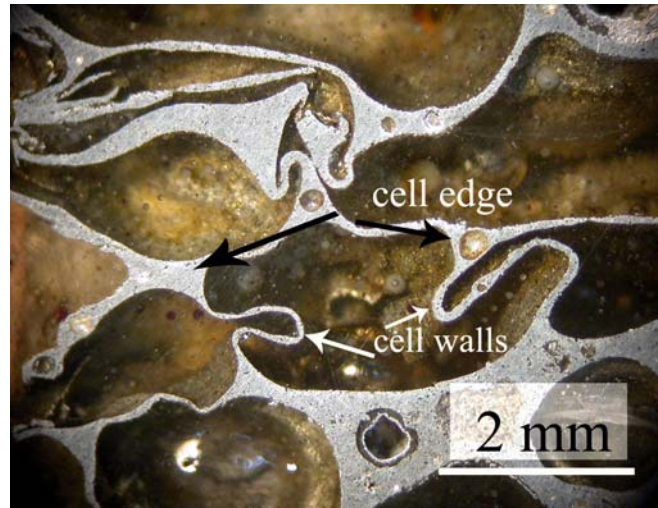


Figure 3.5. Deformation mechanism of Al foam under compressive load
(Source: Yuksel and Guden 2005)

The plastic collapse stress is predicted as (Gibson and Ashby 1997),

$$\frac{\sigma_{pl}^*}{\sigma_{ys}} = 0.3 \left(\frac{\rho^*}{\rho_s} \right)^{3/2} \quad (3.3)$$

for open-cell foams and ,

$$\frac{\sigma_{pl}^*}{\sigma_{ys}} = 0.3 \left(\phi \frac{\rho^*}{\rho_s} \right)^{3/2} + (1 - \phi) \frac{\rho^*}{\rho_s} + \frac{P_0 - P_{at}}{\sigma_{ys}} \quad (3.4)$$

for closed-cell foams. σ_{ys} is the yield stress of solid material.

3.1.3. Densification

Following the collapse region, at a critical strain, the cell walls start to touch each other and, as a result the foam densifies. The stress in this region increases rapidly

and approaches to the strength of the solid foam material. The densification strain (ε_D) is related to relative density with following equation (Gibson and Ashby 1997);

$$\varepsilon_D = 1 - 1.4 \left(\frac{\rho^*}{\rho_s} \right) \quad (3.5)$$

3.1.4. Anisotropy

The anisotropy in cell shape measured by the ratio of the largest cell dimension to the smallest is called the shape-anisotropy ratio (R). The value of R varies from 1 for isotropic foam to 10 for very anisotropic foams (Gibson and Ashby 1997). The relation between the plateau stress and R is calculated using cubic cell model as,

$$\frac{(\sigma_{pl})_3}{(\sigma_{pl})_1} = \frac{2R}{1 + \frac{1}{R}} \quad (3.6)$$

where 3 and 1 refer to the strongest and weakest directions, respectively.

3.2. Terminologies Used in Crush Analysis

In any crushing event of columnar structure, the total absorbed energy (E) is the area under the load-displacement curve (Figure 3.6) and is,

$$E(\delta) = \int_0^{\delta} P \, d\delta \quad (3.7)$$

where δ and P are the displacement and the load, respectively. The corresponding average crushing load (P_a) is calculated dividing the absorbed energy by the displacement,

$$P_a(\delta) = \frac{E(\delta)}{\delta} \quad (3.8)$$

The specific absorbed energy (SAE) shows the capability of a structure to absorb the deformation energy. SAE can be formulated in several bases including per unit mass and volume. SAE per unit mass is expressed as,

$$SAE = \frac{\int_0^{\delta} P \, d\delta}{m_t} \quad (3.9)$$

where m_t is the total mass of the deformation element.

The ratio between the average load P_a and maximum load P_{max} , both calculated in the interval of $\{0, \delta\}$, is defined as the crush force efficiency (A_E):

$$A_E = \frac{P_a(\delta)}{P_{max}(\delta)} = \frac{E(\delta)}{P_{max}(\delta)\delta} \quad (3.10)$$

Total efficiency (T_E) is the total absorbed energy divided by the products of $P_{max}(\delta)$ and total length of deformation element (l):

$$T_E = \frac{E(\delta)}{P_{max}(\delta)l} \quad (3.11)$$

The stroke efficiency is defined as the ratio between the point at which the total efficiency has its maximum value (δ_{max}) and total length of the crushing element,

$$S_E = \frac{\delta_{max}}{l} \quad (3.12)$$

The efficiency terms are directly related to the deformation capacity (D_c), which is the displacement divided by the initial length of the element:

$$D_c = \frac{\delta}{l} \quad (3.13)$$

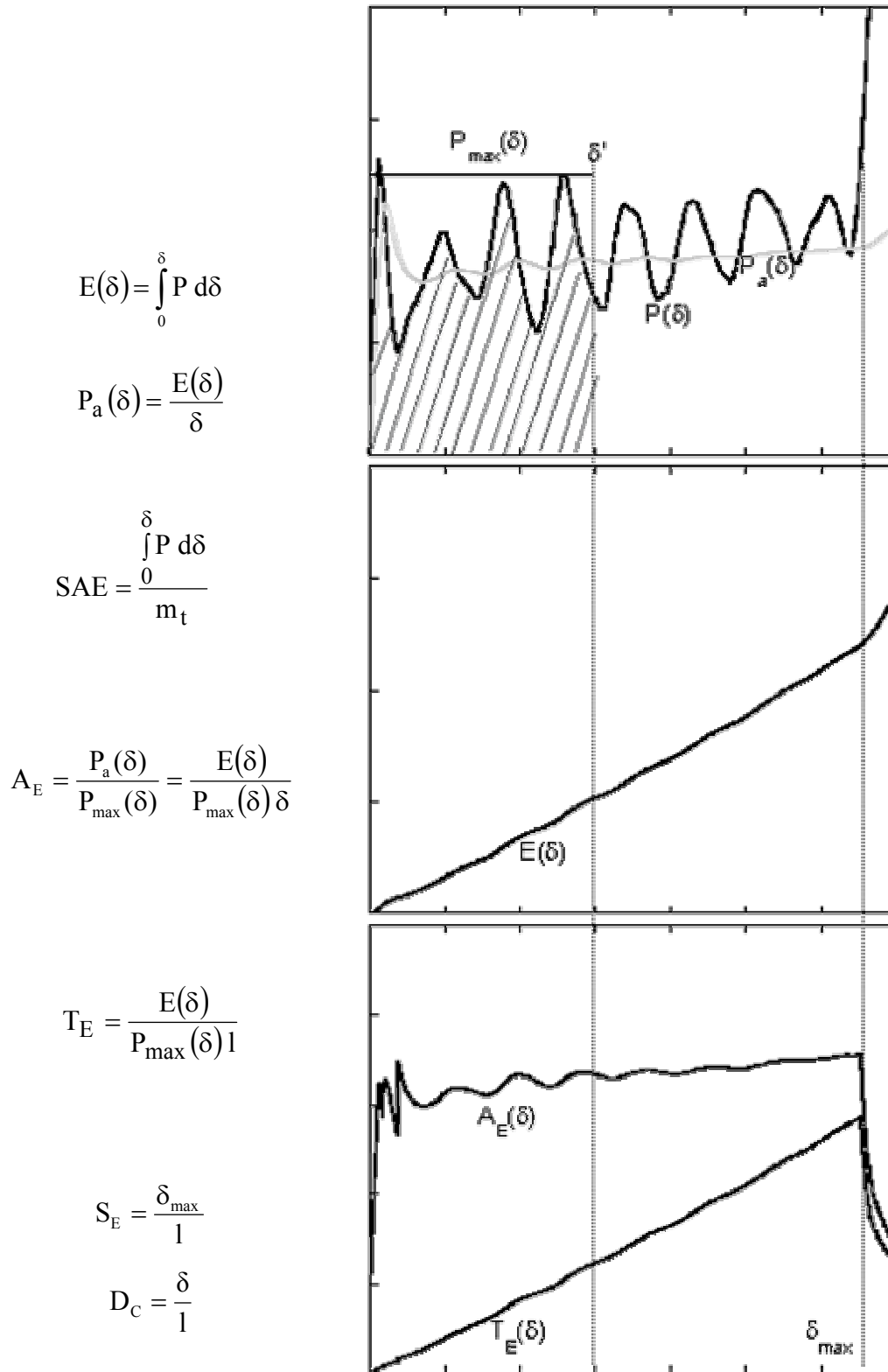


Figure 3.6. Terminologies used in the crush analysis of tubes.

3.3. Crushing Behavior of Composite Tubes

Composite tubes that can be manufactured with many different manufacturing techniques have many diverse applications. The size and the material used differ according to the application area of the composite tubes. Composite tubes can be manufactured from nano-scale to dimensions like a few meters in diameter according to the design and the application.

The energy absorption characteristics of composite materials depend on many parameters as listed in Figure 3.6. Hamada and Ramakrishna (1998) extensively studied the effects of material property variables, geometric variables, and testing variables on the energy absorption capabilities of the composite materials.

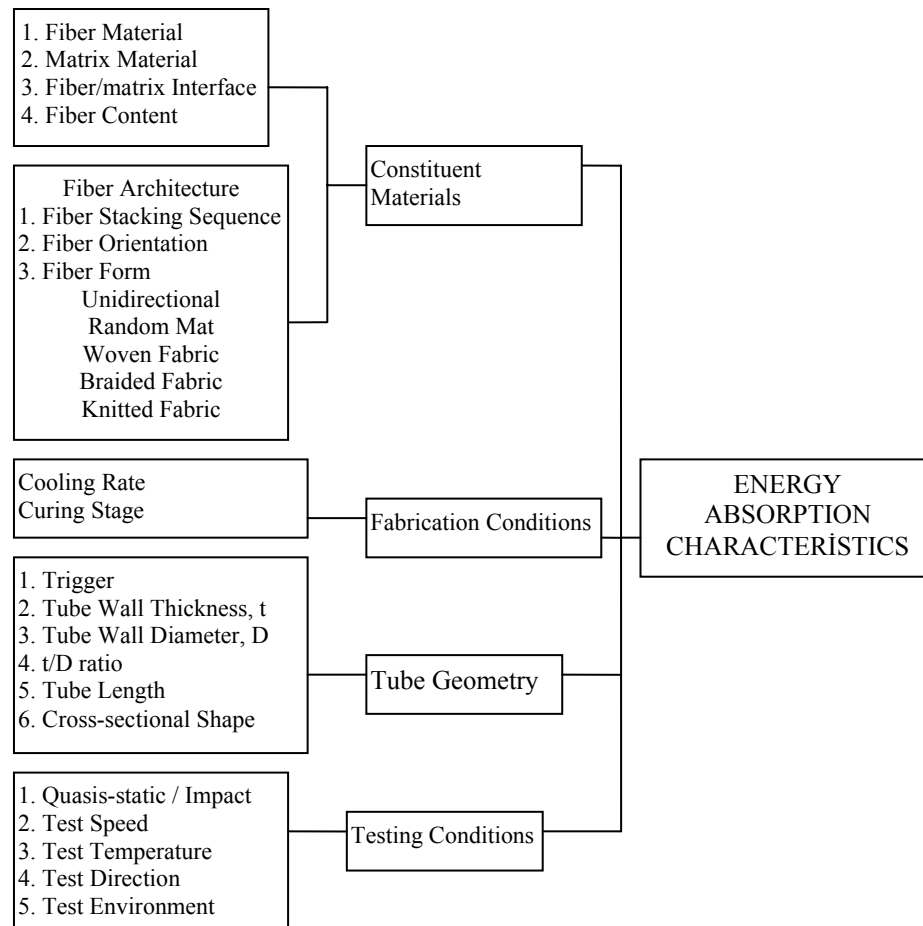


Figure 3.7. Various variables that influence the energy absorption characteristics of composite materials.

(Source: Hamada and Ramakrishna 1998)

Circular cylindrical composite structures deform in compression by at least five possible deformation mechanisms. These are:

1. Fiber micro buckling
2. Euler buckling
3. Tube inversion
4. Progressive crushing
5. Axisymmetric and diamond shape buckling

The schematic representation of these tube deformation mechanism types are shown in Figures 3.8(a-f) (Harte and Fleck 2000, Harte et al. 2000).

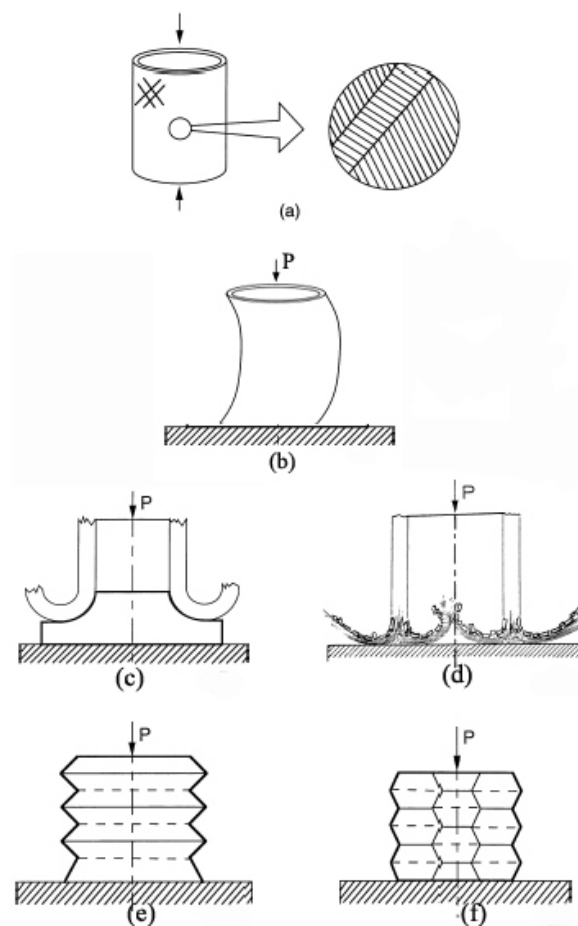


Figure 3.8. Deformation types of tubular composite structures under compression. (a) Fiber micro buckling, (b) Euler buckling, (c) tube inversion, (d) progressive brittle crushing, (e) axisymmetric buckling and (f) diamond shape buckling.

(Source: Harte and Fleck 2000, Harte et al. 2000)

3.3.1. Fiber Micro Buckling

Micro buckling of fibers is a localized failure mode that involves the rotation of fibers within a bandwidth about in tenths of fiber diameters. It is common failure mode for the composite structures and also observed in composite tubes such as shown in Figures 3.9(a) and (b) braided glass fiber reinforced composite tubes (Harte and Fleck 2000). It was observed that when the braid angle (θ) less than 35° fiber microbuckling was dominant crushing mode for braided composite tubes. This mode results in catastrophic failure of the tube and load values abruptly decrease after the initial peak load as seen in Figure 3.9(a). The failure by microbuckling may induce sawtooth like fracture in the tubes (Figure 3.9(b)). The available theoretical results for the micro buckling type of failure of laminated composites were also reviewed and those models were compared with the measured strength of composites in the same study. It was found that most of the calculated values were in good agreement with the measured values. The stress level for the activation of fiber micro buckling mode of failure depends upon the in-plane shear strength of the composite along the local fiber direction, and the magnitude of any imperfection such as fiber waviness.

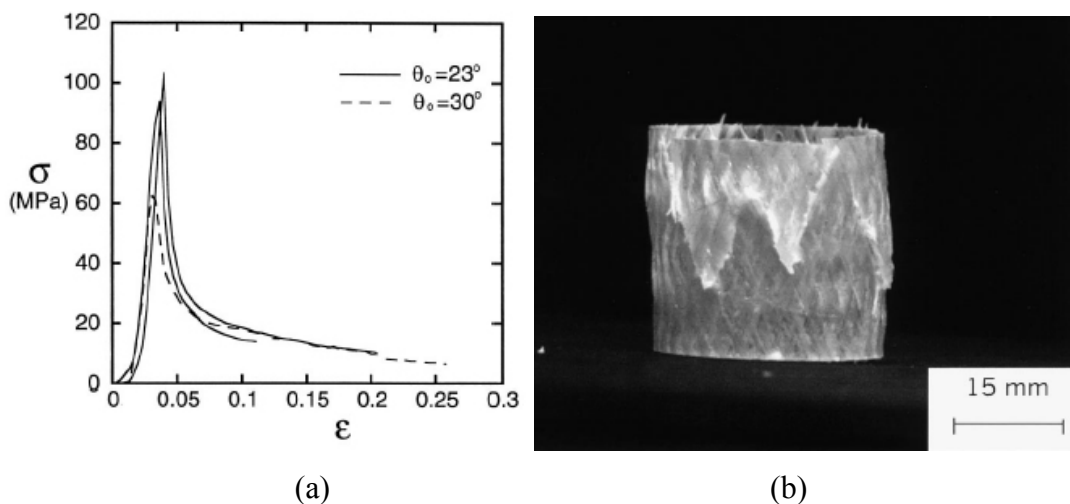


Figure 3.9. (a) Nominal stress-nominal strain behavior for braids of initial helix angle $\theta=23^\circ$ and 30° failing by micro buckling in compression. (b) The sawtooth fracture path of a compressive specimen which has failed by micro buckling.

(Source: Harte and Fleck 2000)

3.3.2. Euler Buckling

Euler buckling is the bending of tube as a strut (Figure 3.8 (b)). Long and thin tubes are likely to fail by Euler buckling before the onset of any other failure mechanism. The buckling will occur at a local non-uniformity in material or geometry. This type of deformation results in very low levels of energy absorption, as failure is restricted to a very localized area of the tube material. This can be easily avoided by a suitable choice of tube length, diameter and tube wall thickness.

3.3.3. Tube Inversion

Tube inversion mechanism is the bending and stretching of a tube to a larger or smaller diameter (Figure 3.8 (c)). To trigger and maintain this type of deformation, an end fixture is needed and as a result of this the weight of the energy absorbing system increases. The steady state inversion of metallic tubes has been analyzed by Al-Hassani et al. (1972).

3.3.4. Progressive Crushing

Progressive crushing is a commonly observed crushing mode for the glass fiber reinforced composite tubes under compression. This mode of failure results in very high levels of energy absorption associated with the large number of micro fractures that occur as the tube crushes. The energy dissipation is due to the generation of fracture surface area, friction between fragments, and from plastic shear of the matrix.

Chiu et al. (1998) investigated progressive crushing in biaxially and triaxially braided composite tubes. Tubes were found to fail by progressive splaying mode of crushing. It was shown in the same study, the average width of the splaying fronds increased with increasing braid angle but decreased with increasing axial yarn content.

Progressive crushing mode of tube deformation may proceed both in fragmentation and splaying modes as shown in Figures 3.10(a) and (b) respectively (Hamada and Ramakrishna 1998). Movement of crushed composite, splaying, can be in outer (external) and/or inner (internal) direction. The effect of the splaying direction (inner or outer) on the static and dynamic tube structures on the load values of a

composite was investigated by Saito et al. (2000). It was shown in Figures 3.11(a) and (b) (Saito et al. 2000) internal spraying absorb more energy than external spraying in static tests. An example for inner/outer splaying mode is also shown in Figures 3.12 (a) and (b) (Turner et al, 2005).

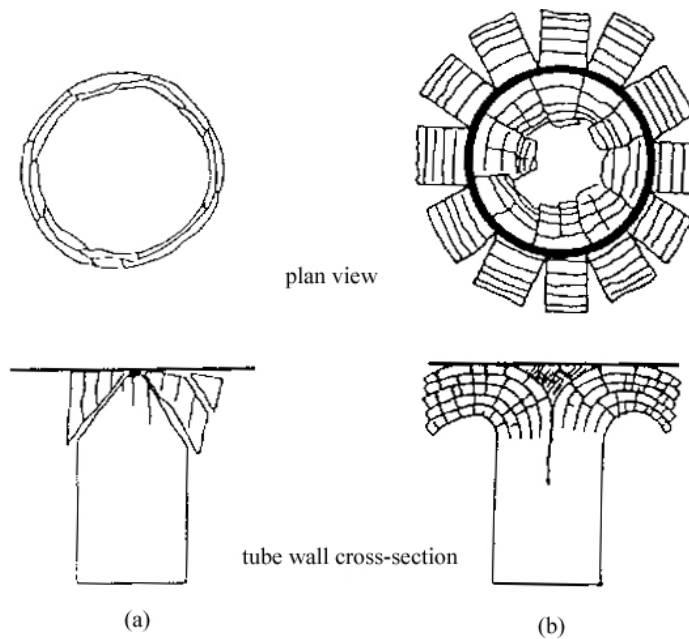


Figure 3.10. Progressively crushing of composite tubes by (a) fragmentation and (b) splaying modes.

(Source: Hamada and Ramakrishna 1998)

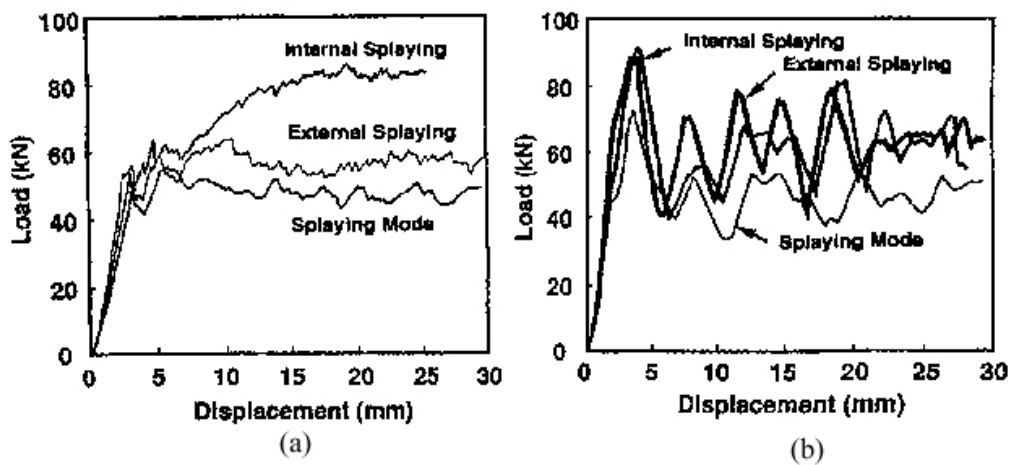
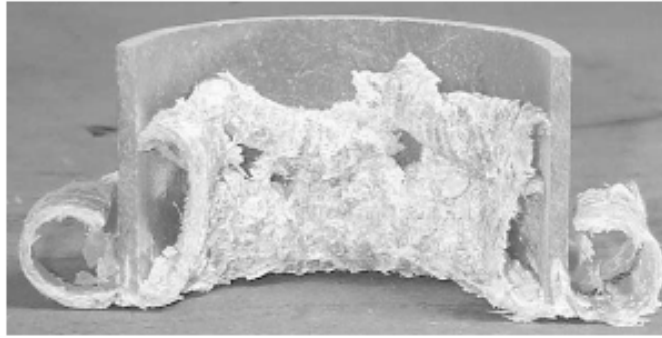


Figure 3.11. Load displacement curves of (a) static and (b) impact tests of composite tubes

(Source: Saito et al. 2000)



(a)



(b)

Figure 3.12. (a) Sectioned crush tube sample showing frond formation and center wall crack, (b) Sectioned non-crimp fabric tube showing frond formation with high degree of post-crush integrity

(Source: Turner et al, 2005)

3.3.5. Axisymmetric and Diamond Shaped Buckling

Axisymmetric and diamond shaped buckling are the two competing progressive shell-buckling modes (Figure 3.8 (e) and (f)). The tube diameter to tube wall thickness ratio (D/t) ratio is the dominant factor whether axisymmetric or diamond shape buckling will occur. Thick isotropic tubes fail by axisymmetric buckling, whereas thin walled tubes fail by diamond buckling (Mikkelsen 1999, Tvergaard 1983). It was observed that specimens having geometries close to the transition can switch from one mode to another during a single test (Andrews et al. 1983). Diamond shaped buckling although mostly observed in metal tubes may also occur in braided composites tubes as depicted in Figure 3.13 (Harte and Fleck 2000).

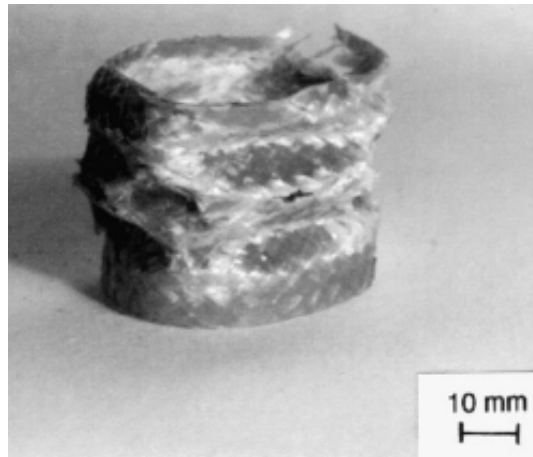


Figure 3.13. Image of a $\theta = 40^\circ$ braid tube failed by diamond shape buckling
(Source: Harte and Fleck 2000)

3.3.6. Crushing Behavior of Filament Wound Tubes

Song and Du (2002) studied the axial and off-axis compression behavior of filament wound tubes in different fiber angles and thickness. Depending on the ply angle various kinds of deformation modes were observed (see Figures 3.14 (a-c)) (Song and Du 2002). It was shown that the energy absorption of the tube decreased with the increasing off-axis loading angle. Axial and lateral compression behavior of filament wound tubes were also studied by Toğulga (2003).

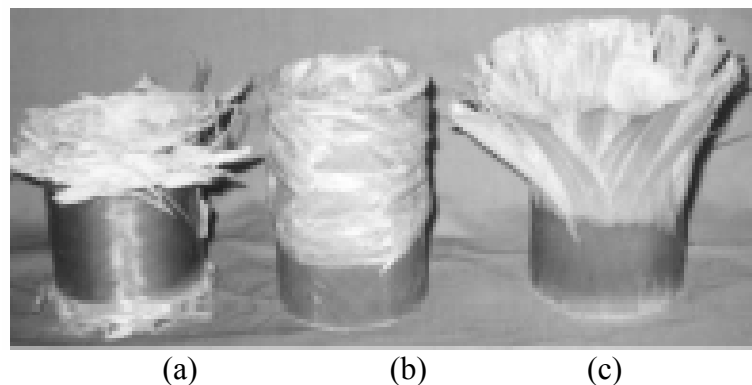


Figure 3.14. Transition of collapse mode with respect to ply angle: (a) $\theta = 75^\circ$, in transverse shearing, (b) $\theta = 45^\circ$ in local buckling, (c) $\theta = 15^\circ$ in lamina bending.
(Source: Song and Du 2002)

3.4. Crushing Behavior of Al Tubes

The first systematic investigation on the classification of crushing types was due to Andrews et al. in 1983. They performed crushing tests on tubes of various t/D and L/D ratios and classified the crushing modes of cylindrical tubes in 7 groups. These are:

1. *Concertina*: axisymmetric and sequential or progressive folding starting at the end of the tube.
2. *Diamond*: asymmetric but sequential folding accompanying a change in the cross-section shape of the tube.
3. *Euler*: bending of tube as a strut.
4. *Concertina and 2 lobe and/or 3-lobe diamond (Mixed)*: Folding first in the concertina mode changing to diamond configuration
5. *Axisymmetric/concertina*: simultaneous collapse along the length of the tube.
6. *2-lobe diamond*: Simultaneous collapse along the tube in the form of the 2-lobe diamond configuration.
7. *Tilting of tube axis*: Shearing of tube on the platen surface in the form of the 2-lobe diamond configuration.

Alexander (1960) studied analytically the crushing behavior of circular tubes. He modeled the concertina mode of deformation basing on the plastic work required for bending and stretching of extensible thin cylinder (Figure 3.15) (Alexander 1960). Alexander's model gives the average crushing load as;

$$P_a \cong 6\sigma_0 t(Dt)^{1/2} \quad (3.14)$$

σ_0 is the mean plastic flow stress;

$$\sigma_0 = \left(\frac{\sigma_{0.2} + \sigma_U}{2} \right) \quad (3.15)$$

where $\sigma_{0.2}$ is proof stress and σ_U is the ultimate tensile stress of tube material.

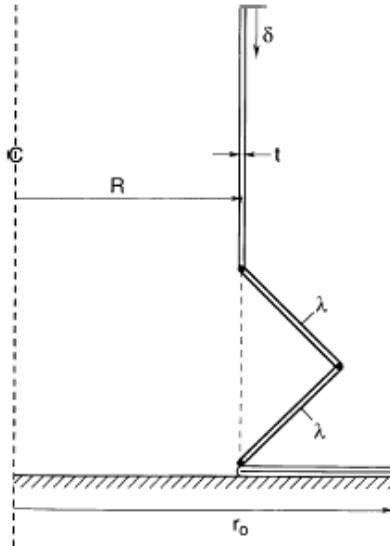


Figure 3.15. Alexander's concertina mode of deformation model.

(Source: Alexander 1960)

Andrews et al. (1983) observed for thin-walled tubes with t/D ratio smaller than 0.013, the deformation mode was diamond and the number of folds increased with decreasing t/D ratio. In this study it was also shown that although the average crushing load and absorbed energy were higher in the concertina mode, the absorbed energy in the development of one complete fold was higher in diamond mode.

Alexander's model was modified by Abramowicz and Jones and they proposed the average crushing load equations in 1984 and 1985 for the concertina mode of deformation (Abramowicz and Jones 1984, Abramowicz and Jones 1986, Jones and Abramowicz 1985) as,

$$P_a \cong \sigma_0 t \left(6(Dt)^{1/2} + 3.44t \right) \quad (3.16)$$

and

$$P_a \cong \sigma_0 t \frac{6\sqrt{Dt} + 3.44t}{0.86 - 0.57\sqrt{t/D}} \quad (3.17)$$

The crushing behavior of polyurethane foam-filled thin-walled metal tubes was investigated at quasi-static and dynamic deformation rates and it was concluded that tube wall interacts with the foam filler deformation and that result in a more tendency for the axisymmetric mode of deformation (Reid et al.1986). It was recently pointed out that the average crushing loads of polyurethane foam-filled Al thin-walled tubes were greater than the sum of the average crushing loads of empty tube (alone) and foam (alone) (Guillow et al. 2001).

Santosa and Wierzbicki (1998) investigated the crushing behavior of Al honeycomb and Al foam-filled metallic box columns both numerically and experimentally and showed that the effect of filler on the tube crushing load was similar when the strong axis of the honeycomb through and normal to the compression axis, proving that both axial and lateral strength of the filler were effective in increasing the crushing load of the tube. Santosa et al (2000) noted that the bonding between filler and tube wall increased the average crushing load of filled tube over the unbounded filled tube when appropriate tube geometry and foam density were chosen. Recently, Al foam filled Al, brass and titanium tubes have been investigated under compression laterally and axially and the increase in specific energy was found to be greater in the lateral direction than in the axial direction (Hall et al. 2002). Kavi (2004) studied the compression mechanical behavior Al foam filled Al tubes and found that the crushing loads of foam filled tubes were higher than the sum of crushing loads of empty tube and foam alone, an effect know as interaction effect (Figure 3.17).

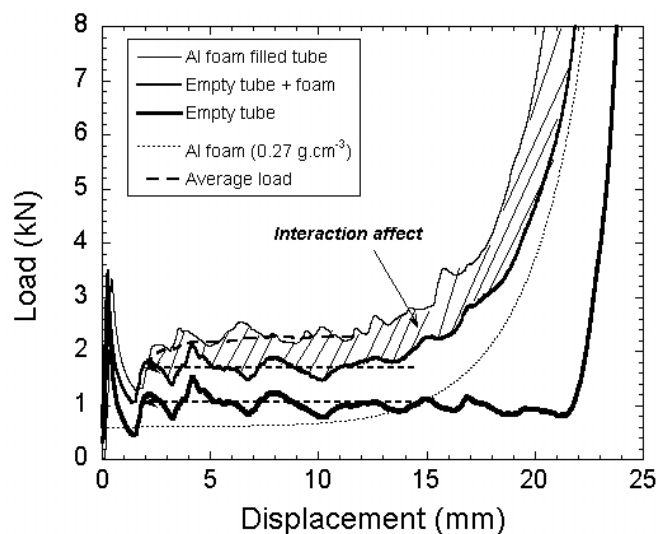


Figure 3.17. Compression behavior of Al foam filled Al tube
(Source: Kavi 2004).

Harte et al. 2000 investigated the compression and tensional behavior of braided glass fiber / epoxy circular tubes with polymer foam fillers. The energy absorption values of tubes were found to increase with foam filling. As shown in Figure 3.18, the foam filling of braided tubes was observed switching into axisymmetric mode in the same study.

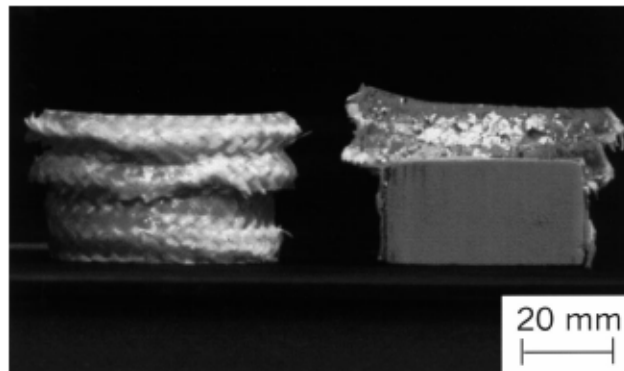


Figure 3.18. Cross-sectioned braided tube with polyurethane core after uniaxial compression, $\theta=40^\circ$

(Source: Harte et al. 2000).

Epoxy foam filling of round Al-composite hybrid tubes improved the axial crush performance of the empty hybrid tubes (Babbage and Mallick 2005). The foam filling of square hybrid tubes in the same study resulted in tube failure either by buckling or by tearing of the tubes at the corners due to the prevention of inner folds by the foam core as seen in Figure 3.19.

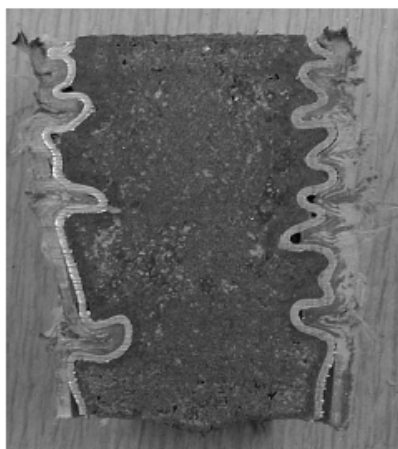


Figure 3.19. Cut-away section of an epoxy foam-filled hybrid tube after the axial test

(Source: Babbage and Mallick 2005).

CHAPTER 4

MATERIALS AND PROCESSING

4.1. Al Closed Cell Foams

4.1.1. Closed Cell Al Foam Preparation

Aluminum closed cell foam investigated in this study was manufactured at İzmir Institute of Technology using a patented powder metallurgical technique known as foaming from powder compacts (Baumeister and Schrader 1992). The method simply consists of mixing aluminum or aluminum alloy powders with an appropriate blowing agent and compacting the mixture to a dense product called foamable precursor. Heating the precursor to its melting point turns the metal compact into a semi-liquid viscous mass and simultaneously causes the blowing agent to decompose. The release of gas from the decomposing of the blowing agent first leads to the formation of pores and then causes the metal to expand into a low-density foam structure. Final step is solidifying this foam structure.

A production line has been constructed for the preparation of aluminum closed foams in the laboratory (Figure 4.1). Production line includes a hydraulic press for compaction of powder (100 tons capacity), a box-furnace for foaming of powder compacts and a specially designed carrier for handling and moving the hot foaming molds (Figure 4.2). For a successful foam manufacture, the purity, particle size and distribution and alloying elements of the raw powder materials should be optimized essentially. Commercial air-atomized aluminum powders (Aldrich) were proved to be of sufficient quality for the melt foaming. The specifications of materials, Al powder and TiH_2 , used to prepare foams are tabulated in Table 4.1. The content of blowing agent in all precursor materials was chosen to be 1 wt%. This amount was found to be sufficient to form foaming in Al compacts.

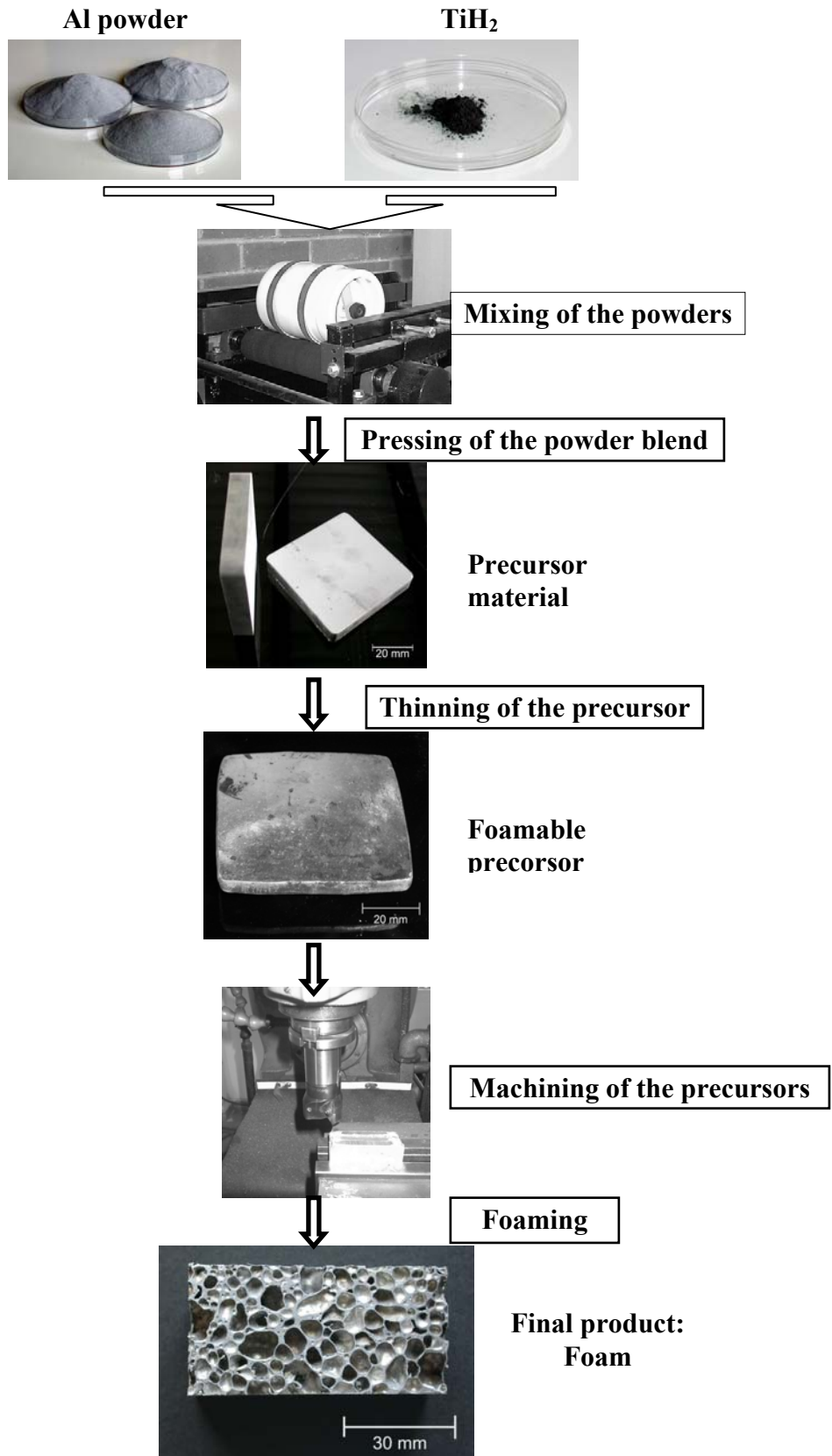


Figure 4.1. Schematic of foam preparation process.

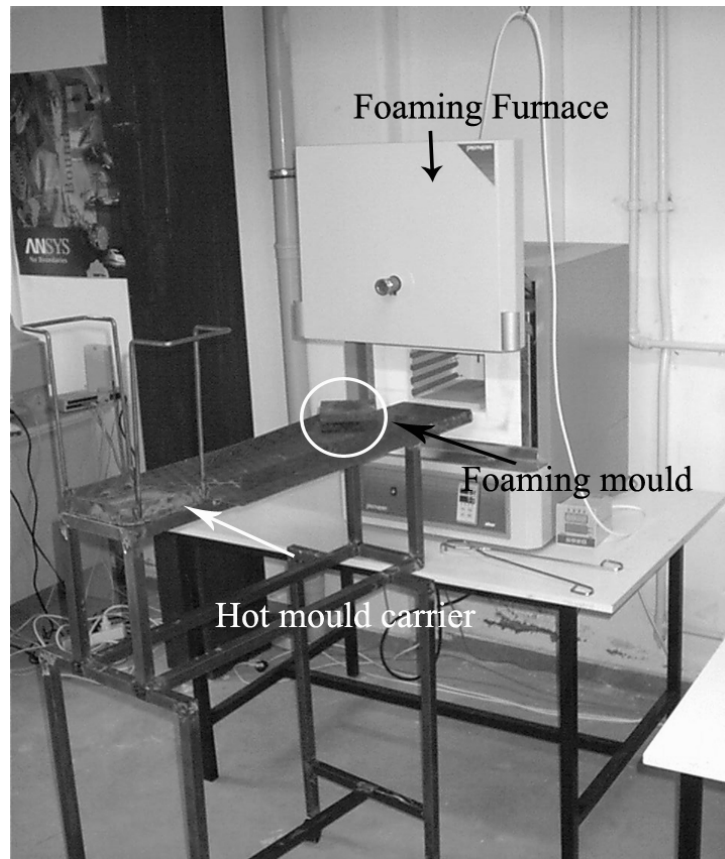


Figure 4.2. Foaming furnace, hot mould carrier and foaming mould.

Table 4.1 Specifications of powders used in foam manufacturing.

Material	Density	Molar mass	Size	Purity
Al powder (Aldrich)	2.702 g/cm ³	26.98 g/mol	< 74 μ	99 %
TiH ₂ (Merck)	3.76 g/cm ³	49.92 g/mol	< 37 μ	>98 %

Homogeneous distribution of Al powder and the blowing agent in the powder mixture is very important for high-quality foams with uniform pore size distributions. Powders were mixed in batches of 129 g blends in a commercial tumbling mixer shown in Figure 4.1. The ingredients were mixed inside a plastic container which was rotated on a rotary mill around 4 hours to form a homogeneous powder mixture. Preliminary investigations were conducted for determining the effect of compaction pressure on the final relative densities of powder compacts for an ultimate goal of producing precursor material in which the blowing agent (TiH₂) was fully embedded into metal matrix. For this purpose the mixture (Al and TiH₂) was cold compacted in the hydraulic press under various compaction pressures in a rectangular ST 37 steel die (Figure 4.3), having a cross-section of 7x7 cm for the powder. Initially dense precursor materials were

prepared at various compaction pressures at room temperature ranging between 100 and 400 MPa. The details of the precursor preparation at different compaction pressures are tabulated in Table 4.2.

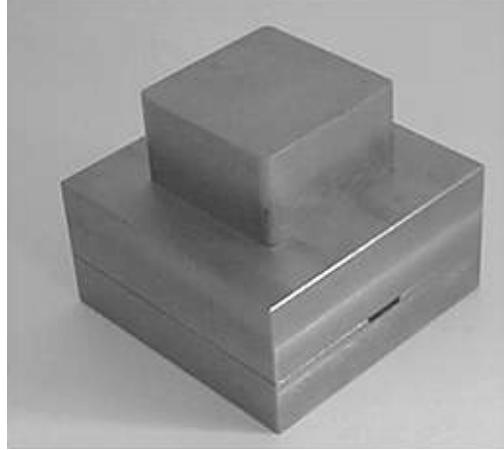


Figure 4.3. Cold compaction die

Table 4.2 Specifications of the initially prepared cold compacted precursors.

Precursor Number	Dimensions (mm)	Mass (g)	Applied Pressure (MPa)	Relative Density (%)
1	11.8 x 70.08 x 70.08	129.532	100.1	82.24
2	11.09 x 70.10 x 70.16	129.944	150.1	88.13
3	10.56 x 70.14 x 70.10	129.278	200.2	92.10
4	10.21 x 70.14 x 70.18	129	300.2	94.94
5	10.15 x 70.13 x 70.16	128.746	300.2	95.30
6	9.58 x 70.07 x 70.08	123.817	400	97.30

The maximum relative density obtained in these compacts was 97% at the highest pressure applied (400 MPa). Initial foaming experiments conducted on the precursors listed in Table 4.2 resulted in poor foaming. Due to the relatively low densities of compacts, the released H₂ from the decomposition of the blowing agent escaped before the melting of precursor. In order to increase the final relative densities further, the partially compressed precursor materials were hot forged at 350 °C. The compacts for hot forging were prepared in the hydraulic press under a pressure of 200 MPa, with a relative density of 92% (Figure 4.4(a)) and a thickness of 10 mm. The thickness of the compact was reduced to 7 mm by hot forging (Figure 4.4(b)) and the relative density of the precursor materials further increased to ~99%.

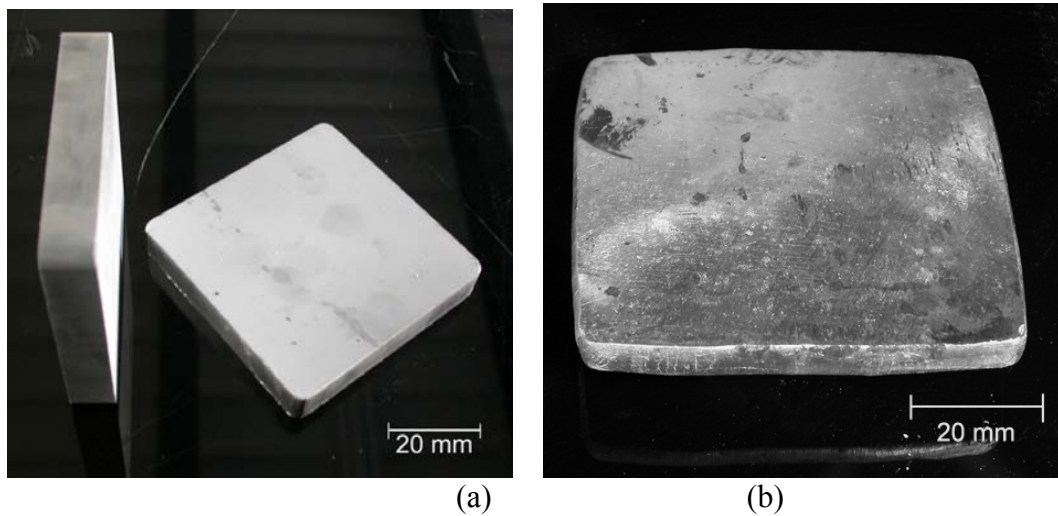


Figure 4.4. (a) Cold compacted precursor (92% dense) and (b) hot forged precursor (99% dense).

As a result of open die forging the cross-sectional area of the precursor increased and cracks formed at the edges. In order to remove the cracks, cross-sectional area of precursor was machined according to the geometry of the foaming mould (Figure 4.5). Flat side surfaces also provided good thermal contact with the foaming mold which is very important for foaming step.

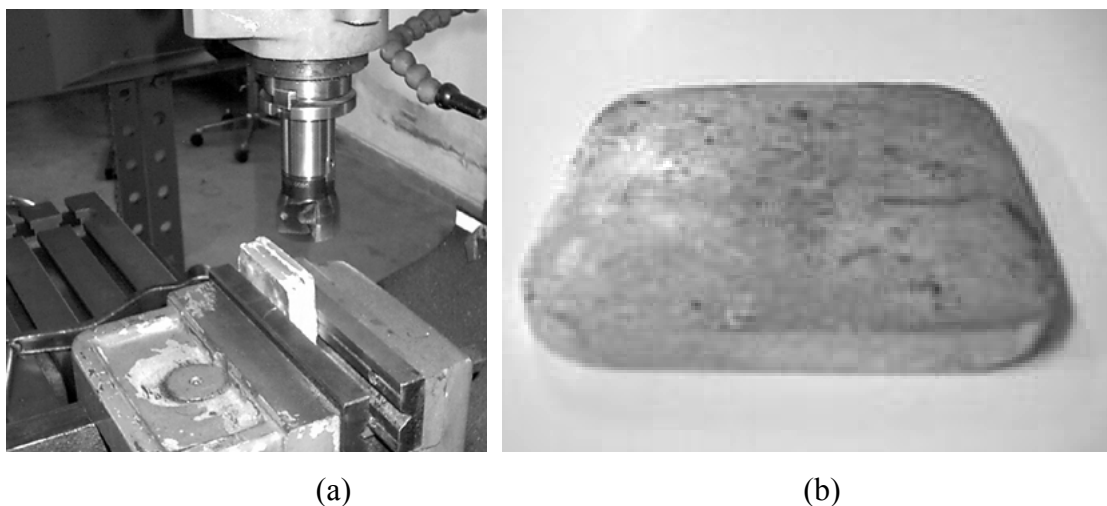


Figure 4.5. (a) Machining of the forged precursor material and (b) machined precursor.

In a final step the machined hot forged precursor material was foamed by heating it above its melting point in a foaming mold, having a cross-sectional area of 8x8 cm and a height of 3.5 cm. The precursor was inserted into a pre-heated (750°C)

steel mold providing expansion only in the vertical direction (Figure 4.6). After precursor insertion, the steel mold was closed at the top. The inserting and removing specimen took less than 10 seconds. The preheated foaming mold also provided heat for the foaming process. During foam insertion the furnace temperature dropped about 50°C for 2 minutes then the temperature increased again to 750°C. Since the inner dimensions of the foaming mold was the same with the precursor cross-section, after a certain furnace holding time it expanded vertically and filled the mold.

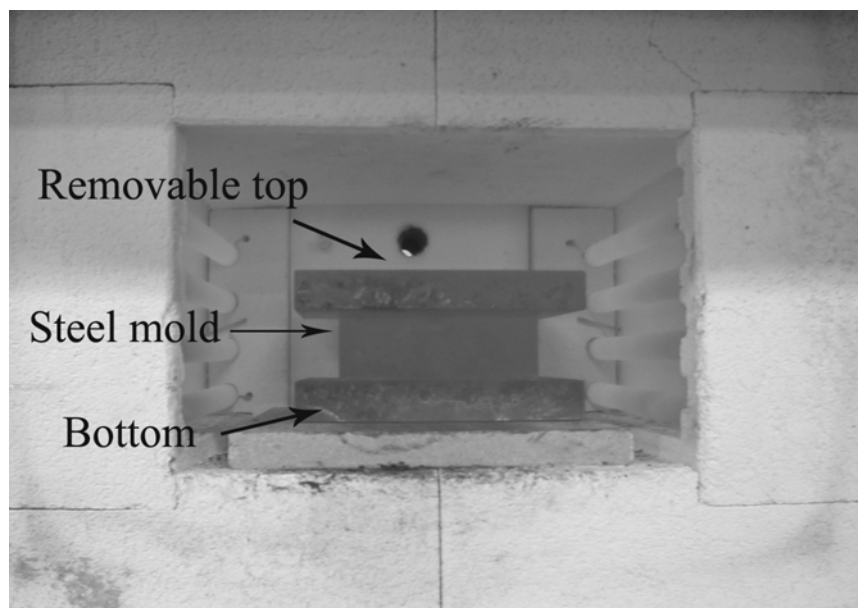


Figure 4.6. Foaming in the furnace with a steel mold closed at the top and bottom.

Initial foaming experiments were conducted in order to find out an optimum furnace holding time that would completely fill the mold. It was found that at a furnace holding time of about 5 minutes precursors completely filled the mold (Figure 4.7). The final expansion obtained about the 4 times the initial thickness of the precursor, see Figure 4.8. After the specified furnace holding time the foaming mold containing the liquid foam was taken from the furnace. In order prevent the collapse of liquid foam the liquid foam was quickly cooled together with foaming mold. Following cooling methods were applied: 1) plunging the mould into large water filled reservoir 2) slow cooling by spraying water on foaming mold 3) cooling by air without any intervention. It was found that plunging the mould into a large water filled reservoir resulted in solidification of the liquid foam nearly with same dimensions of liquid foam. In other

methods it was found that foam collapse was substantial. By simply changing the furnace holding time, foam plates having different densities were obtained and used in filling of composite tubes as will be explained in following sections.

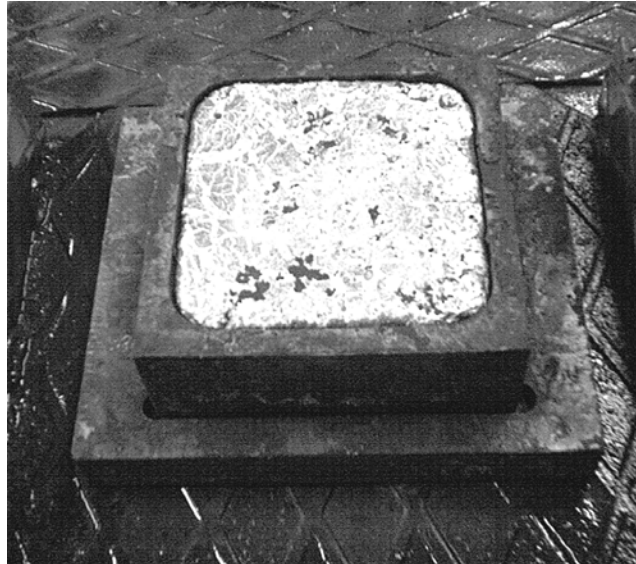


Figure 4.7. Foamed precursor that completely filled foaming the mold

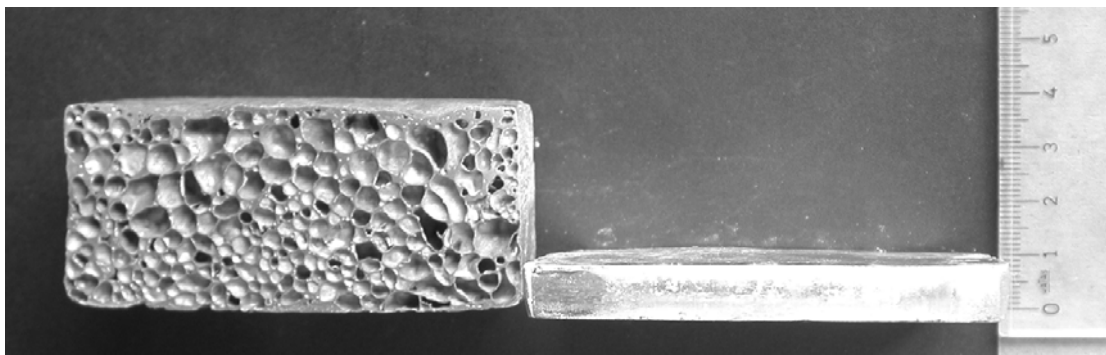


Figure 4.8. Pictures of Al foam and precursor material, showing 4 times expansion of initial thickness of the precursor.

4.1.2. Aluminum Foam Filler Sample Preparation

The regions near to the skins of Al foam contains denser metal layer as compared with the interior sections. Further, a dense foam layer also forms near the bottom of the foam sample, mainly due to the liquid foam drainage. At the interior of the foam plate more homogenous cell structure was found and therefore for the foam-filling of composite tubes, cylindrical foam samples were cut with electrical discharge

machine normal to the thickness of the plate or normal to the foam expansion direction. In each foamed plate, four foam fillers of 25 mm and 27 mm in diameter and length respectively were cut with the electrical discharge machine (Figure 4.9). A cylindrical foam sample cut from the foam block is shown in Figure 4.10. All machined foam fillers were cleaned using acetone bath and then dried for 2 hours at 180°C. The density of fillers was measured after drying by simply dividing the weight to the volume of the sample.



Figure 4.9. View of machining foam fillers using electrical discharge machine.

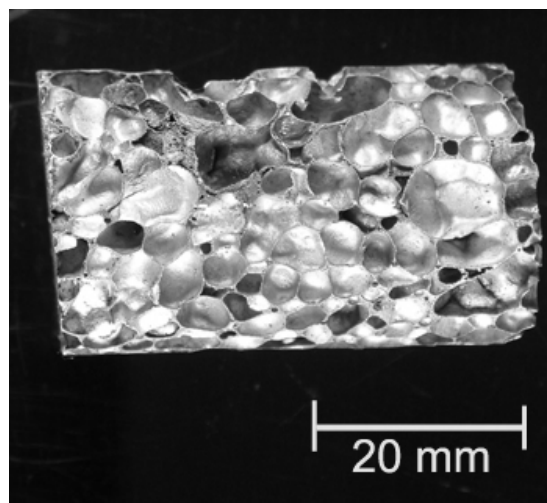


Figure 4.10 An electrical discharge machined cylindrical Al foam sample.

4.1.3. Compression Mechanical Properties of Al Foams

Figure 4.11 shows the compressive stress–strain curves of the prepared Al foams of three different densities, 0.27, 0.35 and 0.43 g/cm³ (Kavi et al. 2004). In order to see the repeatability of compression stress-strain behavior of foams with the same density, two tests results are shown in Figure 4.11. It is also noted in Figure 4.11, the plateau stresses of foams are not constant and increase with increasing strain. It is supposed that foams having homogeneous cell size and cell size distribution show steady plateau stress in collapse region. But in reality, differences in cell size and cell distribution cause the collapse of weak cells before the collapse of strong cells. This leads to increase in the stress values in the collapse region.

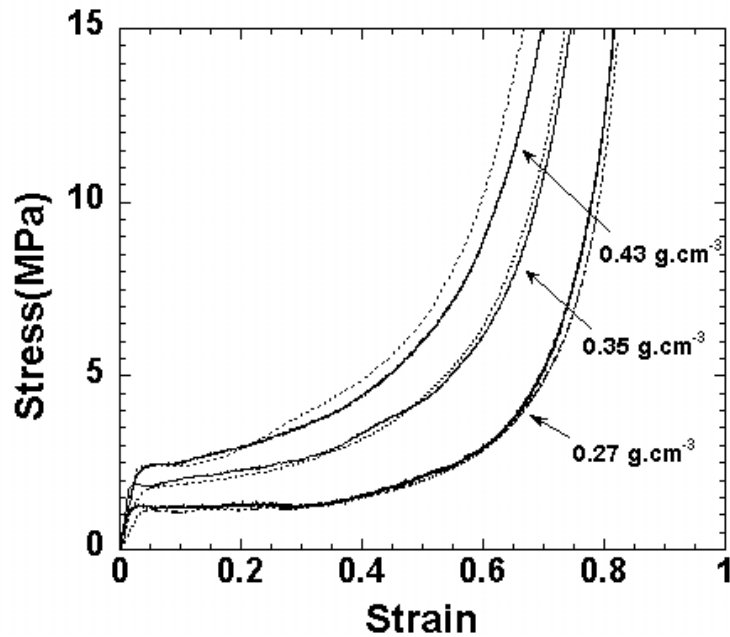


Figure 4.11. Compressive stress-strain curves of the prepared Al foams at various densities.

The plateau stress varied with the foam density as depicted in Figure 4.12 (Kavi et al. 2004); as the relative density increased the plateau stress increased. It is of great advantage to be able to describe the strain hardening properties of the aluminum foams by a simple model. Such model has been proposed by Hannsen et al. (2002) for the compression stress-strain behavior of Al foams and the constitutive model was also

validated by using non linear finite element code LS-DYNA. The strain-hardening model proposed is given by the following equation:

$$\sigma = \sigma_p + \gamma \frac{e}{e_D} + \alpha \ln \left[1 / \left(1 - \left(\frac{e}{e_D} \right)^\beta \right) \right] \quad (4.1)$$

where σ_p , e , e_D , γ , α and β are the plateau stress, strain, compaction strain, linear strain hardening coefficient, scale factor and shape factor respectively.

$$e_D = 1 - \frac{\rho_f}{\rho_b} \quad (4.2)$$

Because of its simplicity, the above-given model was also used to construct the stress-strain relation of the prepared Al foams. Experimental stress-strain curves corresponding to a specific density were fitted with Equation 4.1. The coefficients of Equation 4.1 are also listed for each density in Table 4.2 (Kavi et al. 2004). The constructed stress-strain curves are presented in Figure 4.11 together with experimental curves. Generally satisfactory agreements are found.

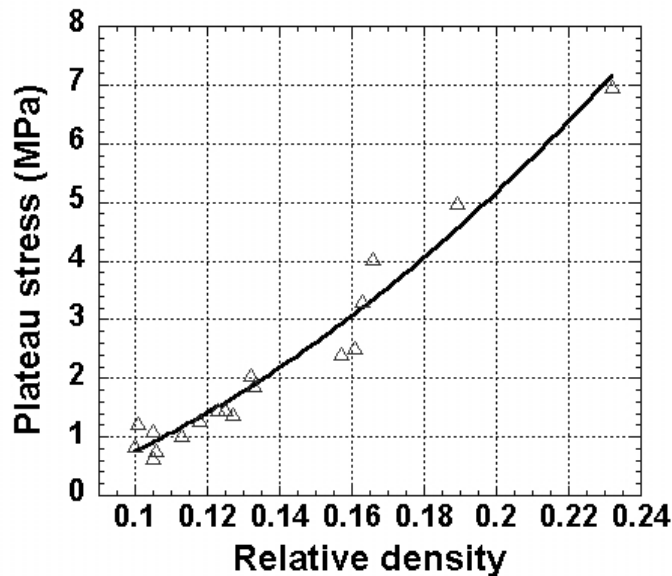


Figure 4.12. Typical plateau stress vs. relative density curves of the Al foams.

(Source: Kavi et al. 2004)

Table 4.3 Coefficients of Equation 4.1 for each foam density studied.

Foam density (g.cm ⁻³)	σ_p	γ	α	β
0.27	1.24	0.2	17	6
0.35	1.96	1.7	17	5
0.43	2.44	1.7	18	4

4.2. Preparation of Glass Fiber Reinforced Composite Tubes

Two manufacturing techniques were used to prepare composite tubes: filament winding and tube rolling. An E-glass type, continuous fiber tow and fiber fabric were used as reinforcement material (Figures 4.13). The matrix material is an iso-polyester resin (blend of isophthalic acid and maleic anhydride or fumaric acid), and was prepared by mixing with 1.5 wt% hardener solution containing 5wt% Mek-peroxide as the active material and 0.28 wt% curing agent solution containing 6 wt% cobalt octoat as the active material.

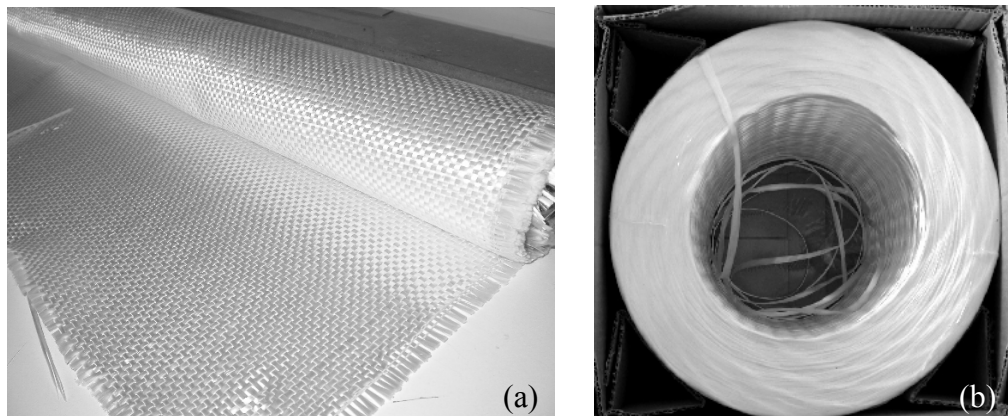


Figure 4.13. Glass fibers used to prepare tubes, (a) fiber fabric and (b) continuous fiber tow.

4.2.1. Filament Winding

A filament winding set up was constructed on a lathe and both the rotation speed of the mandrel on which the fibers wound and the speed of crosshead of the lathe were

important parameters for adjusting fiber angle. After initial trails, lathe was adjusted to form fiber winding at a 65° to the mandrel axis. The picture of the used mandrel (25 mm in diameter) and the metal ring used to de-mold the tube after post curing are seen in Figure 4.14.

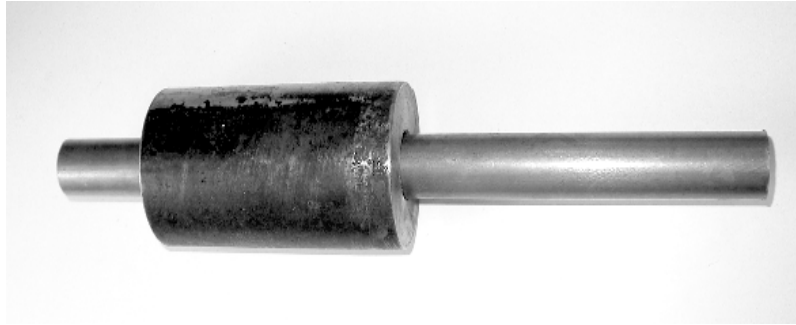


Figure 4.14. Mandrel and the de-molding ring.

The fiber tow was impregnated by the thermosetting resin bath attached to the crosshead of the lathe and one fiber tow was wound on each rotation of lathe. For ease of removal of tube, the mandrel was initially polished and a release agent was applied on its surface. After the winding process, the tubes were initially cured at room temperature for four hours, rotating on the lathe to prevent downward resin flow. The dried composite tubes were then post cured in a furnace at 120°C for two hours. After the cooling, the tubes were de-molded from the mandrel and then sectioned into 27 mm long compression specimens. The tubes manufactured by filament winding process are shown in Figure 4.15.

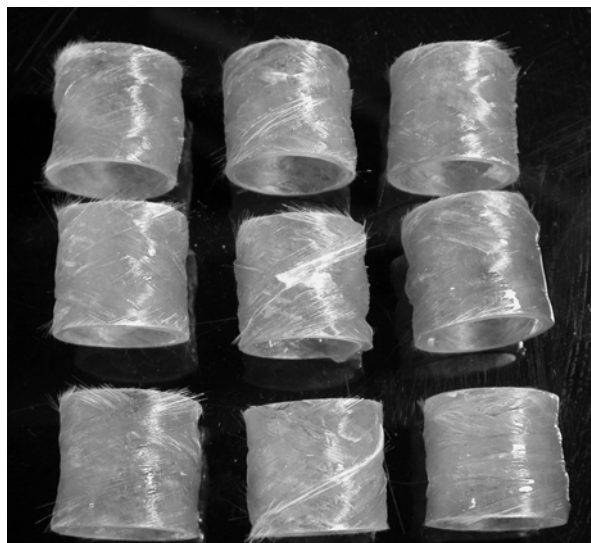


Figure 4.15. Sectioned filament wound composite tube test specimens.

4.2.2. Tube Rolling

The mandrel used for filament winding process was also used for tube rolling (Figure 4.16). As in the filament winding process, a releasing agent was spread on the surface of the mandrel for ease de-molding. Woven glass fabrics in various fabric areal densities were used as the reinforcement for polyester matrix composite tubes. These fabrics were first cut into rectangular sections and then impregnated by the resin. Then the section was hand rolled on the mandrel. The rolled tubes initially cured at room for about four hours. Post curing was conducted in a furnace at 120° C for two hours. After post curing, the tube was de-molded and sectioned into 27 mm long compression test tube samples as shown in Figure 4.16.

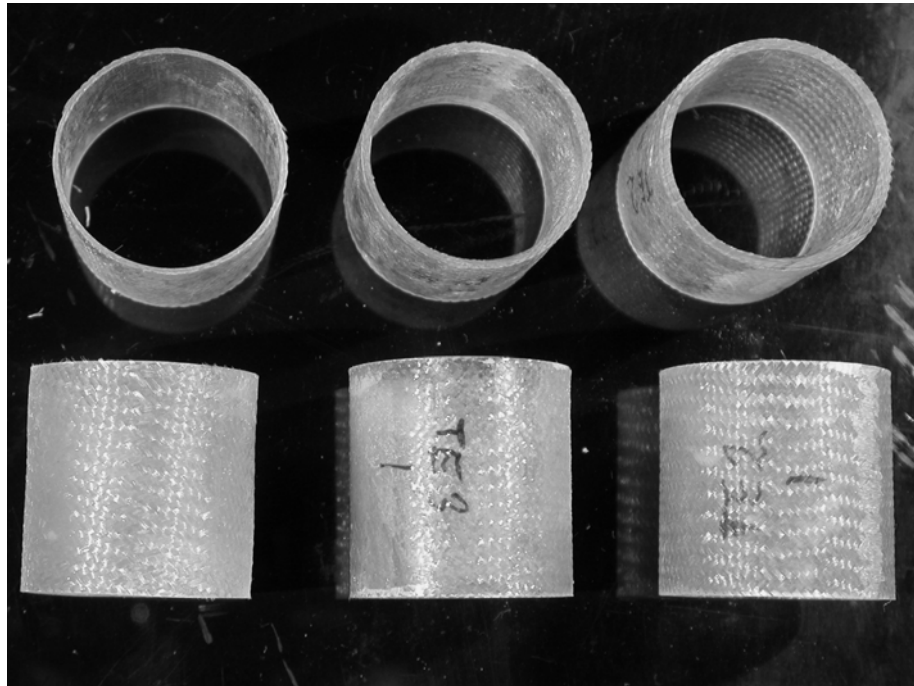


Figure 4.16. Rolled and cut to length composite tube compression test specimens.

CHAPTER 5

PREPARATION OF EMPTY, FOAM-FILLED, HYBRID AND FOAM FILLED HYBRID TUBES

5.1. Composite Tubes

The main geometrical parameters of the composite tube as shown Figure 5.1 include thickness (t), length (l), radius (r), mass. An important geometrical parameter is the fiber angle (θ), the angle between the fiber and tubes axis as depicted in Figure 5.1. The inner diameter of all composite tubes (25 mm) including empty and foam filled composite and empty and foam-filled aluminum-composite hybrid tubes tested in this study was kept approximately equal to its length (27 mm) in order to prevent Euler buckling.

There are five test groups involved testing of composite tubes and these are:

- 1) filament wound tubes (FW),
- 2) rolled tubes of different fabrics (TA),
- 3) rolled tubes with two different fiber angles (TB),
- 4) rolled tubes with varying thicknesses (TE) and
- 5) Al-foam filled rolled tubes (TF).

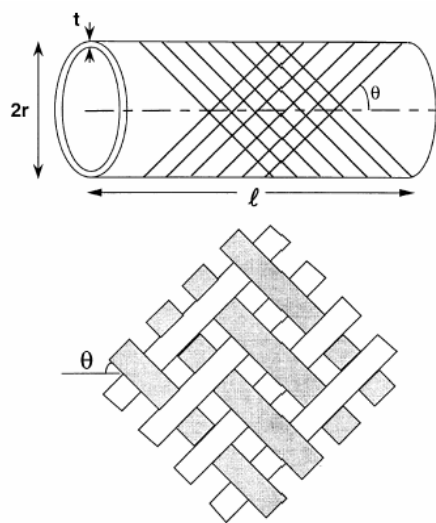


Figure 5.1. Representation of geometrical parameters of fiber reinforced composite tubes (Harte et al. 2000).

5.1.1. Composite Tubes Prepared by Filament Winding

The filament wound tubes were cut to 27 mm length compression test specimens upon removing from the 25 mm diameter cylindrical steel shaft. Typical side and cross-sectional views of the tubes are shown in Figures 5.2(a) and (b), respectively. Owing to the processing method, the prepared tubes wall thicknesses and outer diameter show variations along the tube length as depicted in Figures 5.2(a), (b) and (c). A close inspection of the tubes has also shown that the fiber orientation and fiber angle are also varied along the tube length. The control of the geometrical parameters of the tubes using filament wound method is rather difficult for tubes with such small diameter and wall thickness.

The fiber angle and the average wall thickness in these wound tubes were around 65 degrees and 2 mm respectively.

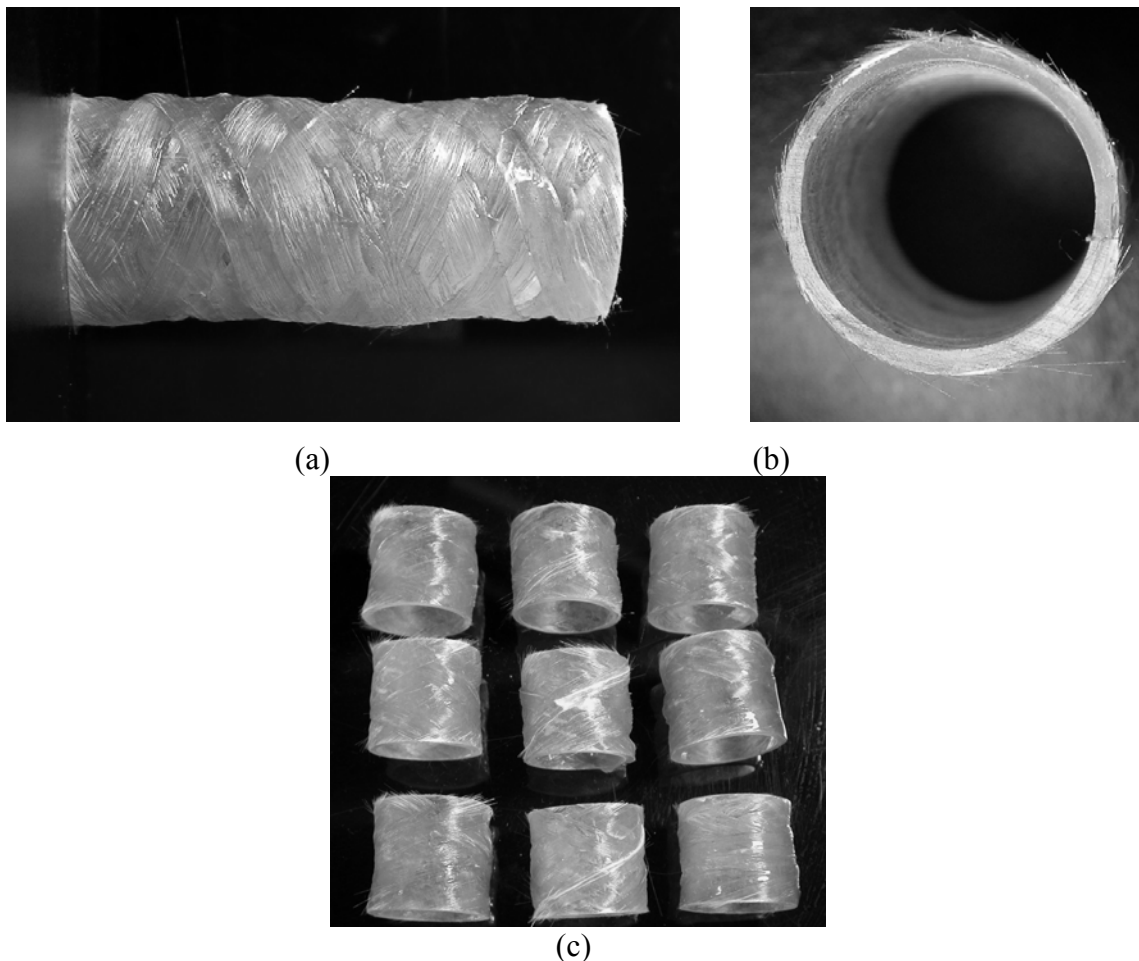


Figure 5.2. Filament wound tubes: (a) side and (b) cross-sectional view and (c) compression test specimens.

5.1.2. Composite Tubes Prepared by Tube Rolling Method Using Different Fabrics

Using tube rolling method four different groups of tubes of 0/90 fiber orientations varying in fabric areal density and thicknesses were prepared and investigated for the quasi-static crushing behavior. The prepared tubes wall thicknesses and fabric areal densities are tabulated in Table 5.1. The tubes prepared by the tube rolling method show relatively more homogenous wall thicknesses and fiber orientation along the tube wall as compared with the tubes prepared by the filament winding (Figures 5.3(a) and (b)).

Table 5.1. Wall thickness and fabric areal density of composites with 0/90 fiber lay-up.

Test number	Wall thickness (mm)	Fabric areal density (g/m ²)
1	0.86	100
2	0.71	280
3	1.07	280
4	1.53	280

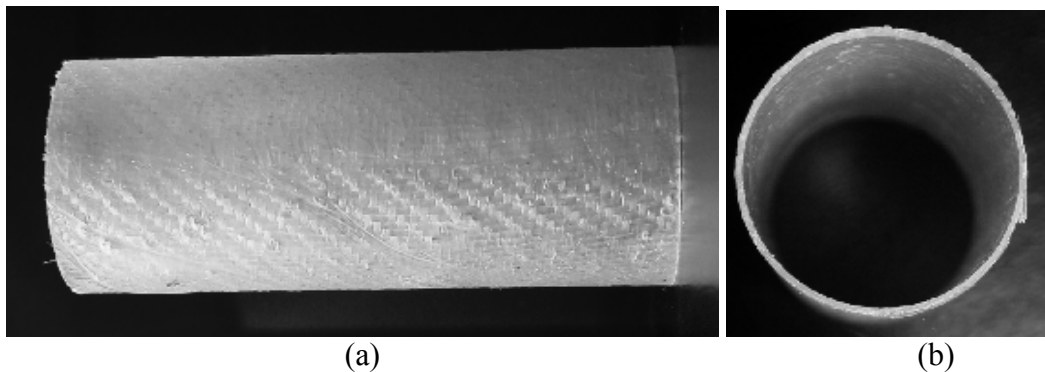


Figure 5.3. Rolled tube showing homogeneous outer diameter and thickness: (a) side and (b) cross-sectional view.

5.1.3. Composite Tubes Prepared by Tube Rolling Method with Different Fiber Angles

The effects of fiber angle on the crushing behavior of tubes were investigated with fiber angles of 0/90 and 45/45 degrees using E-glass fiber fabric of 2x2 twill [0,90] fiber construction and 165 g/m² areal density (Figures 5.4(a) and (b)). Tubes with 0/90 fiber angle was coded as TB1 and 45/45 degrees as TB2. The tubes had an average wall thickness of 0.50 mm. The Fiber fabric used in these tubes was used in the rest of the study.

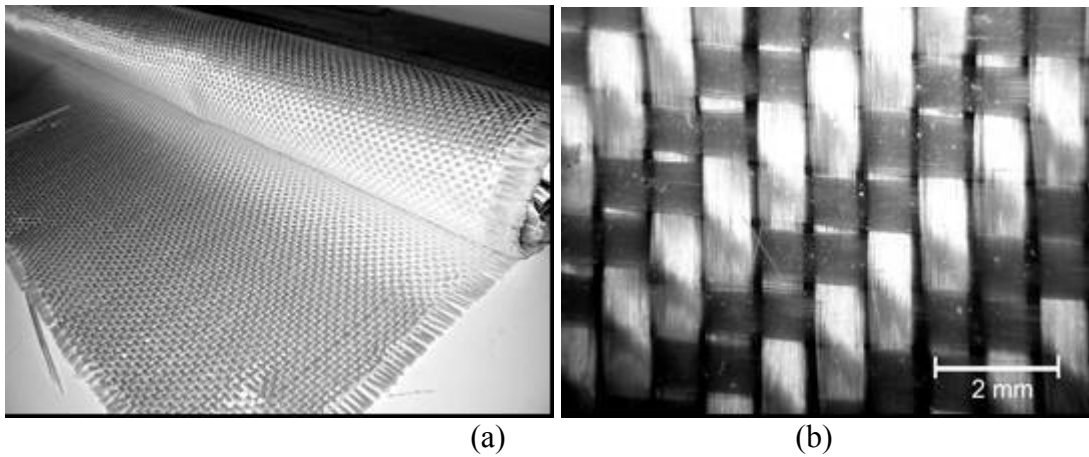


Figure 5.4 (a) E-glass woven fabric with (b) 2x2 twill fiber construction.

5.1.4. Composite Tubes Prepared by Tube Rolling Method with Different Wall Thickness

Tubes with three different wall thicknesses of 45/45 fiber angle were prepared using E-glass fiber fabric of 2x2 twill [0,90] fiber construction and 165 g/m² areal density in order to investigate the effects of wall thicknesses on the crushing behavior of the tubes. The thicknesses of these tubes as shown in Figure 5.5 varied between 0.44 and 1.34 mm. In the first group tests coded as TE1 in Table 5.2 the average tube thicknesses is 0.55 mm. The second and third group tests are sequentially coded as TE2 and TE3 and the average tube thicknesses are 0.82 and 1.32 mm, respectively. The top view of tube of each group is shown in Figure 5.5. The volume percentages of the fibers in these tubes were determined by matrix burn out in a preheated furnace at 650°

C for 120 minutes and found about 50% , which varied only slightly with thickness of the tubes.

Table 5.2. Geometric parameters of composite tubes prepared for determining the thickness effect.

Test group	Specimen code	Wall thickness (mm)	Length (mm)	Mass (g)	D/t ratio
1	TE1.1	0.62	27	2.15	42.3
	TE1.2	0.53	27	2.09	49.2
	TE1.3	0.49	27	2.16	53.0
	TE1.4	0.41	27	2.13	62.9
	TE1.5	0.59	27	2.23	44.4
2	TE2.1	0.74	27	3.20	35.8
	TE2.2	0.87	27	3.18	30.7
	TE2.3	0.86	27	3.27	31.1
3	TE3.1	1.30	27	5.13	21.2
	TE3.2	1.32	27	5.17	20.9
	TE3.3	1.34	27	4.92	20.7

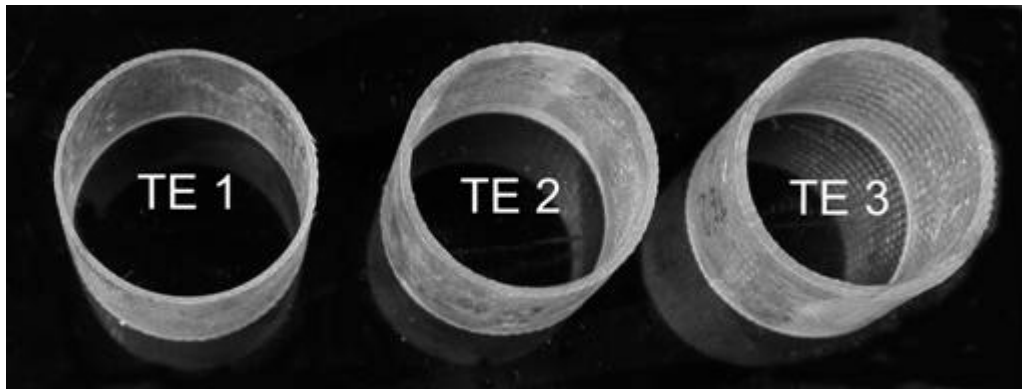


Figure 5.5. Rolled tubes of different thickness coded as TE.

5.1.5. Aluminum Foam-Filled Rolled Composite Tubes

In order to determine the effect of foam filling on the composite crushing behavior, E-glass fiber fabric of 2x2 twill fiber (165 g/m^2) composite tubes with 45/45 fiber angle and wall thicknesses of 0.56-0.65 mm were filled with foams of varying density between 0.25 and 0.61 g/cm^3 . The fillers were machined with outer diameter the same as the inner diameter of the tube with close tolerances using an electrical discharge machine (Figure 5.6(a)). The filler fitted inside tube without imposing pressure. A layer of polyester resin was swept onto the inner surfaces of the tube before fitting the

filler so that after curing the filler tightly bonded to the surfaces of the tube (Figure 5(b)). The properties of the filled tubes are listed in Table 5.3.

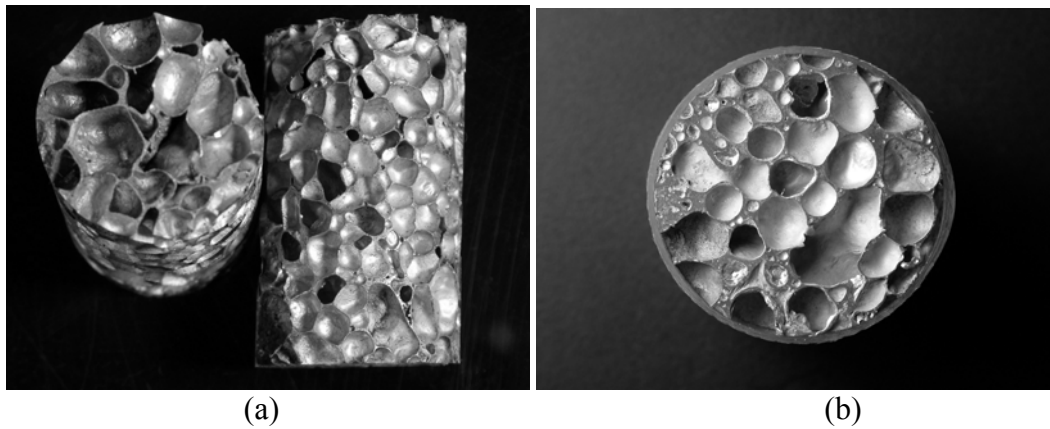


Figure 5.6. (a) machined filler Al-foam samples and (b) foam filled composite tube with thickness of 0.56 mm.

Table 5.3. The properties of the foam filled composite tubes.

Specimen code	Foam density (g/cm ³)	Wall thickness (mm)	Tube mass (g)	Total mass (g)	Length (mm)
TF1-2	0.25	0.64	2.40	5.64	27
TF1-4	0.29	0.56	2.77	6.49	27
TF4-2	0.32	0.59	2.61	6.73	27
TF4-6	0.33	0.49	2.19	6.2	27
TF4-7	0.33	0.59	2.18	6.45	27
TF1-5	0.34	0.65	2.75	7.12	27
TF1-9	0.44	0.56	2.73	8.39	27
TF1-13	0.61	0.63	2.97	10.78	27

5.2. Hybrid Tubes

Empty and Al foam filled aluminum-composite hybrid tubes were tested in order to determine effect of metal tube and foam filling on the crushing behavior of the composite. Empty and Al-foam filled hybrid tubes coded as TTE and TTF, respectively. In these tests a deep-drawn Al tube produced by METALUM Company of Turkey and received in 25 mm diameter with 0.29 mm wall thickness were used. The yield and ultimate strength of the tube material was previously determined by Toksoy (2003) at a quasi-static strain rate of $\sim 1 \times 10^{-3} \text{ s}^{-1}$. The ultimate tensile stress (σ_U), 0.2% proof strength ($\sigma_{0.2}$) and Vickers hardness number of the tube material are listed in Table 5.4

(Toksoy 2003). Tubes were machined to 27 mm in length using a diamond saw. Geometric and material parameters of tested empty tube are listed in Table 5.5.

Table 5.4 Mechanical properties of Al tube material

Materials	σ_U (± 10 MPa)	$\sigma_{0.2}$ (± 10 MPa)	Σ_0 $(\frac{\sigma_{0.2} + \sigma_U}{2})$	Vickers hardness number
99.7% Al	170	112	141	58

Table 5.5 Geometric parameters of tested empty Al tube

Tube Material	Outer Diameter (mm)	Thickness (mm)	Length (mm)	Mass (g)	D/t ratio
%99.7 Al	25	0.29	27	1.72	86.2

5.2.1. Empty Hybrid Tubes

The Al tubes having the outer diameter same with that of composite tubes were inserted inside and bonded using polyester resin as the adhesive to the composite tubes. Rolled E-glass fiber fabric of 2x2 twill fiber (165 g/m^2) composite tubes with 45/45 fiber angle and wall thicknesses ranging between 0.53 and 0.72 mm were tested in the hybrid tubes. Before insertion the surfaces of the Al tubes were cleaned with acetone and then dried. The side and top view of a hybrid tube are shown in Figure 5.7 and the properties of the tested tubes are tabulated in Table 5.6.

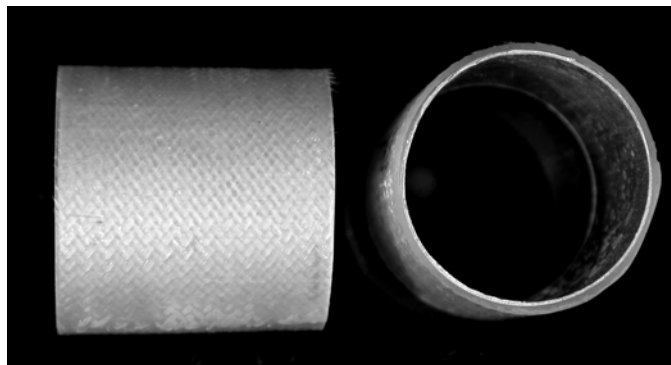


Figure 5.7. Empty aluminum-composite hybrid tubes.

Table 5.6. Properties of empty hybrid tubes.

Specimen code	Total mass (g)	Composite tube wall thickness (mm)	Length (mm)
TTE1.1	4.29	0.53	27
TTE1.2	3.63	0.61	27
TTE1.3	4.28	0.53	27
TTE1.4	4.58	0.72	27
TTE4.2	4.15	0.60	27
TTE4.3	3.93	0.59	27

5.2.2. Al-Foam Filled Hybrid Tubes

The properties of the foam filled hybrid tubes are tabulated in Table 5.7. Rolled E-glass fiber fabric of 2x2 twill fiber (165 g/m²) composite tubes with 45/45 fiber angle and wall thicknesses ranging between 0.47 and 0.63 mm were tested in the foam filled hybrid tubes. At all surfaces polyester resin was used as adhesive. The foam density in these tubes was kept almost constant around 0.4 g/cm³. Figure 5.8 shows the top view and layers of a foam filled hybrid tube.

Table 5.7. Properties of al foam filled hybrid tubes.

Specimen code	Foam density (g/cm ³)	Composite tube thickness (mm)	Composite tube mass (g)	Total mass (g)	Length (mm)
TTF 1	0.39	0.60	2.44	8.82	27
TTF 2	0.41	0.47	2.19	8.98	27
TTF 3	0.40	0.62	2.49	9.33	27

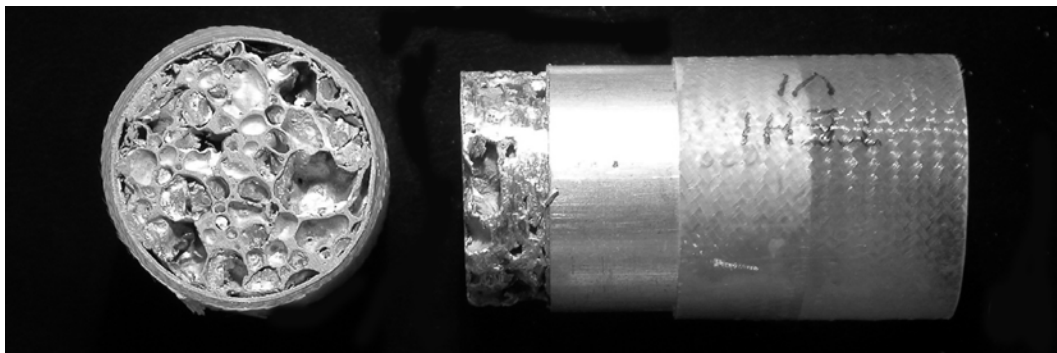


Figure 5.8. Al foam-filled hybrid tube top views and layers.

5.3. Compression Tests and Calculations Methods

The quasi-static compression testing of prepared test specimens were carried out using a fully computerized SHIMADZU testing device with cross head speed of 25 mm/min. Compression tests results were digitally recorded as time, load and displacement data. In few tests, the deformation sequence was also recorded using a digital video camera to analyze the deformation stages clearly. Time data taken was used in this analysis.

Load and displacement data were used to investigate the crush load behavior of the specimen and to calculate absorbed energy value by the help of trapezoidal rule in calculating the area under the load curve, as mentioned in Section 3.2.

The compression tests were made between parallel flat compression plates of the compression test machine without any other compression apparatus used.

CHAPTER 6

RESULTS AND DISCUSSION

6.1. Compression Behavior of Empty Tubes

6.1.1. Single Composite Tubes

The load-displacement curves of the filament wound empty composite tubes of thickness varying around 2 mm are shown in Figure 6.1. The initial peak load or maximum load (P_{max}) in each curve shown in this figure is followed by fluctuating crushing loads, from which a mean crush load (P_m) can be calculated. As is shown in the same figure, qualitative mean crushing loads of the tubes determined by discarding the initial peak load region vary greatly between the tests from a lowest crushing load of 4.3 kN to a highest crushing load of 13 kN. The filament wound tubes failed partly by buckling and partly by the separation of wound continuous fiber tows (Figures 6.2(a) and (b)). Since the thickness of the tube varied location to location, the buckling started from the thinnest section of the tube, leading to a significant load values variations between the different tubes.

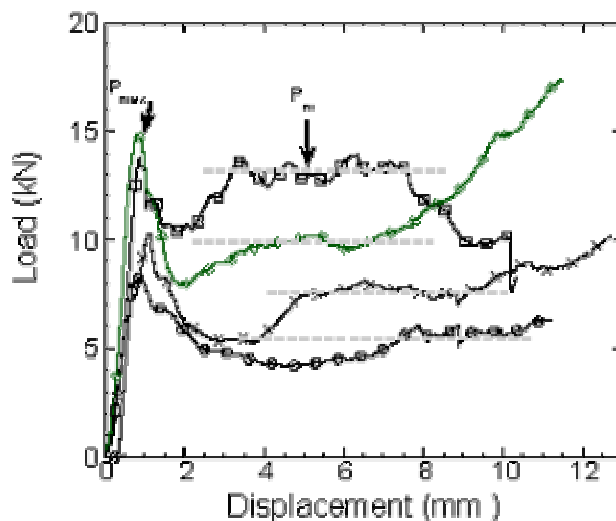


Figure 6.1. Load-displacement curves of filament wound composite tubes.

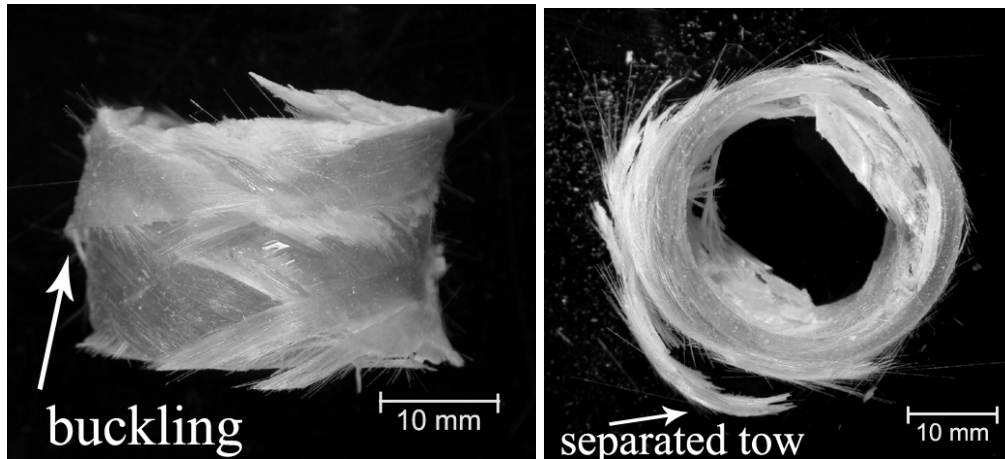


Figure 6.2. Photographs of a filament wound composite tube failed by (a) buckling and (b) separation of tows.

The load-displacement curves of the rolled tubes (0/90 fiber orientation and 100 and 280 g/cm² fabric areal densities) in varying thickness are shown in Figures 6.3(a) through (d). The load-displacement curves shown in these figures and subsequent microscopic analysis on the crushed tube samples have further clarified the crushing mechanisms involved. Two crushing modes are distinguishable: (a) progressive crushing mode (Figure 6.4(a)) and (b) catastrophic failure of two ways; (i) compressive shear (Figure 6.4(b)) and/or (ii) axial splitting of the tube wall (Figure 6.4(c)), the same as the crushing modes proposed by Ramakrishna and Hamada (1998) previously. The catastrophic failure mode, as previously noted by Ramakrishna and Hamada (1998), is characterized by a sudden drop in load values following an initial peak load as seen in Figure 6.3(b) for a composite tube of 0.71 mm thick. The catastrophic failure modes absorb little energy, hence they are of little interest to crash worthy structures and mostly observed in brittle glass and carbon fiber reinforced epoxy and polyester matrix composites (Ramakrishna and Hamada, 1998). Figures 6.3(a-d) show few trends of the effects of fabric areal density and the thickness of the tubes on the deformation mode, hence crushing load values. Firstly, increasing the areal density from 100 to 280 g/cm² at almost constant wall thickness (Figures 6.3(a) and (b)) shows a trend of increasing the number of occasions for the catastrophic failure. Secondly, increasing the thickness of the tubes (Figures 6.3(b-d)) however increases the crushing loads and tends to promote the progressive crushing mode. These results should be however taken cautiously since they are based on the limited number of tests and as well as specific to the composite tubes investigated.

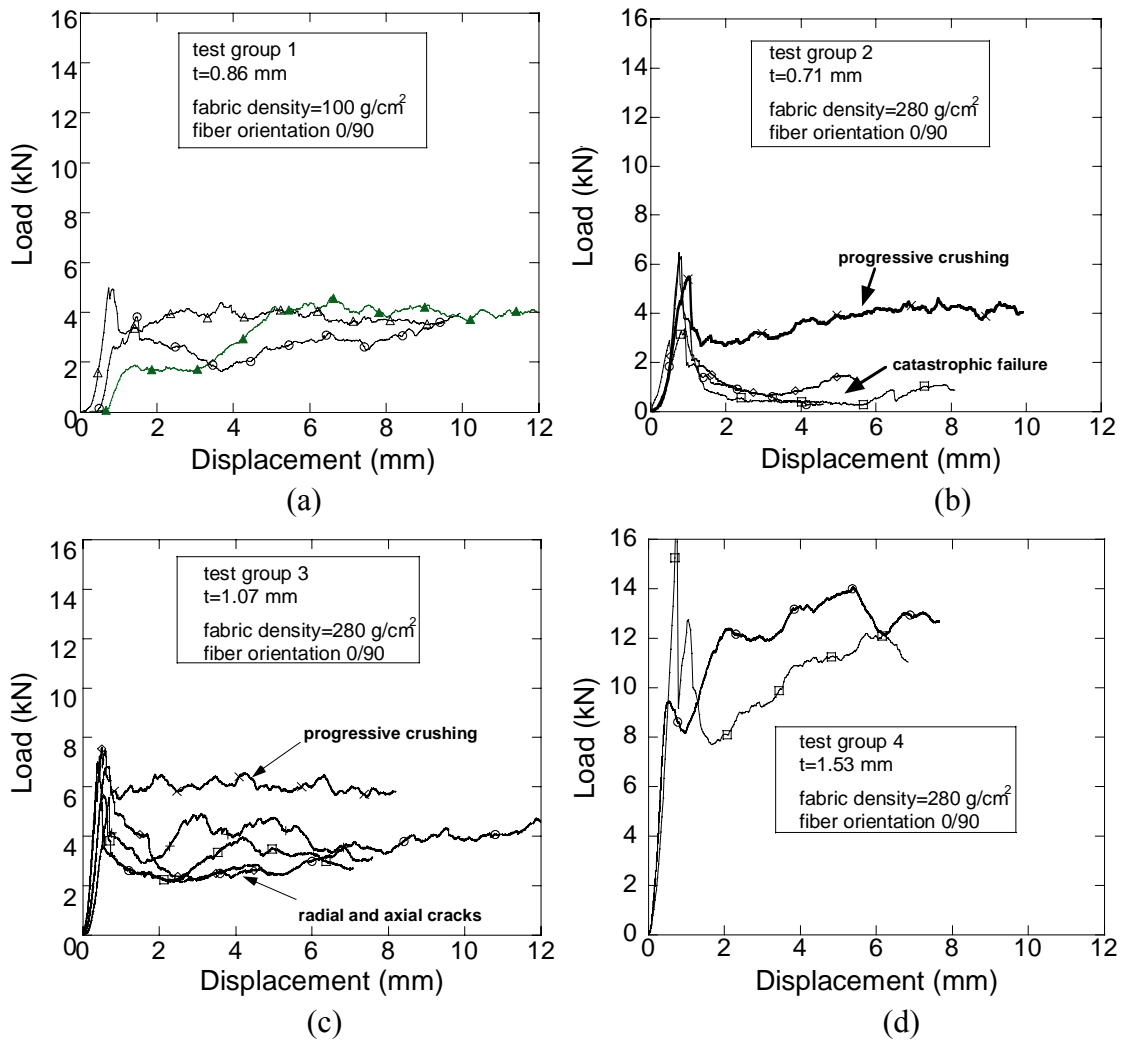


Figure 6.3. Load-displacement curves of composite tubes manufactured by tube rolling with two different fabric densities and varying thickness: a) 100 g/cm², $t=0.86$ mm and 200 g/cm², b) $t=0.71$ mm, (c) $t=1.07$ mm and d) $t=1.53$ mm.

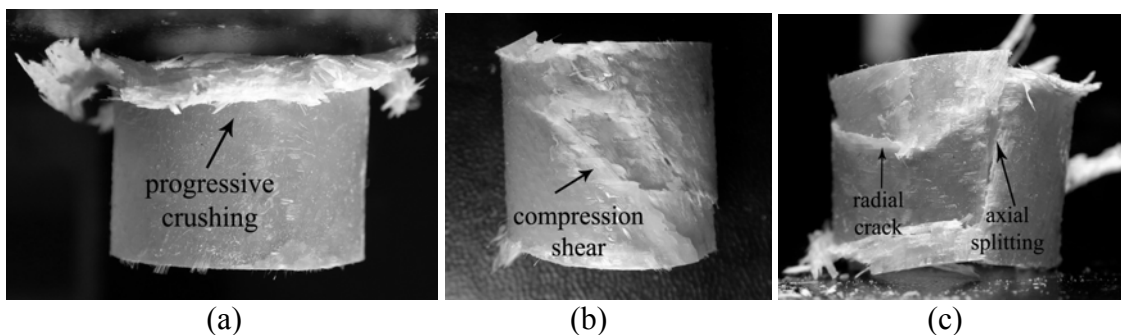


Figure 6.4. Crushing modes of the composite tubes of 0/90, a) progressive crushing and catastrophic failure (b) compression shear and (c) axial splitting and radial crack.

Figures 6.5 (a), (b) and (c) shows the load displacements curves of the composite tubes with three different average wall thickness of 0.55, 0.82 and 1.32 mm and 45/45 fiber angle prepared using E-glass fiber fabric of 2x2 twill [0,90] fiber construction with 165 g/m² areal density, respectively. The thickness of these tubes as shown in Figures 6.5 (a-c) varied between 0.44 and 1.34 mm. Except two tests, one of them is the thickest tube (1.32 mm) and the other one is the in thinnest tube (t=0.55 mm), the crushing mode is progressive crushing. In Figure 6.6(a), the load-displacement curve of a 0.5 mm thick tube deforming in progressive crushing mode is shown. The corresponding deformation views of the tube at various displacements as numbered in Figure 6.6(a) are shown in Figure 6.6(b). The tube deform elastically until a peak load, number 1 in Figure 6.6(a), thereafter localized deformation near the compression test platen-specimen contact region starts to form and proceeds along the length of the tube (see 2 in Figure 6.6(b)).

It is known that progressive crushing mode can be achieved by chamfering one of the ends of the composite tube (Ramakrishna 1998, Jimenez et al. 2000). When the compressive load is applied, the load at the tip of the chamfer end of the tube increases significantly, leading to microfracture initiating and the progression of the crushing zone. The form of crush zone is dependent on many factors including tube geometry, fiber orientation, test condition and etc. The progressive crushing mode of the tube in the studied composite tubes is believed to trigger from the one of the tube ends due to the imperfections at the end faces partly introduced during the sectioning of the tubes with diamond saw and the imperfect contact of the tube end faces with the compression test platen. Delaminations introduced during sectioning may likely trigger the crushing deformation from one of the ends of the tube. The imperfect contact between tube and compression test platen may increase the load locally in the contact area and lead to crushing start from the end of the tube. The increased numbers of occasions of progressive crushing in the thinnest tube simply support the later phenomenon since thinner the tube wall, higher the probability of in-contact area at the surface of the tube.

Following the initial peak load due to the localization of the deformation in an area near the one of the tube ends, the load decreases until number 3 in Figure 6.6(a). After this point deformation mode switches to progressive crushing and load values increases to an average value as seen in Figure 6.6(a). Further deformation proceeds in outward splaying mode (Figure 6.6(b)). Similar deformation modes were also observed previously in a glass fiber/epoxy composite (Saito et al., 2000).

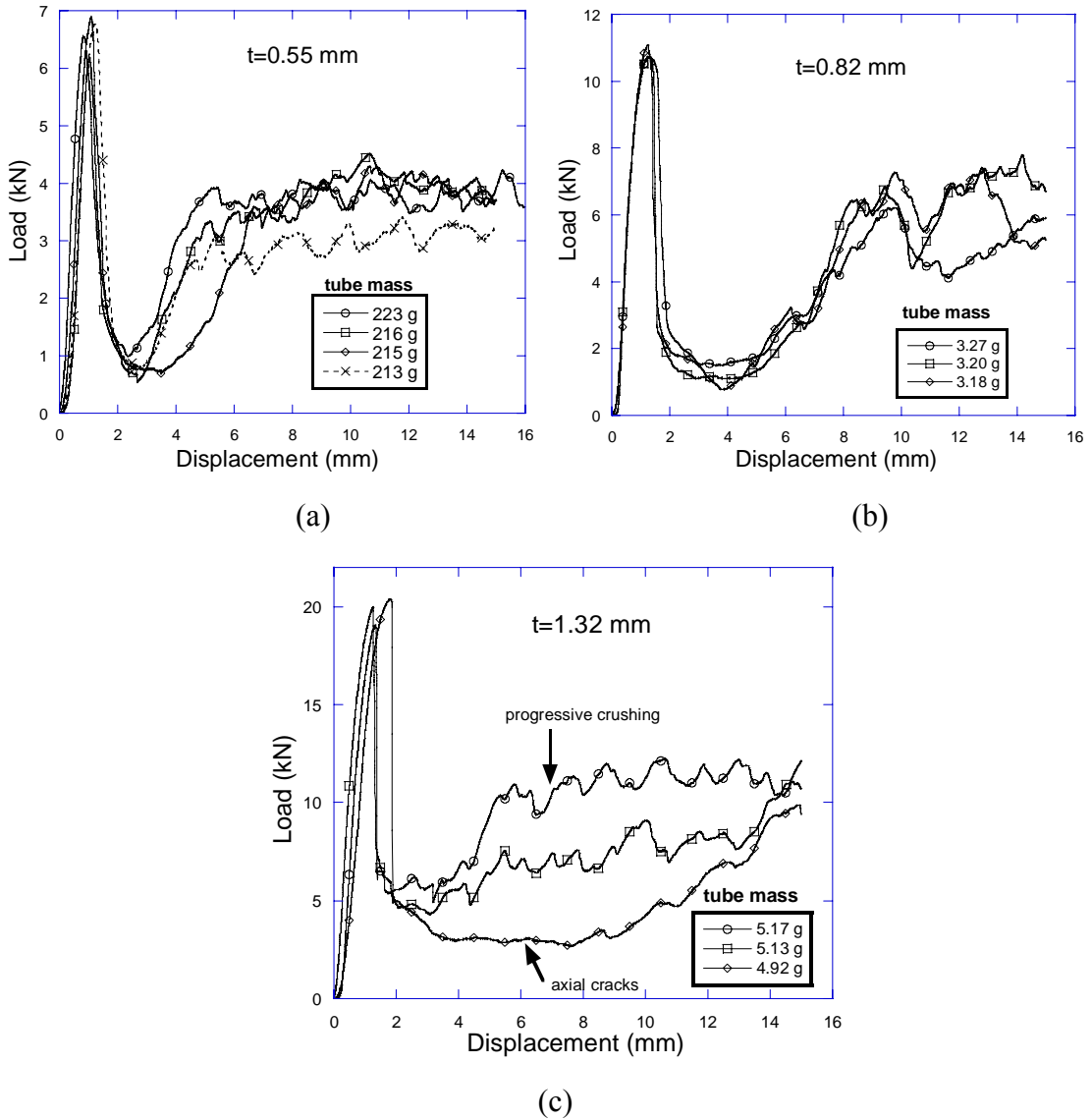
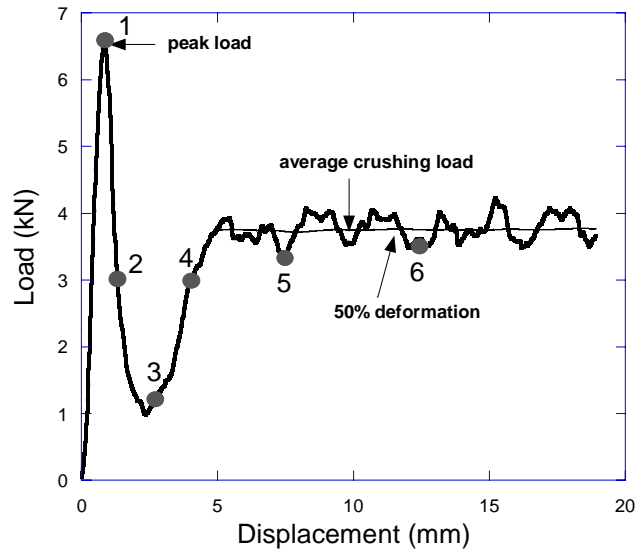
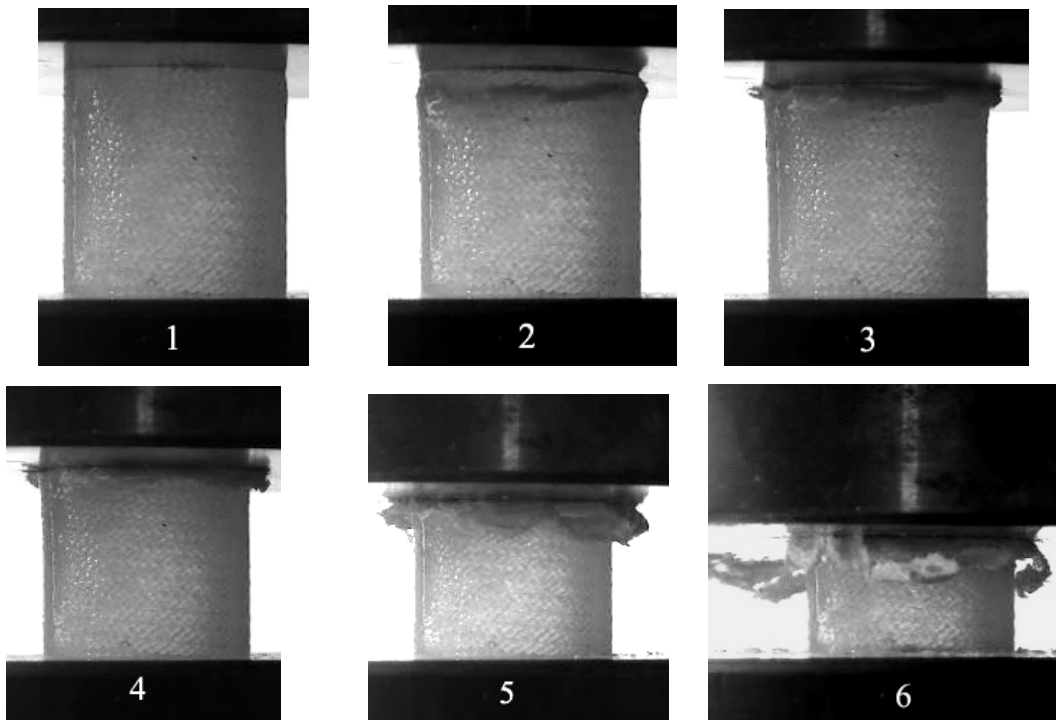


Figure 6.5. Load-displacement curves of the composite tubes with 45/45 fiber angle prepared using E-glass fiber fabric of 2x2 twill fiber construction of 165 g/m² areal density, average wall thickness: (a) t = 0.55 mm (b) t = 0.82 mm and (c) t = 1.32 mm.



(a)



(b)

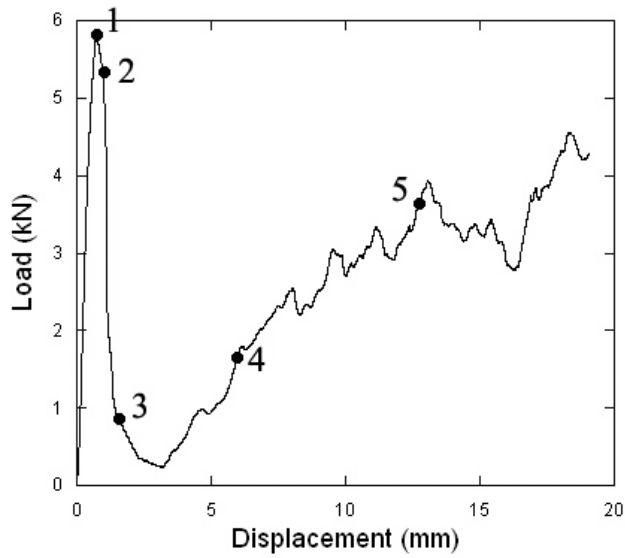
Figure 6.6. (a) Load-displacement curve of a composite tube with 45/45 fiber angle prepared using E-glass fiber fabric of 2x2 twill fiber construction of 165 g/m² areal density, wall thickness 0.41 mm and (b) corresponding view of the deformation at various displacements numbered in (a) showing progressive crushing mode.

The mean crush loads of the tubes were calculated in the region of progressive crushing of the load-displacement curves as show in Figure 6.6(a). The mean crush and maximum or peak loads, energy absorption and specific energy absorption corresponding to 50% deformation and corresponding deformation mechanisms of the tubes are tabulated in Table 6.1. The progressive crushing mode increases both mean crush loads and energy and SAEs as compared with catastrophic failure mode in the tubes of similar thickness.

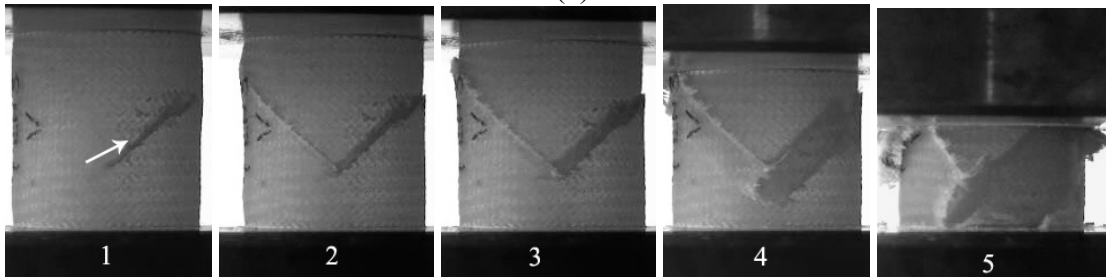
Table 6.1. Compression test results of empty composite tubes with 45/45 fiber angle.

Average Thickness (mm)	Specimen code	Maximum Load (kN)	Mean crush load %50 Deformation (kN)	Deformation mechanism	Energy absorbed %50 deformation (joule)	SAE %50 deformation (joule/g)
0.55	TE1.1	6.89	3.87	Progressive	45.31	21.09
	TE1.2	6.19	3.88	Progressive	48.08	22.93
	TE1.3	6.77	3.01	Progressive	41.27	19.11
	TE1.4	6.56	3.77	Progressive	45.03	21.14
	TE1.5	5.84	2.80	Axial cracks	28.44	13.52
0.82	TE2.1	10.75	6.45	Progressive	69.32	21.66
	TE2.2	11.08	6.24	Progressive	67.88	21.31
	TE2.3	10.73	5.09	Progressive	63.44	19.39
1.32	TE3.1	19.97	7.69	Axial cracks	115.08	22.43
	TE3.2	20.37	4.82	Axial cracks	82.03	15.88
	TE3.3	19.07	10.72	Progressive	147.00	29.82

Figures 6.7(a) and (b) show the load-displacement curve and deformation history (as function of displacement) of a composite tube sample failed by catastrophic failure, respectively. The composite tube seen in Figure 6.7(b) failed by forming the compressive shear regions, two shear lines, forming along the diagonal axis of the tube. Following the maximum load, the load values decreases to a minimum thereafter the load values increases as two shear-cups compressed completely. In addition to compression shear mode, axial splitting of the tube is observed in catastrophically failed composite tube samples as shown in Figure 6.7(b). Microscopic analyses of the failed samples of catastrophic modes have shown matrix and fiber cracking and fiber/matrix interface debonding (Figures 6.8(a-c)).

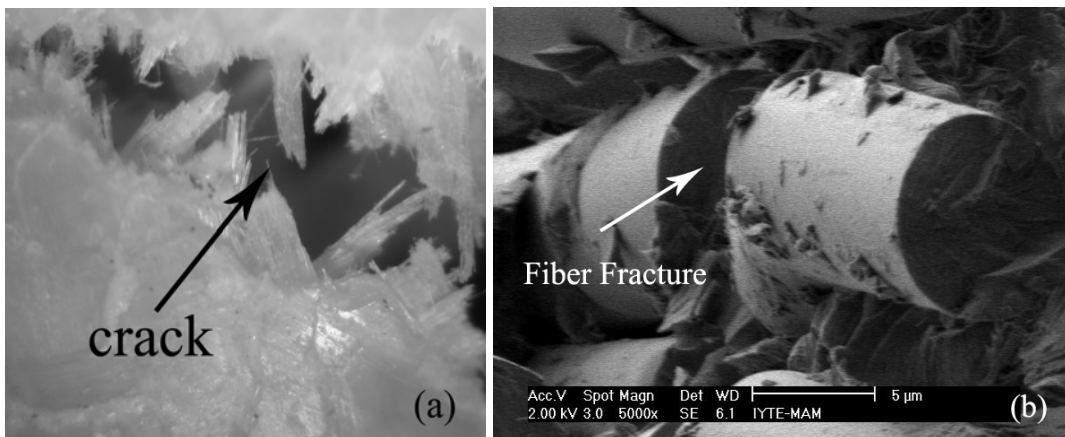


(a)



(b)

Figure 6.7. (a) Load-displacement curve of a composite tube with 45/45 fiber angle prepared using E-glass fiber fabric of 2x2 twill fiber construction of 165 g/m² areal density, wall thickness 0.59 mm and (b) corresponding view of the deformation at various displacements numbered in (a) showing catastrophic failure crushing mode.



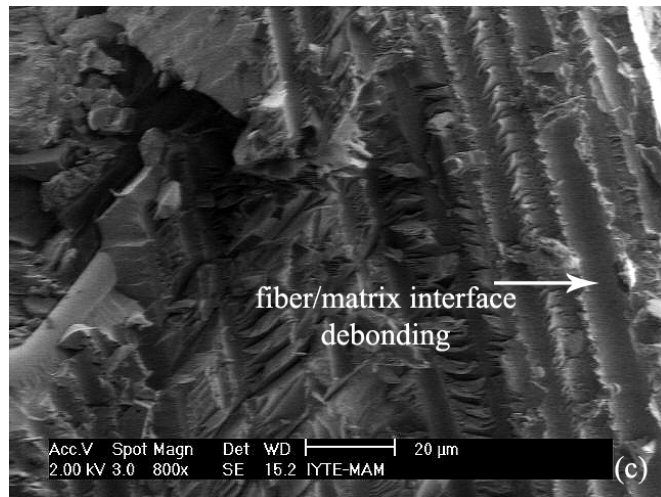
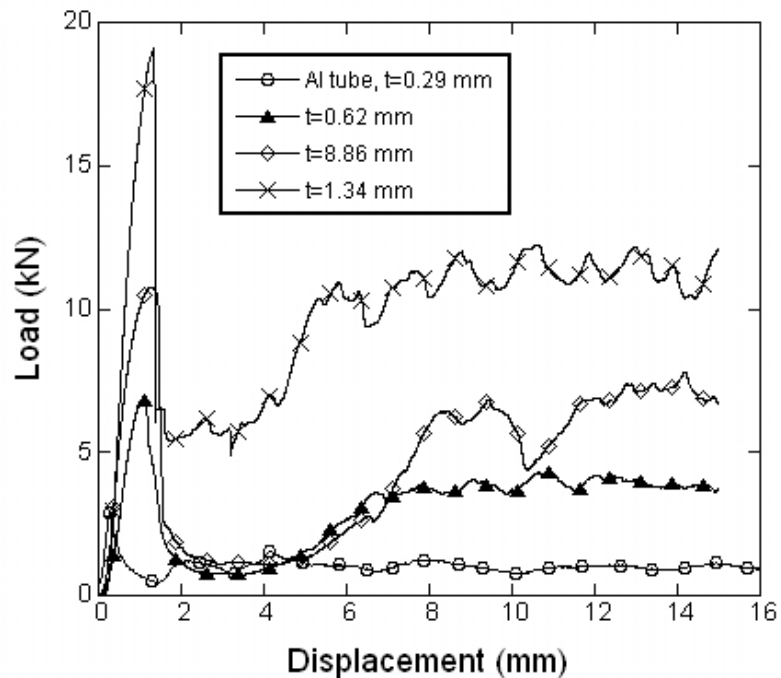


Figure 6.8. Micrographs showing (a) a crack on the surface of a tube, formed as result of fiber and matrix fracture b) a broken fiber and c) fiber/matrix interface debonding in the crack region.

In Figures 6.9(a) and (b) the load-displacement and SAE curves of the empty composite tubes with different thickness and empty Al tube are shown for the comparison purposes. In these curves, only the tubes showing progressive crushing mode are included. Both maximum and mean loads of the tubes increase with tube thickness hence tube mass (Figure 6.9(a)). While SAE values of the tubes with thickness of 0.62 and 0.86 mm are very similar, 1.34 mm thick tube shows relatively higher SAE values (Figure 6.9(b)). It is also noted in Figure 6.9(b) that Al tube of 0.29 mm in thickness and 27 mm in length shows relatively low SAE values as compared with composite tubes. The crushing mode of the same Al tube was previously investigated by Toksoy et al. (2005). It, in its empty form, crushes in the diamond mode of deformation. Figure 6.10(a) further shows the variation of tube mass with maximum and mean loads of the composite tubes with 45/45 fiber orientation. Tube mass is used in this graph rather than tube thickness, since tube mass is a measure of both volume and density of the tube and form a basis for the comparison of SAE values. It is further an average property while thickness is measured locally. As seen in this figure, increase in tube mass increases the maximum and mean loads of the composite tubes. Although the maximum loads are not affected by the failure mode, the mean load values are relatively low for the catastrophic failure mode as seen in Figure 6.10(a). The SAE values of the composites calculated at 50% deformation shows a weak dependence to

the tube mass when it is calculated using mean crush force (N/kg). The average SAE value of the composite tube based on the mean crush force is about 1.65 N/kg as shown in Figure 6.10(b). The use of mean crush loads in the calculation rather than calculating SAE over the all displacement range also reflects a more accurate energy absorption calculation since the mean crush force is almost constant in the progressive crushing region. Therefore, one may consider it as a basis for the comparison as well as a method for the calculation of SAE values of the composite tubes providing that it does not change significantly with the displacement. This is also valid for the empty Al tubes. Figure 6.11 shows the variations of load, mean crush load and SAE values (calculated using mean crush load) of investigated Al tube with displacement. After the initial peak load, similar to the composite tubes, mean crush load changes slightly with displacement between 1.02 kN and 1.11 kN. Similarly, SAE values based on the mean crush force also show weak dependence of the displacement in the same region, varying between 0.60-0.64 N/kg. Figure 6.11 also shows few crushing features of empty Al tube. The rising part of the load-displacement curve at the later stages of the deformation seen in this curve corresponds to the densification region of the diamond lobes formed progressively until 22 mm displacement. The number of peak maximums also corresponds to the total number of lobes or folds formed.



(a)

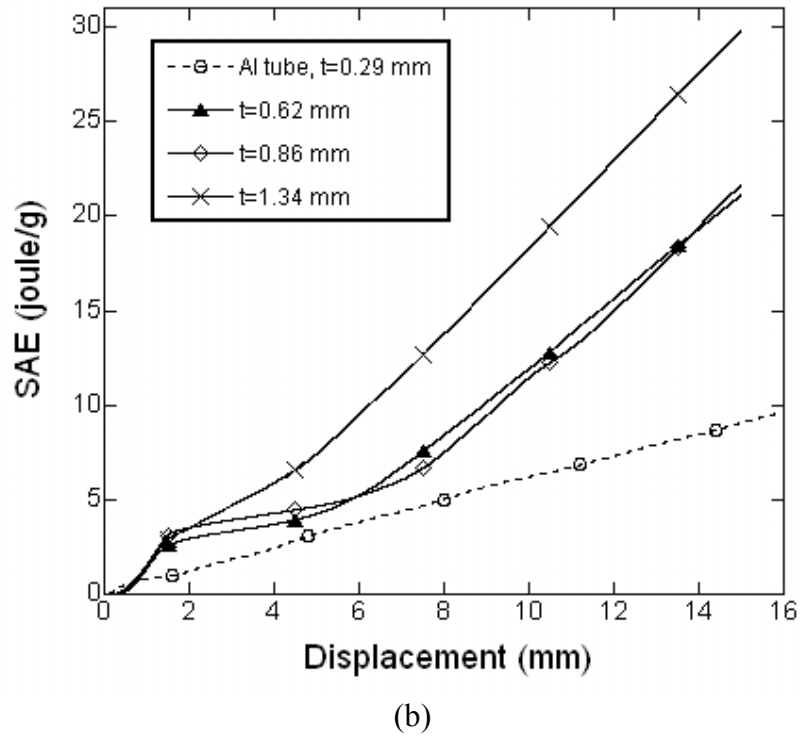
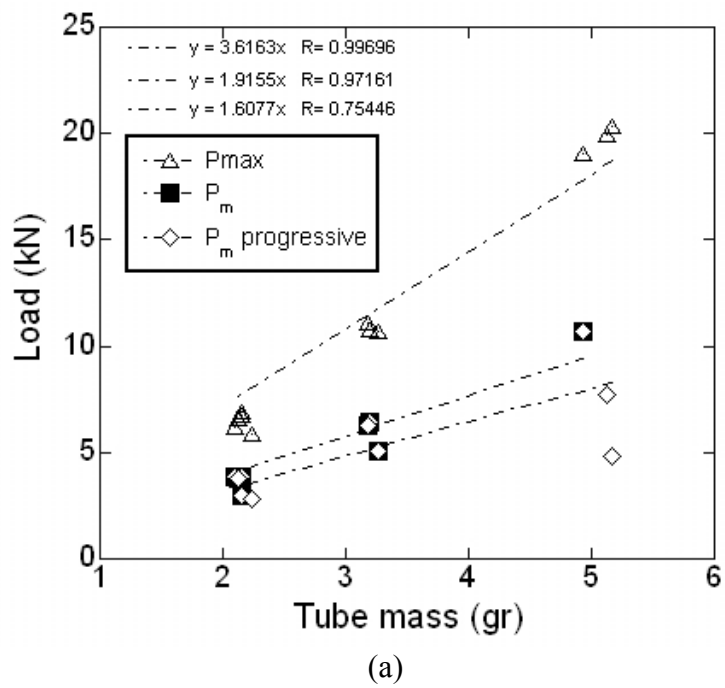
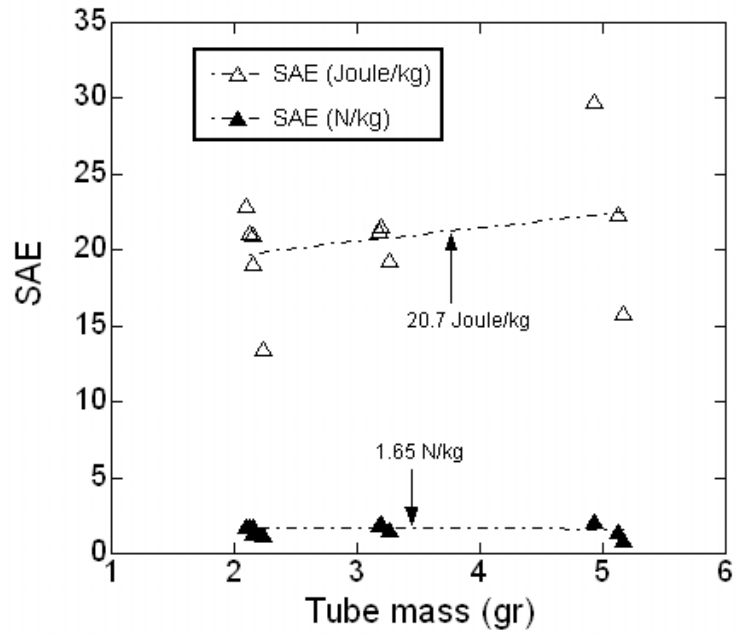


Figure 6.9. Comparison of the (a) load and (b) SAE values of the empty composite tubes of different thickness and empty Al tube.





(b)

Figure 6.10. (a) Effect of the tube mass on the maximum and mean loads and (b) SAE values of empty composite tubes with 45/45 fiber angle.

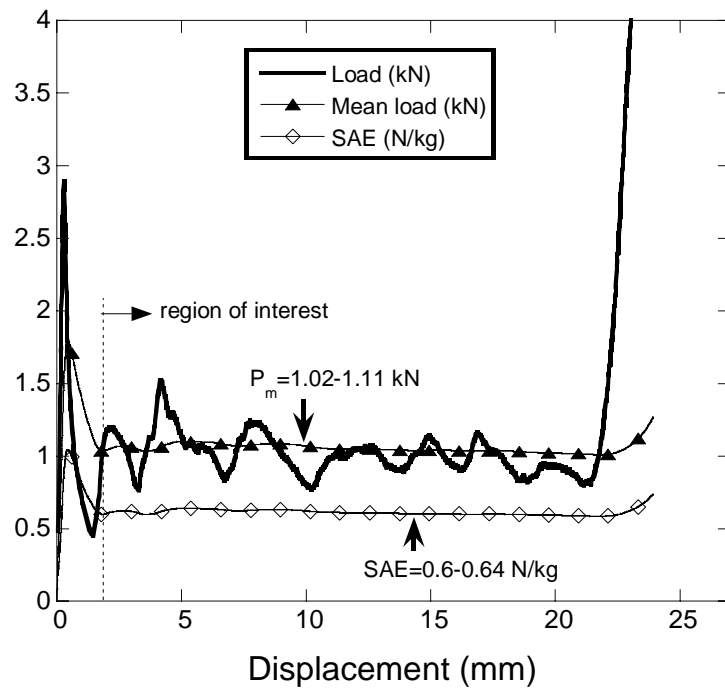


Figure 6.11. Load, mean load and SAE basing on the mean load vs. displacement curves of empty Al tube of 27 mm in length and 0.29 mm in thickness

6.1.2. Empty Al and Composite Hybrid Tubes

Six compression tests were conducted on Al and composite (45/45 fiber orientation and $t=0.53-0.72$ mm) hybrid tubes and the typical load-displacement curves of these tests are shown in Figure 6.12. Two deformation mechanisms are observed; progressive crushing and compression shear. The measured compression test parameters are also tabulated in Table 6.2. Similar to empty composite tubes, compression shear mode decreases the mean crushing loads and corresponding SAE values. The compression shear failure is also found to be promoted at low mass of hybrid tubes as shown in Figure 6.13(a). The same figure also shows a trend of increasing maximum and mean loads with increasing tube mass. The variation of tube mass in each sample may partly be due to a higher average tube thickness than the measured tube thickness and a higher amount of adhesive (polyester) used between composite and Al tube. The latter may provide a good bonding between the tubes hence promotes progressive crushing. The effect of crushing mode on the SAE values of the hybrid tubes is shown in Figure 6.13(b). As seen in this figure, tube samples failed by compression shear have relatively low SAE values, around 0.8 N/kg, while progressive crushing mode results in higher values of SAE, ranging between 1.25 and 1.6 N/kg. The average SAE value of four tests of progressive crushing is found 1.426 N/m. The empty composite tubes having a similar composite tube thickness with hybrid tube however have higher average SAE value, 1.7 N/kg (see Figure 6.13(c)). However, as is expected hybrid tubes have higher SAE values than empty Al tubes as shown in Figure 6.13(c).

Table 6.2. Compression test results of Al-Composite hybrid tubes.

Specimen code	Maximum Load (kN)	Mean load at %50 Deformation (kN)	Deformation mechanism	Energy absorbed (joule)	SAE (joule/g)	SAE (N/kg)
TTE1.1	10.921	6.4451	Progressive crushing	90.46	21.08	1.5024
TTE1.2	7.8313	3.2078	Compression shear	40.31	11.09	0.88369
TTE1.3	10.393	5.8589	Progressive crushing	82.01	19.18	1.3689
TTE1.4	11.195	7.2853	Progressive crushing	89.07	19.46	1.5907
TTE4.2	7.4400	5.1700	Progressive crushing	54.10	13.00	1.2458
TTE4.3	6.4000	3.1500	Compression shear	33.2	8.600	0.80153

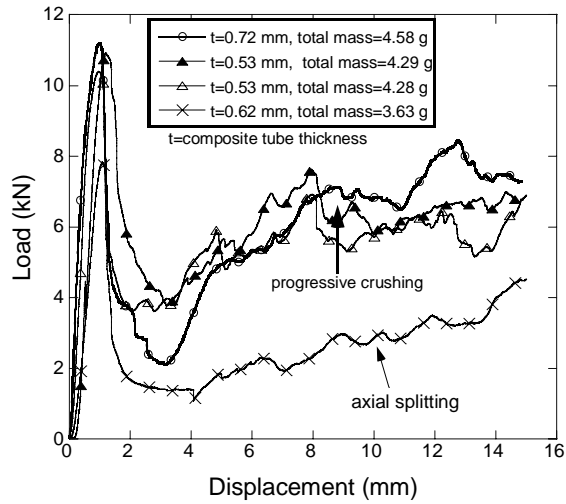


Figure 6.12. Load vs. displacement curves of hybrid tubes.

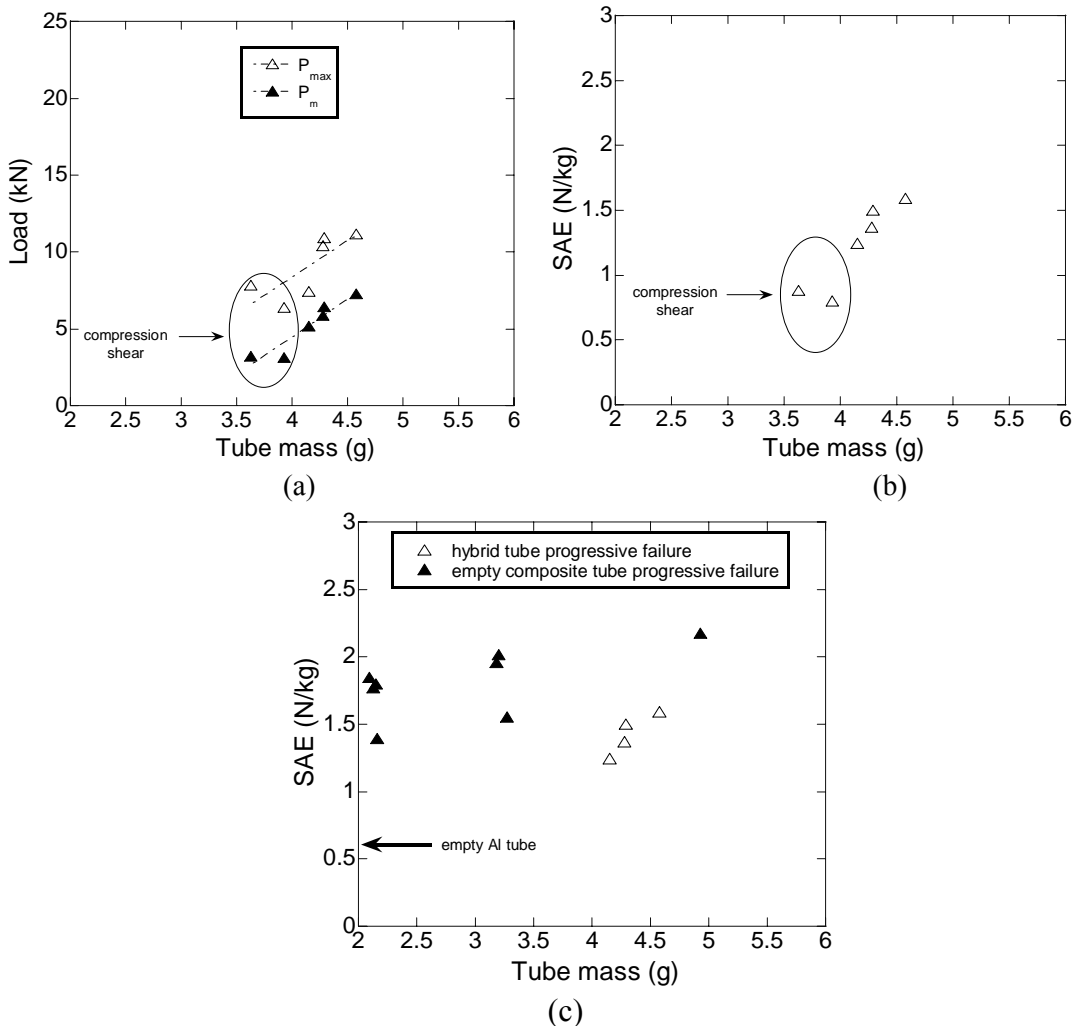
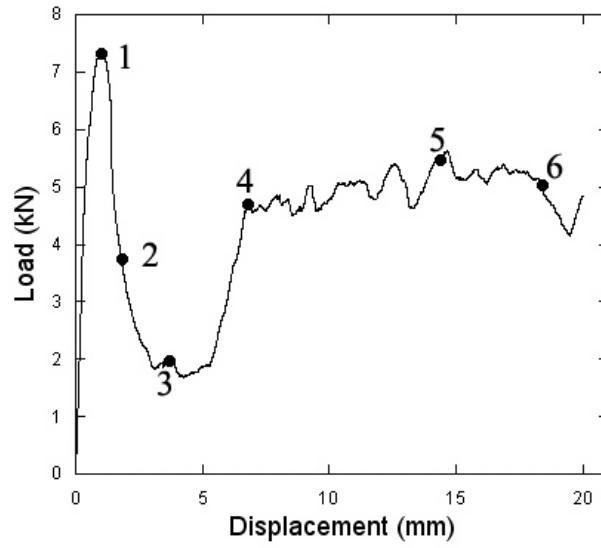


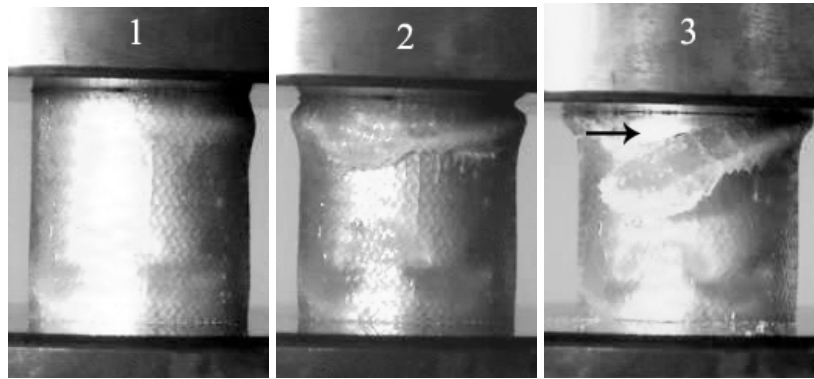
Figure 6.13. Effect of the tube mass on the (a) maximum and mean loads and (b) SAE values of hybrid composite tubes with 45/45 fiber angle and (c) comparison of SAE values of hybrid tubes with empty composite and Al tubes.

Figures 6.14(a) and (b) show the typical load-displacement curve and deformation history, as function of displacement, of a composite hybrid tube sample failed by progressive crushing, respectively. Following the initial peak load due to the localization of the deformation in an area near the one of the tube ends, the load decreases until number 3 in Figure 6.14(a). This behavior is very similar to that of the empty composite tube in the initial deformation region. In hybrid tubes it is also noted that metal tube folding triggers from the same place that composite tube deformation triggers for the progressive crushing. A relatively large composite detached from the Al tube surface is also seen in Figure 14(b). Similar to empty composite tube, after number 3 in Figure 6.14(b) deformation mode switches to progressive crushing mode and load values reaches a constant mean crush load as seen in Figure 6.14(a). Further deformation proceeds in outward splaying mode (Figure 6.14(b)).

Figures 6.15(a) and (b) show the typical load-displacement curve and deformation history as function of displacement of a composite tube sample failed by compression shear, respectively. The failure mode seen in Figure 6.15(b) at number 2 is a compressive shear line along the diagonal axis of tube. This results in detachment of a large composite piece from the surface of the Al tube as marked by arrows in Figure 6.15(b). In same figure at number 4, the proceeding diamond mode of Al tube deformation is clearly seen. Following the maximum load, the load values increases as the composite and Al tube deform together, seen at the later stages of the deformation (number 5 and 6 in Figure 6.15(b)). Therefore, contrary to the catastrophic failure modes reported previously by Ramakrishna and Hamada (1998), the load values progressively increases to the level of the progressive crushing mode because the crushing proceeds with deformation of composite and Al tube together following after detachment of the composite piece formed by compression shear failure.

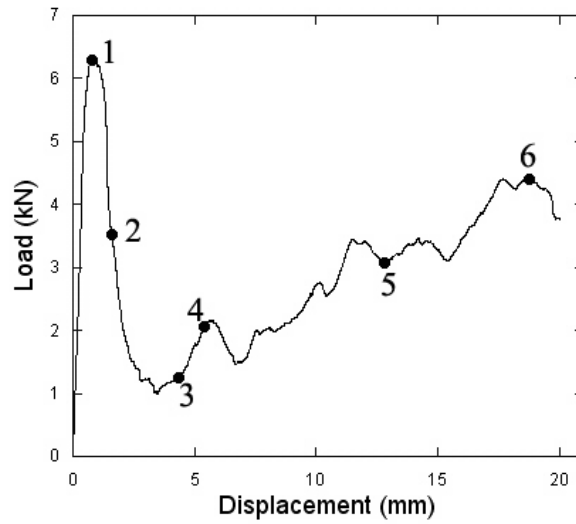


(a)

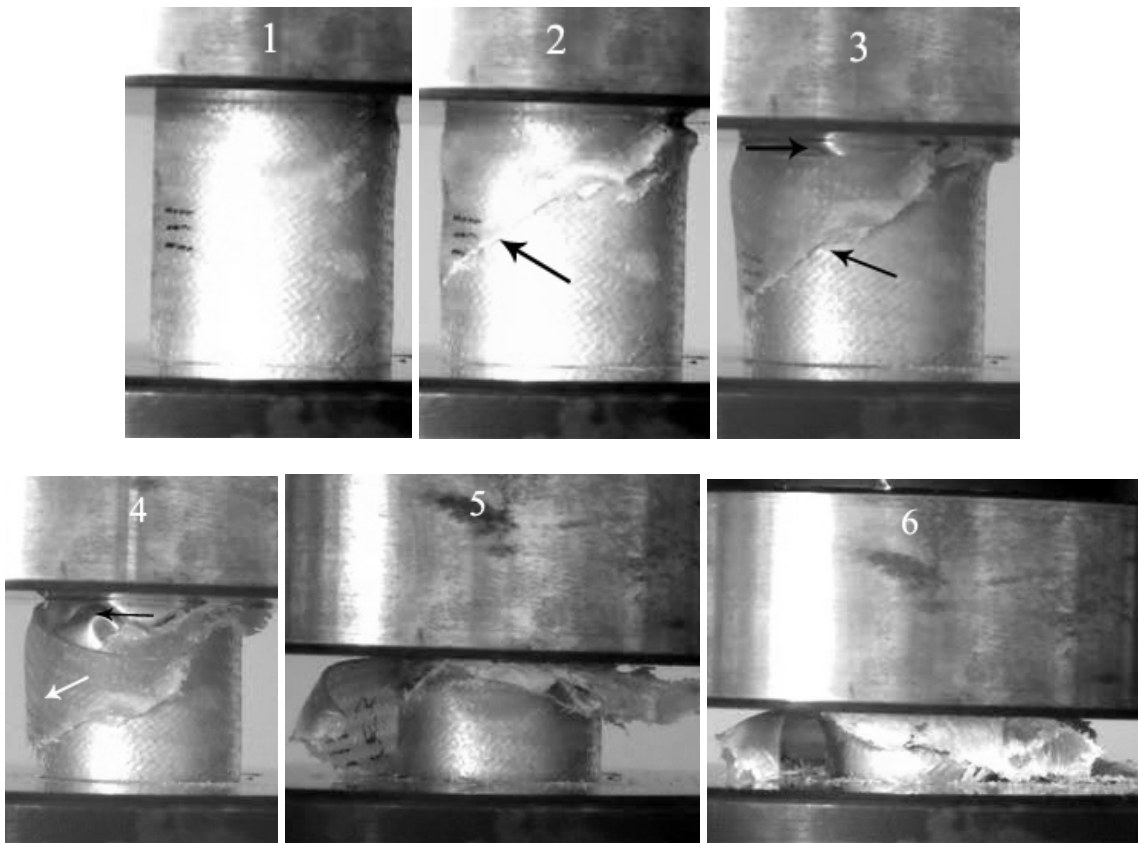


(b)

Figure 6.14. (a) Load-displacement curve of a hybrid tube with 45/45 fiber angle and (b) corresponding view of the deformation at various displacements numbered in (a) showing progressive crushing mode.



(a)

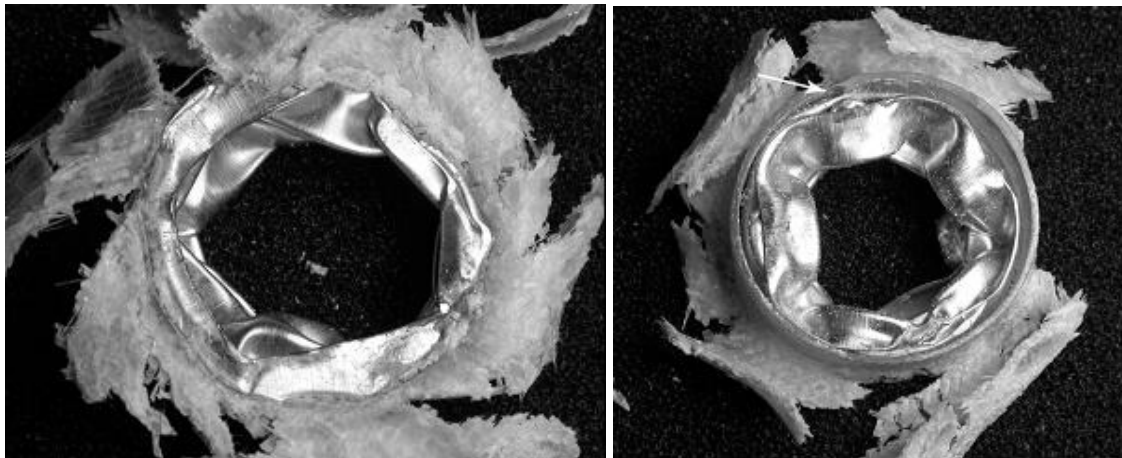


(b)

Figure 6.15. (a) Load-displacement curve of a hybrid tube with 45/45 fiber angle and (b) corresponding view of the deformation at various displacements numbered in (a) showing compression shear mode crushing mode.

Since the crushing modes of composite tube of the hybrid tube structure and empty composite tube are very much similar, it may be concluded that the

deformation of hybrid tubes is dominated by the composite tube deformation. The deformation mode of Al tube is however changed significantly in progressive crushing mode. Figures 6.16 (a) and (b) shows deformed shape of a hybrid tube in progressive crushing after 20 mm displacements, taken from back and front of the crushing direction, respectively. For comparison, in Figures 6.17(a) and (b) the back and front view of crashed empty tube are sequentially shown. Although the deformation mode of Al tube in hybrid tubes are similar to the diamond mode of empty tube, the shape and the geometry of the folds are not as homogeneous as the empty tube diamond mode. The change in the deformation mode of Al tube in hybrid tube is due to the prevention of the outer folding of the Al tube. This is clearly seen in Figure 6.16 (a), where Al tube folds are thoroughly through the inside. Although the empty tube shows a 4-sided diamond mode of deformation, the numbers of sides increases in the hybrid tube. Since the composite tube wall in the samples failed by compression shear is partly effective in constraining Al tube, the diamond mode deformation is more similar to that of empty Al tube except again the numbers of the fold sides increase in hybrid tube particularly at the later stages of the deformation (Figure 6.18).



(a)

(b)

Figure 6.16. Pictures of the progressive crushed hybrid tube after 20 mm deformation in (a) from back and (b) from front.

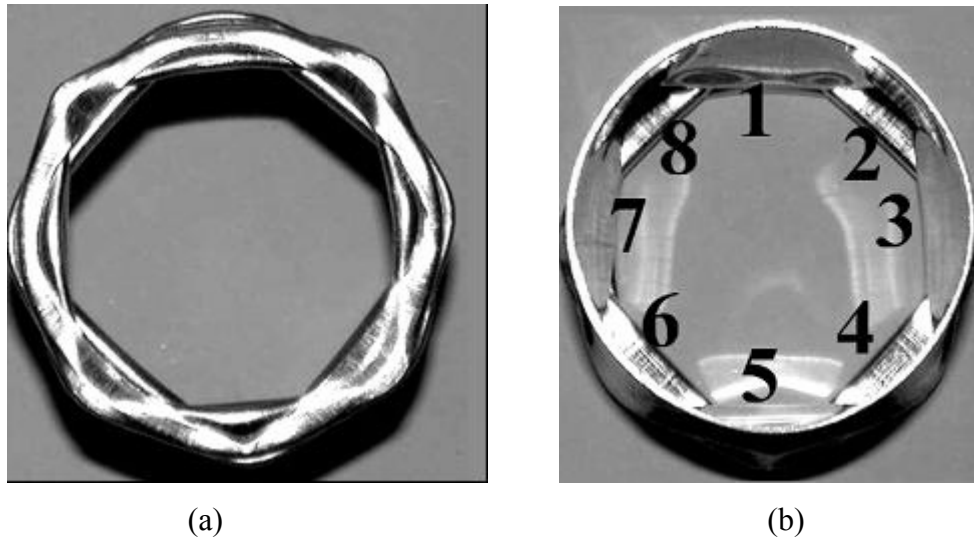


Figure 6.17. Partially crushed empty Al tube: (a) back and (b) front views.

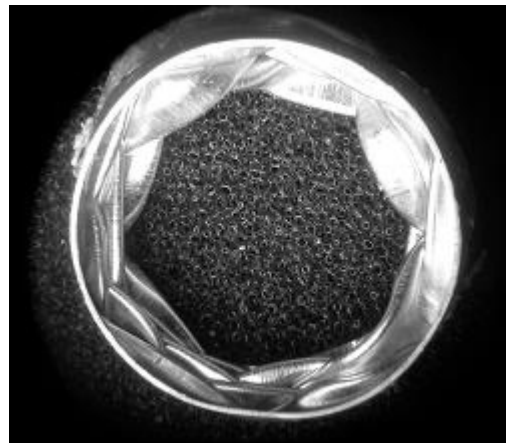


Figure 6.18. Pictures of the hybrid tube after 20 mm deformation in Figure 6.14 taken from the backside of the crushing.

Figure 6.19 shows the load-displacement curves of hybrid tube deforming in progressive crushing together with empty composite and Al tube and the mathematical sum of the loads of the empty composite and Al tube. The higher load values of hybrid tube that empty composite load + empty Al tube load basically shows an interaction effect between Al and composite tube. The interaction as stated above a result of the change of deformation mode in Al tube due to the constraining effect of the composite tube. The interaction is also seen in Figure 6.20, in which the SAE values of the hybrid tubes are compared with those of empty composite and Al tube and composite+Al tube. The hybrid tube shows higher SAE values than those of composite+Al tube. Since the energy absorption in the initial region of the deformation

is predominantly affected by the triggering process, the hybrid tube shows higher SEA values than empty composite tube, while at increasing displacements SAE values of the empty tubes exceed those of hybrid tubes (see circle in Figure 6.20). A simple calculation based on the average mean loads of empty composite, Al tubes and hybrid tubes shows an increase in the mean crush load of hybrid tubes as high as 2.3 times of the mean crush load of empty Al tube. This values is also comparable with experimentally found strengthening coefficients of Al foam filled Al tubes, ranging between 1.7 and 2.8, the higher value of strengthening arises from the use of adhesive between foam filler and tube (Toksoy et al. 2005).

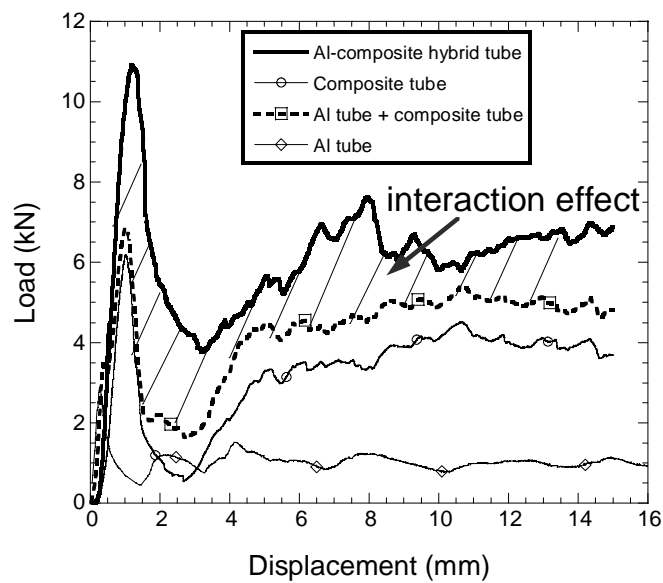


Figure 6.19. Comparison of crushing loads of hybrid tubes with empty composite and composite tubes and their sum.

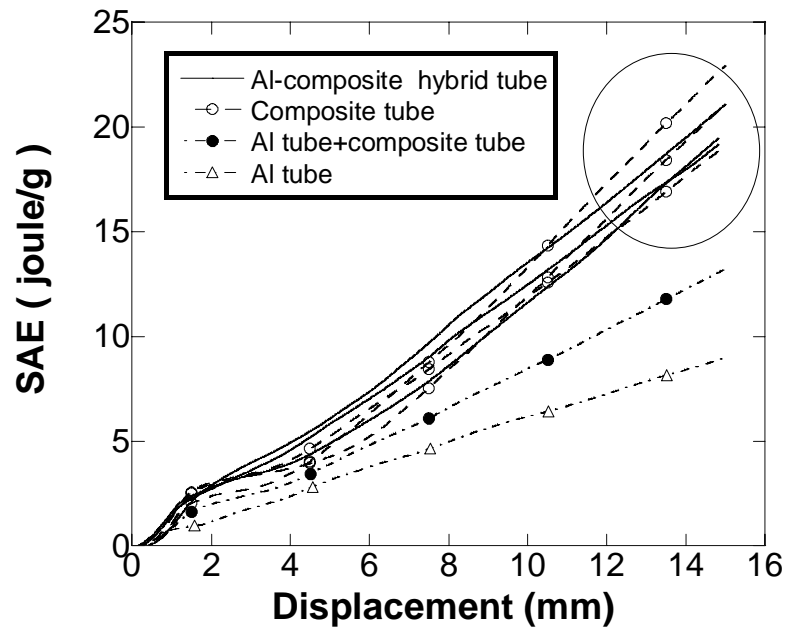


Figure 6.20. Comparison of SAE values of the hybrid tubes with empty composite and Al tubes and their sum.

6.2. Compression Behavior of Al-Foam Filled Tubes

6.2.1. Al-Foam Filled Composite Tubes

The compression load-displacement curves of Al foam filled and empty tube are shown in Figure 6.21. As the foam density increases, as clearly seen in these curves, load values increase. It is also noted in Figure 6.21 that foam filling (a) induces a continuously increasing load values following the initial peak loads and (b) reduces the magnitude of load drop following the peak load. The latter suggests that foam imposes a more stable tube crushing triggering and deformation. This is also supported by that the failure due to the compressive shear is not observed in foam filled composite tubes. The failure mechanisms of a foam filled tube are seen in Figures 6.22(a) and (b) which is very similar to the progressively crushing empty tubes except the magnitude of load drops following the peak load decreases in the filled tubes as noted previously. The compression tests results of the foam filled tube are listed in Table 6.3. As noted in this table also in Figure 6.23, foam density has a pronounced effect in increasing maximum and mean crush loads of the composite tubes.

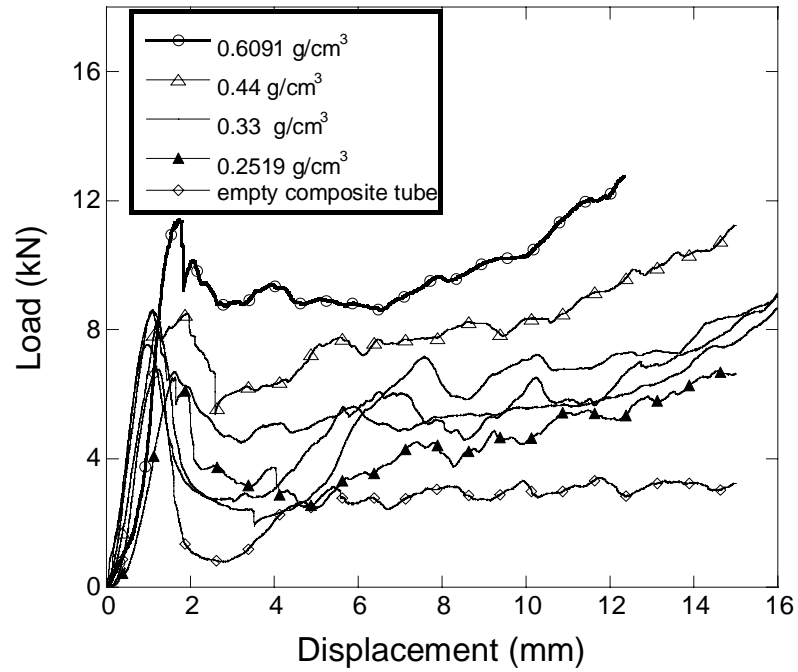
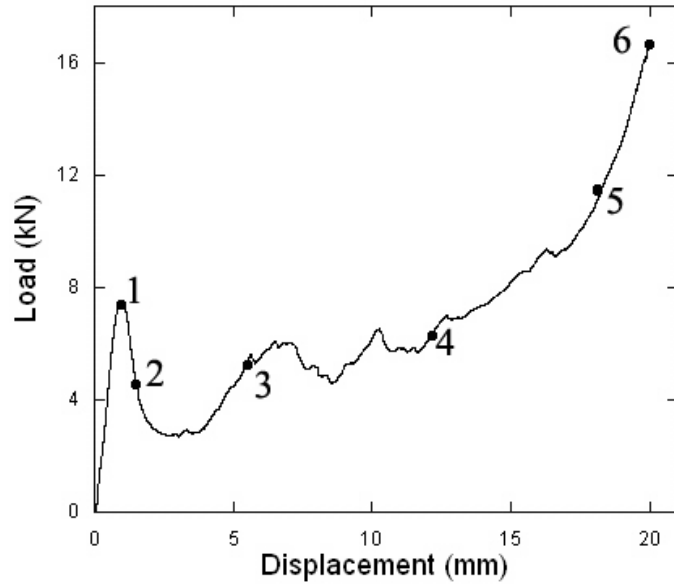


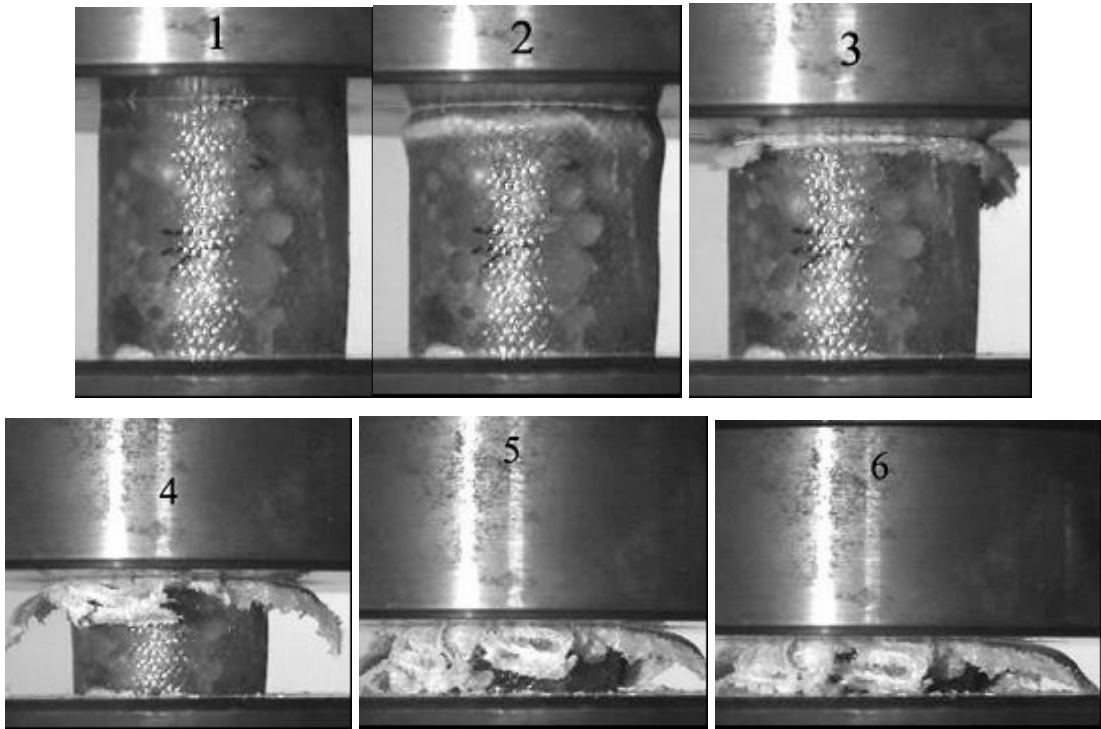
Figure 6.21. Load-displacement curves of foam filled and empty composite tubes.

Table 6.3 Compression test results of Al-foam filled composite tubes.

Specimen code	Foam Density (g/cm ³)	Maximum Load (kN)	Mean load at %50 Deformation (kN)	Deformation mechanism
TF1-2	0.2519	6.71	5.32	Progressive crushing
TF1-4	0.2904	8.53	7.79	Progressive crushing
TF4-2	0.32	10.18	7.27	Progressive crushing
TF4-6	0.33	9.96	7.00	Progressive crushing
TF4-7	0.33	9.68	6.46	Progressive crushing
TF1-5	0.3410	9.36	8.19	Progressive crushing
TF1-9	0.4410	11.24	9.09	Progressive crushing
TF1-13	0.6091	12.749	10.76	Progressive crushing



(a)



(b)

Figure 6.22. (a) Load-displacement curve of a foam filled (0.33 g/cm^3) tube with 45/45 fiber angle and (b) corresponding views of the deformation at various displacements numbered in (a) showing progressive crushing mode.

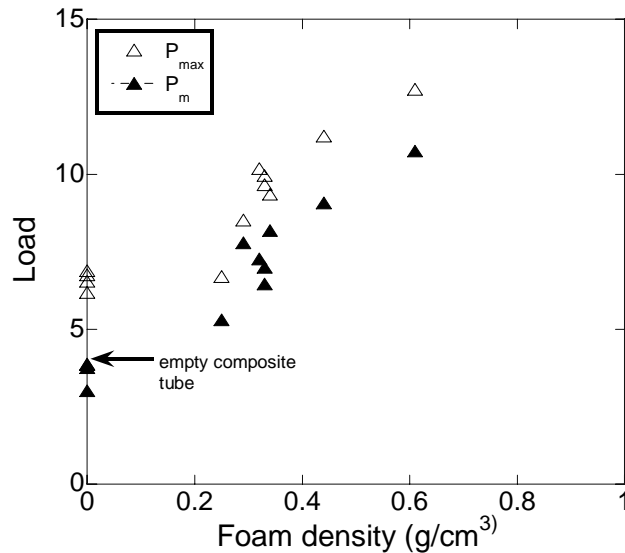
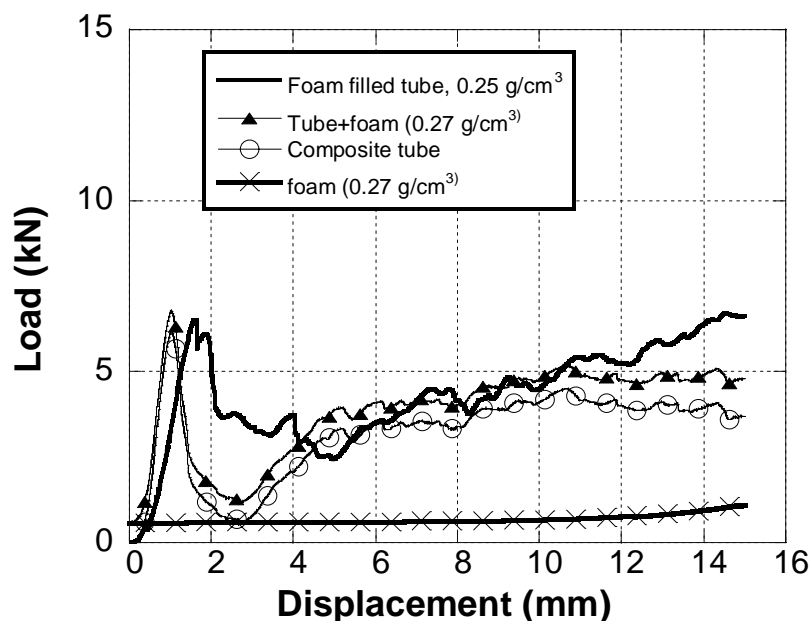


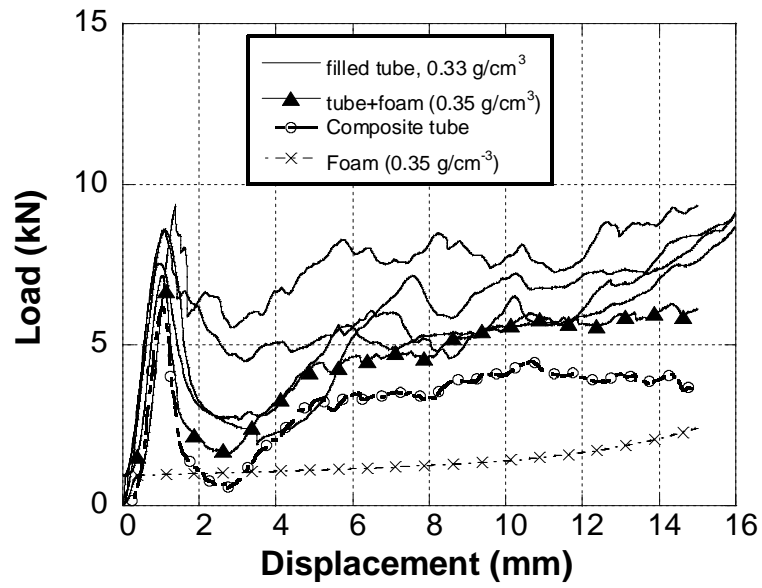
Figure 6.23. Maximum and mean crush loads vs. foam densities in filled and empty tubes.

In Figures 6.24 (a), (b) and (c) the compression load values of 0.25, 0.33 g/cm³ and, 0.44 and 0.27 g/cm³ foam filled tubes are compared with corresponding crush loads of empty composite and Al foam and their mathematical sum. In Figures 6.24, two different effects of foam filling are detected. First, although foam filling increases the crush loads just after the peak load, it is ineffective to increase the crushing loads of the composite tube in the progressive crushing region as seen in Figure 6.24(a) for 0.25 g/cm³ foam filling. Second, the foam filling results in crushing loads higher than that of the sum of crushing loads of empty tube and foam as depicted in Figure 6.24(c) for 0.44 and 0.29 g/cm³ foam filled composite tubes. The results for the same density foam filling even show both trends. In Figure 6.24(b) although two test results of 0.33 g/cm³ foam-filling show higher crush loads than the sum of crush loads of foam and tube, other two tests show similar crush loads of foam filled tubes with the sum of crush loads of foam and tube. In Figure 6.22(b) it is also noted that the magnitude of the load drop following the peak load is higher in the foam filled tubes of lower crushing loads in the progressive crushing region. Based on these findings following deformation mechanisms are proposed. First, when the tube crushing deformation triggers, the foam and tube separates or partially separates and deformation of the tube and foam proceeds separately, leading to no interaction between tube and foam. Second, tube and foam deform together at all displacements, resulting in an interaction effect that increase the

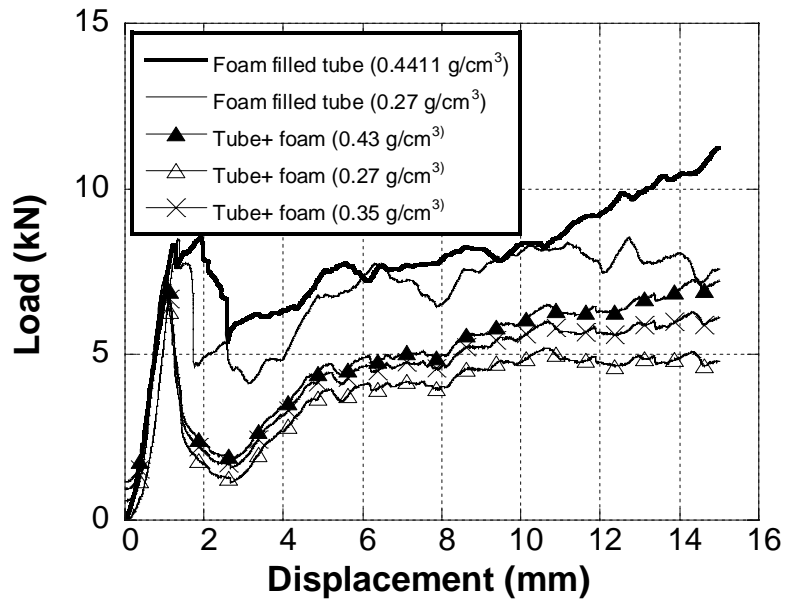
foam filled tube crush loads over the sum of the crush loads of empty tube and foam. The interaction effect may be partly because the composite tube confines the foam core (Poisson ratio of Al foam is greater than 0) and the deformation of tube drive the foam deformation in and that has higher foam plate load than the average foam plateau load. In free form, the foam deformation starts from the weakest linkage. Therefore, the adhesive between foam and tube may play a critical role in the deformation of foam filled tubes. The effect of interaction on the SAE values of filled tube is seen in Figure 6.25. At a similar foam density, in the case of interaction, filled tube shows higher SAE values than foam+tube but still it has lower values than empty composite tube. With the limited interaction at the initial stage of deformation, filled tube show the same SAE values with those of foam+tube if one disregards the initial high crushing loads experienced by the foam filled tube. Finally it should be noted that the variations in foam crushing loads at the same foam density and in composite tube at the same weight may also be responsible for the measured two different modes of deformation in filled tubes. To clarify these effects, systematic tests will be conducted on the foam filled tubes in future.



(a)



(b)



(c)

Figure 6.24. Comparison of foam filled tube crush loads with empty composite and Al foam and their sum (a) 0.25 g/cm^3 , (b) 0.33 g/cm^3 and (c) 0.44 and 0.27 g/cm^3 .

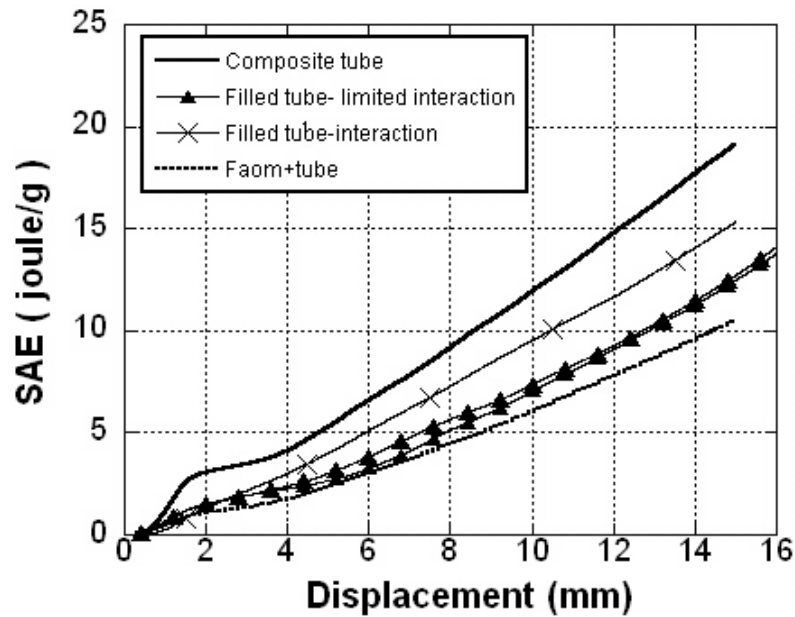


Figure 6.25. Comparison of SAE values of the foam filled tubes with empty composite and the sum of composite tube and the foam.

6.2.2. Al-Foam Filled Al-Composite Hybrid Tubes

Three hybrid tubes were filled with an average foam density of 0.40 g/cm^3 , ranging between $0.39\text{-}0.41 \text{ g/cm}^3$. The load-displacement curves of the foam filled hybrid tubes are shown in Figure 6.26 together with those of empty hybrid and empty composite tube. As is seen in this figure, foam filling is not effective in increasing load values of empty hybrid tube until about at large displacements 10 mm over empty hybrid tubes. The load-displacement curves of hybrid tubes, the sum of the crush loads of composite and Al tube and foam and foam filled composite and Al tube are shown in Figures 6.27(a) and (b), respectively. The hybrid tube shows very similar crush load values with the sum of the crush loads of composite tube, Al tube and Al foam (Figure 6.27(a)). Al foam densities used for comparison is noted to be higher the density of foam used in the filled tubes, but the difference between them is so small to affect significantly above findings. Foam filled hybrid tube although shows higher crushing loads than foam filled Al tube, it shows lower crushing loads than filled composite tube at the similar foam densities (Figure 6.27(b)). Again, the difference in the foam densities between filled tubes is small and although it will be effective in lowering and raising the curves, it will not change the general trends.

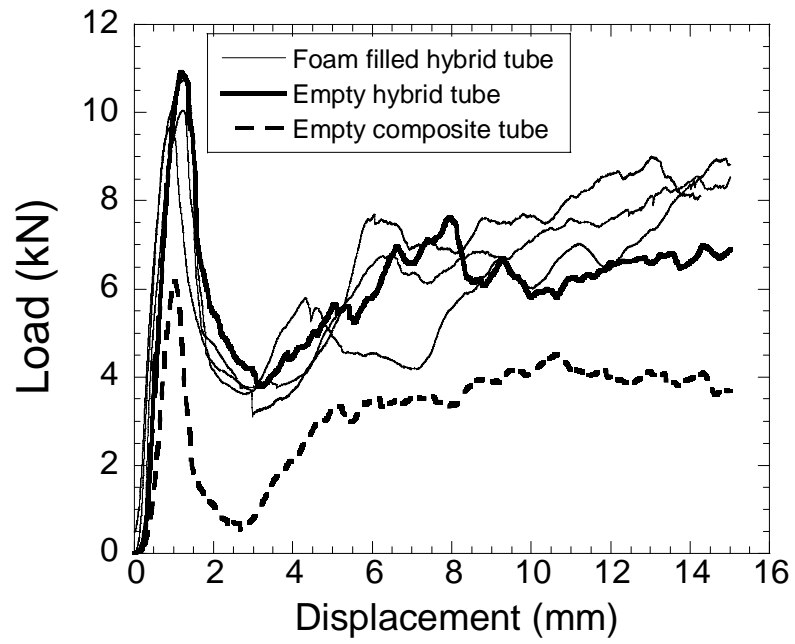
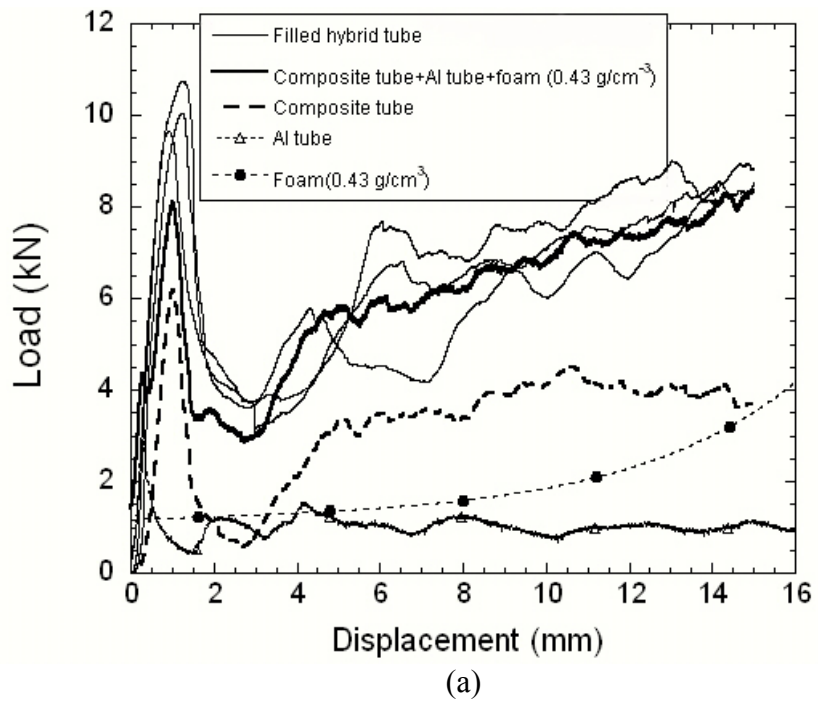


Figure 6.26. Load-displacement curves of foam filled hybrid, empty hybrid and composite tubes.



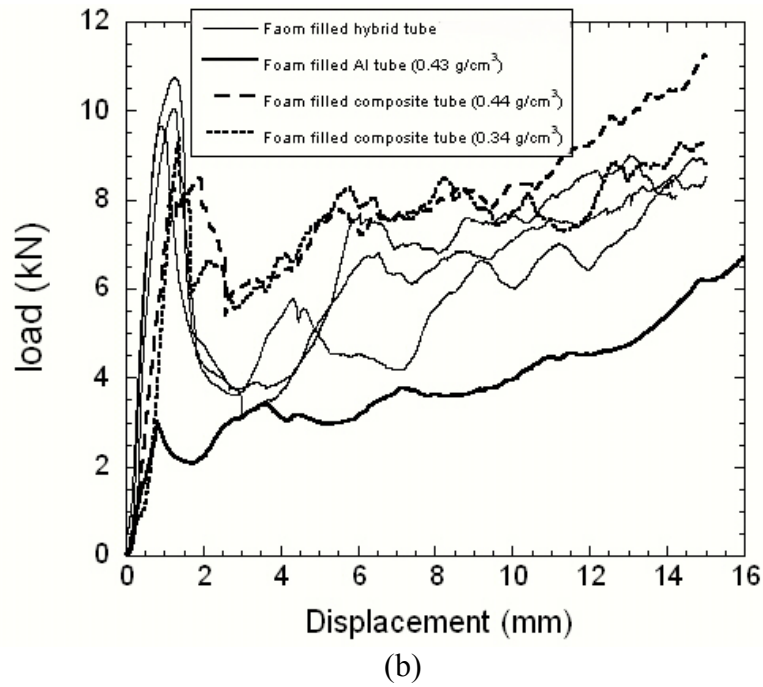


Figure 6.27. Comparisons of load-displacement curves hybrid tube with (a) the sum of crush loads of composite tube, Al tube and foam and (b) foam filled composite and Al tubes.

In hybrid tubes, the folding of metal tube will be restricted both by the foam filler and composite tube. The resistance imposed by the filler and the composite is also effective in the initial stages of the deformation since it is found that the composite fails by axial cracks at later stages of deformation as shown in Figure 6.28(a). In empty hybrid tubes, although metal tube crushes in inhomogeneous diamond mode, it deforms in concertina mode in the foam filled hybrid tube as depicted in Figure 6.28 (b). This deformation mode is very much similar to the deformation mode of Al foam filled Al tubes (Figure 6.29(a)) as previously noted by Kavi et al. (2004). Although the concertina folds in the foam filled Al tube are uniform in shape and thickness and they are mostly outward of the filler, in hybrid tubes the folds are not as regular as in case of foam filled Al tube and tend to form through the inside of the foam (Figure 6.29(b)). The irregular folds are most probably resulted from the fractured composite pieces entrance between the fold as depicted in Figure 6.29(c). This also confirms that although composite fails by axial cracks it remains attached to Al tube and provides a partial confinement for the tube deformation. This also explains the higher crushing loads of foam filled hybrid tubes than those of foam filled Al tube at the similar foam densities.

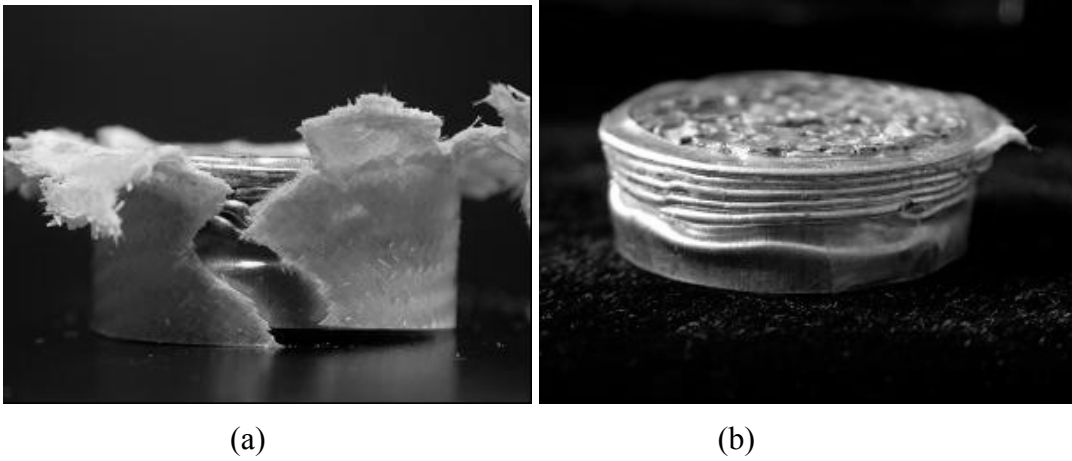


Figure 6.28. (a) Image of the Al-foam filled hybrid tube after compression (b) deformation mechanism of the Al tube of the foam filled hybrid tube,

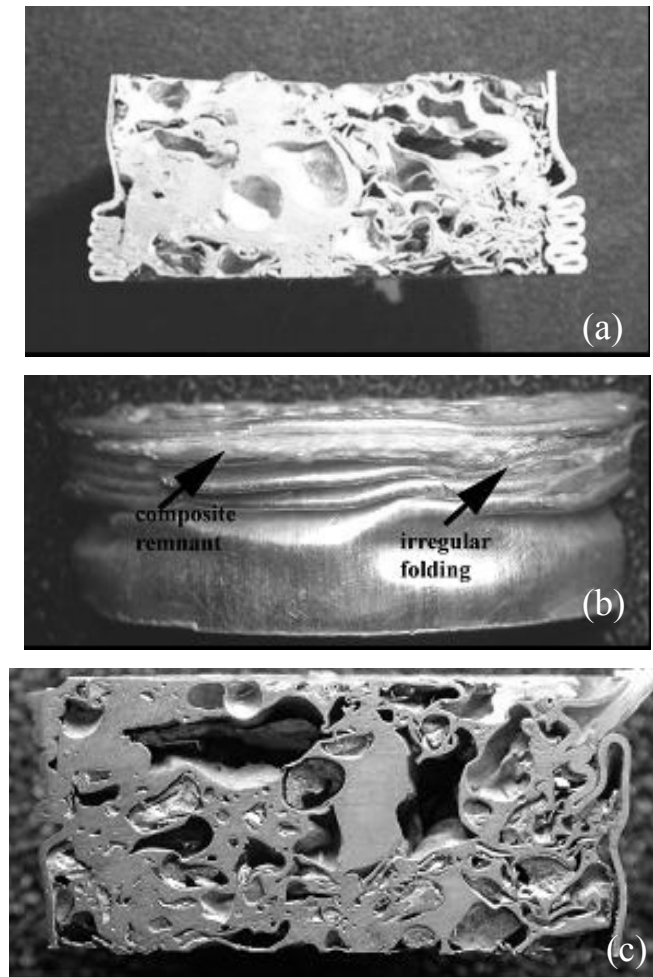


Figure 6.29. Deformed views of (a) foam filled Al tube (Kavi et al., 2004) and (b) and (c) foam filled hybrid tube

In Figure 6.30, the SAE values of empty and foam filled hybrid and composite tubes are shown as a function of displacements. Based on the mean crush load SAE calculation, empty composite tubes show higher energy absorption than hybrid tubes as explained previously. This is also seen in Figure 6.30 if one compares the slopes of SAE-displacement curves of empty composite and hybrid tubes. A similar but more pronounced effect is also seen in the foam filled composite and hybrid tubes. In foam filled tubes with interaction effect, foam filling results in higher SAE values than hybrid tubes.

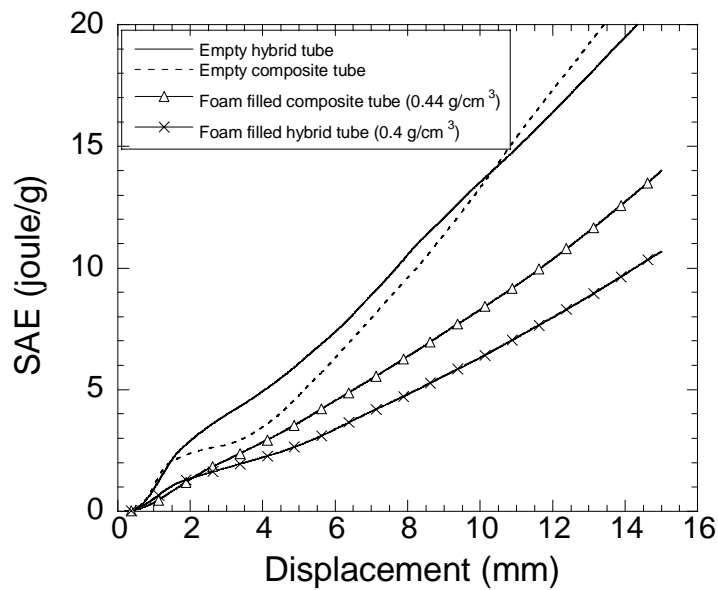


Figure 6.30. SAE vs. Displacements of empty hybrid and composite tube and foam filled hybrid and composite tubes.

CHAPTER 7

CONCLUSIONS

An experimental study has been conducted in order to determine the effects of foam filling on the composite and hybrid (Al metal and composite) composite tubes. Tubes and fillers used in the experiments were prepared using filament winding and tube rolling, and foaming from powder compacts methods, respectively. The quasi-static crush tests were conducted on the empty, hybrid and foam filled E-glass fiber fabric (2x2 twill fiber construction of 165 g/m^2 areal density) composite tubes with 45/45 fiber angle. The deformation sequences of the tubes were recorded during the tests in order to identify the crushing modes of tubes. Based on the experimental results the following can be concluded

1. Two failure mechanisms, progressive crushing and catastrophic failure (compression shear) were observed in the testing of empty composite tube. The progressive crushing mode led to higher crushing loads hence Specific Absorbed Energies (SAE).
2. The predominant progressive crushing mode of empty tubes of thinner wall section was attributed to the surface end inhomogeneity. This was supported by a higher frequency of compressive failure mode in the thicker tubes.
3. Empty composite tubes showed almost a constant mean crush load in the progressive crushing region, which allowed the calculation of SAE values based on the mean crush load.
4. In hybrid tube, the deformation mode of Al tube was found to be a more complex form of the diamond mode of deformation, leading to higher SAE values than the sum of the SAEs of empty composite and empty metal tube. The increased load and SAE values of hybrid tubes were attributed to the interaction between composite and metal tube.
5. Based on the SAE mean crush load calculation it was found that empty composite tube absorbed more energy than hybrid tube, if only the progressive crushing mode was taken into account.

6. The foam filling of the composite tubes came with two different results. It increased the foam filled tube crush loads over the sum of the crush loads of empty composite and foam. In the latter case, although foam filling stabilized the initial region of the load-displacement curves of the filled tubes, it was found to be not effective in increasing foam filled tube crush load over the sum of the crush loads of empty composite and foam in the progressive crushing region. These two effects were discussed in terms of possible interactions between composite tube and foam.
7. The foam filling of hybrid composite tubes was found to be ineffective in increasing crush loads and hence SAE values over the sum of the crush loads of composite tube, Al tube and foam. The observed failure mechanism of the filled hybrid tubes were found to be in accord with the above statement in that composite tubes failed by axial splitting due the resistance imposed by the foam filler to Al metal tube folding hence ineffective in effecting metal tube folding.

REFERENCES

- Abramowicz, W. and Jones, N. 1984. "Dynamic axial crushing of circular tubes", *International Journal of Impact Engineering*, 2, 263-81.
- Abramowicz, W. and Jones, N. 1986. "Dynamic progressive buckling of circular and square tubes", *International Journal of Impact Engineering*, 4, pp. 243-269.
- Al-Hassani, S.T.S., Johnson, W. and Lowe, W.T. 1972. "Characteristics of inversion tubes under axial loading". *J.Mech.Eng.Sci.*, 14 (6), pp. 370-381.
- Alexander, J. M. 1960. "An approximate analysis of the collapse of thin cylindrical shells under axial loading", *Quarterly Journal of Mechanics and Applied Mathematics*, 13, pp. 10-15.
- Andrews, K.R.F., England, G.L. and Ghani, E. 1983. "Classification of the axial collapse of cylindrical tubes under quasi-static loading.", *Int.J. Mech.Sci.*, 25 (9/10), pp. 687-696
- Babbage, J.M. and Mallick, P.K. 2005 "Static axial crush performance of unfilled and foam-filled aluminum composite hybrid tubes", *Composite Structures*, 70, pp. 177-184
- Banhart, J. and Baumeister, J. 1998. "Production Methods for Metallic Foams", MSR Symposium Proceeding, San Francisco, Vol.521, pp.121-132
- Banhart, J. 1998 "Production Methods for Metallic Foams", Metal Foam Symposium, Symposium Proceedings, (Delaware, Oct. 7-8, 1997), Verlag Pub. Bremen,
- Banhart, J. 2000. "Manufacturing routes for metallic foams", *JOM*, 52 (12), pp.22-27.
- Banhart, J. 2000. "Metallic foams: challenges and opportunities", Eurofoam, (MIT-Verlag, Bremen), pp. 13-20.
- Baumeister, J. and Schrader, H. 1992. US Patent No.5151246
- Baumgartner, F., Duarte, I. and Banhart, J. 2000 "Industrialization of powder compact foaming process", *Advanced Eng. Mater.*, 2, pp.168-174.
- Chiu, C.H., Tsai, K. and Huang, W.J. 1998. "Effects of braiding parameters of energy absorption capability of triaxially braided tubes", *J.Comp. Mater.*, 32 (21), pp.1964-1983
- Gergely, V. and Clyne, B. 2000. "The Formgrip process: foaming of reinforced metals by gas release in precursors", *Adv. Eng. Mater.*, 2, No:4, pp. 175-178.

- Gibson, L.J. and Ashby, M.F. 1997., *Cellular Solids: structures and properties*, Second edition, Cambridge University Press,
- Gibson, L. J. and Simone, A. E. 1997. "Aluminum foams: structure and properties", Mechanics and materials seminar, 3 April, 1997.
- Guillow, S.R., Lu, G. and Grezbieta, R.H. 2001. "Quasi-static compression of thin-walled circular aluminum tubes", *Int. J. Mech. Sci.*, 43, pp.2103-23.
- Hall, I.W., Güden, M. and Claar, T.D. 2002. "Transverse and longitudinal crushing of aluminum-foam filled tubes", *Scripta Materialia*, 46, pp.513-518.
- Hamada, H. and Ramakrishna, S. 1998. "Energy absorption characteristics of crash worthy structural composite materials" *Engineering Materials*, Vols.141-143, pp 585-620
- Hannsen, A.G., Langseth, M. and Hopperstad, O.S. 2002. "Crush behaviour of foam based components: validation of numerical simulations", *Advanced Engineering Materials*, 4, pp. 771-776.
- Harte, A. and Fleck, N. 2000. "Deformation and failure mechanisms of braided composite tubes in compression and torsion", *Acta Materialia*, 48, pp. 1259-1271.
- Harte, A., Fleck, N. and Ashby, F. 2000. "Energy absorption of foam-filled circular tubes with braided composite walls" *Eur.J.Mech. A/Solids* ,19 , pp. 31-50.
- Jimanez, M.A., Miravete, A., Larrode, E. and Revuelta, D. 2000. "Effect of trigger geometry on energy absorption in composite profiles", *Composite Structures*, 48, pp.107-111
- Jones, N. and Abramowicz, W. 1985. " Static and dynamic axial crushing of circular and square tubes", in *Metal Forming and Impact Mechanics.*, edited by Reid, S.R., (New york: Pergamon Pres), pp. 225-47.
- Kavi, H., Yüksel, S., Tanoğlu, M. and Güden, M., 2004. "Crushing behavior of aluminum foam filled aluminum tubes", 10th Denizli Material Symposium & Exhibition, 14-16 April, Conference Proceeding, pp. 42-49.
- Kavi, H. 2004. "Investigation of compression mechanical behavior of aluminum foam filled metal tubes", MS Thesis, Izmir Institute of Technology.
- Kathuria, Y.P. 2001 " Laser assisted aluminum foaming", *Surface and coatings Technology*, 142- 144, pp. 56-60.
- Kitazono, K., Sato, E. and Kuribayashi, K. 2004. "Novel manufacturing process of closed cell aluminum foam by accumulative roll-bonding", *Script. Mater.*, 50 ,pp. 495-498.
- Ko, F.K. 1998. "Braiding", in *Engineered Materials Handbook Vol.1*, edited by ASM International Handbook Commity, pp.519-528.

- Maiti, S. K., Gibson, L. J. and Ashby, M. F. 1984. "Deformation and energy absorption diagram for cellular solids", *Acta Metall.*, Vol. 32, 11, pp. 1963-1975.
- Martin, J.D. and Sumerak J.E. 1998. "Pultrusion", in *Engineered Materials Handbook Vol.1*, edited by ASM International Handbook Commity, pp.533-543.
- Mikkelsen, L.P. 1999. "A numerical axisymmetric collapse analysis of viscoplastic cylindrical shells under axial compression." *Int. J. Solids and Structures*, 36, pp. 643-668.
- Miyoshi, T., Itoh, M., Akiyama, S. and Kitahara, A. 2000. "Alporas aluminum foam: production process, properties, and applications", *Adv. Eng. Mater.*, 2, No:4, pp. 179- 183
- Peters, S.T. and Humphrey, W.D. 1998. "Filament Winding", in *Engineered Materials Handbook Vol.1*, edited by ASM International Handbook Commity, pp.503-518.
- Prakash, O., Sang, H. and Embury, J. D. 1995. "Structure and Properties of Al-Si Foam", *Mater. Sci. Eng.*, A199, pp. 195-203.
- Ramakrishna, S. and Hamada, H. 1998. "Energy Absorption Characteristics of Crash Worthy Structural Composite Materials", *Engineering Materials*. Vols.141-143, pp. 585-620.
- Reid, S.R., Reddy, T.Y. and Gray, M.D. 1986. "Static and dynamic axial crushing of foam filled sheet metal tubes", *Int. J. Mech. Sci.*, 23, pp. 295-322
- Roy, P.A. 1998. "Tube Rolling", in *Engineered Materials Handbook Vol.1*, edited by ASM International Handbook Commity, pp.569-574.
- Saito, H., Inai, R., Yokoyama, A. and Hamada, H. 2000. "Basic Study of Progressive Crushing Mechanism", *Engineering Materials*. Vols.177-180, pp. 321-326.
- Santosa, S. and Wierzbicki, T. 1998. "Crash behavior of box columns filled with aluminum honeycomb or foam", *Comp. Struct.*, 68, pp.343-67.
- Santosa, S., Wierzbicki, T., Hanssen, A.G. and Langseth, M. 2000. "Experimental and numerical studies of foam-filled sections", *International Journal of Impact Engineering*, 24, pp. 509-534.
- Singace, A.A. and Elbosky, H. 1995. "On the eccentricity factor in the progressive crushing of tubes", *International Journal of Solid Structures*, 32, pp.3589-3602.
- Singace, A.A. and Elbosky, H. 1996. " Further experimental investigation on the eccentricity factor in the progressive crushing of tubes", *International Journal of Solid Structures*, 33, No. 24, pp. 3517-3538
- Song, H.W. and Du, X.W. 2002. "Off-axis crushing of GFRP tubes", *Composites Science and Technology*, 62, pp. 2065-2073.

- Toğulga, M. 2003. "The effects of the microstructure on the durability, mechanical and thermal properties of polymer composite pipe materials for geothermal applications", MS Thesis, Izmir Institute of Technology.
- Toksoy, A.K. 2003. "Quasi-static compression behavior of empty and polystyrene foam filled aluminum tubes", Master Thesis, Izmir Institute of Technology.
- Toksoy, A.K., Tanoglu, M., Guden, M. and Hall, I.W. 2005. "The effect of adhesive on the strengthening of aluminum foam-filled circular tube", *International Journal of Material Science Letters*,
- Turner, T.A., Warrior, N.A., Robitaille, F. and Rudd C.D. 2005. "The influence of processing variables on the energy absorption of composite tubes", *Composites, Part A*, 36, pp. 1291-1299.
- Tvergaard, V. 1983. "On the transition from a diamond mode to an axisymmetric mode of collapse in cylindrical shells.", *Int. J. Solids Structures*, 19 (10), pp. 845-856
- WEB_1, 2005. Industrial Heating, 15/02/2005, <http://www.industrialheating.com/CDA/ArticleInformation/coverstory/BNPCoverStoryItem/0,2830,12062,00.html>
- WEB_2, 2004. Net Composites, 15/8/2004, <http://www.netcomposites.com/filament%20winding>
- WEB_3, 2004. Net Composites, 15/8/2004, <http://www.netcomposites.com/pultrusion>
- Wierzbicki, T., Bhat, S.U., Abramowicz, W. and Brodtkin, D. 1992. "A two folding elements model of progressive crushing of tubes", *International Journal of Solids and Structures*, 29, pp. 3269-3288.
- Yu, C., Eifert, H., Banhart, J. and Baumeister, J. 1998 "Metal foaming by a metallurgy method: production, properties and applications", *Journal of Materials Research Innovations*, 2 (3).
- Yuksel, S. and Guden, M. 2005. "SiC-particulate aluminum foams produced by powder compacts: foaming and compression behavior", *Journal of Materials Science*, in press.